Mechanical Characteristics of Geogrid-Reinforced Gravel in Large-Scale Triaxial Tests

大型三軸試験による ジオグリッド補強礫の力学的特性

by

Ho Thang Van

Signature	Date	Seal
Advisor:		
Co-Advisor:		

A thesis submitted in partial fulfillment
of the requirements for the degree of

Master of Engineering

Department of Civil Engineering
University of Tokyo
Tokyo, Japan
September, 2012

ABSTRACT

Gravel materials are commonly used in the construction of civil engineering infrastructure ranging from pavements to foundations, embankments or dams. In their design life, these structures are subjected to both monotonic and cyclic loads. Geogrids have been used to improve the performance of these structures in many projects. The properties of geogrids and the interaction between geogrids and gravel materials often govern the extent of improvement.

The aim of this study is to examine the effect of geogrid reinforcement on the peak strength and the stiffness of large prismatic gravel specimen. To implement objectives of this study, a series of large-scale triaxial tests were conducted on unreinforced and reinforced gravel specimens of 50 cm in height and 23 cm times 23 cm in cross-section, using an apparatus developed at the Institute of Industrial Science, University of Tokyo (Anh Dan et al. 2006). The material used was crushed sandstone originated from Tochigi prefecture in Japan. In addition to the variation of the cell pressure, the test series also includes the variation of geogrid types. As the specimens were in rectangular prismatic shape with relatively large dimensions as depicted above, placing LDTs in vertical as well as horizontal directions was possible to detect strains locally in those directions. All specimens were initially kept under isotropic consolidation and then sheared with triaxial compression (TC). The experimental study also includes the investigation of the stress distribution in the soil mass with and without reinforcement and the strain distribution along reinforcement. The vertical and horizontal local stress distribution in the soil were measured by placing earth pressure cells at pre-specified locations/depth within the specimen. The strain distribution along the geogrid was recorded using electrical resistance strain gauges that were instrumented at different locations along the geogrids.

Test results show a significant increase of the peak strength and stiffness due to geogrids. The PP geogrids perform better than Combi-grid in combination with gravelly soil. The test results also show that the relative reinforcing effect is higher for small lateral confining pressures, as in case at small depths. In addition, geogrid reinforcement does not show any significant improvement in small strain stiffness of granular specimen,

except for the case with Japanese geogrid. From these results, a simplied model is proposed to measure the confining effect of reinforcement.

ACKNOWLEDGEMENT

The acknowledgement section of this dissertation is too short to contain all the praise and thanks deserved by all the people who have helped me in my graduate career. I hope that the people listed here with a few lines following realize how much they have meant to me.

The greatest thankfulness is extended to my advisor Prof. Dr. Junichi Koseki for his kind supervision during two years of study. Thanks to his unlimited patience and kind clarification during every moment that I had problems. His invaluable advice, nonstop interest, continuing supports always encourage me going forward. I would also like to express my sincere gratitude to Assc. Prof. Dr. Reiko Kuwano for her guidance in every step of my research. Without their support and tutelage, writing this dissertation could not have been finished. Not only with academic matters but they were also there to mentor me to have a good life in Japan as a foreign student. I am also greatly indebted to my co-advisor Assc. Prof. Dr. Taro Uchimura who has had valuable advice, discussion and constructive criticism throughout this thesis.

Many thanks to Koseki and Kuwano Laboratory staff members as well. Heartfelt thanks to Mr. Takeshi Sato for helping me be familiar with the working of apparatuses, teaching me how to prepare transducers and rendered his tactful advices. I also earnestly appreciate Dr. Stanislav Lenart for guiding and assisting me to conduct experiments in a proper way and gave me valuable advices during he did as Research Associate in Koseki Laboratory. Special thanks also to Ms. Michie Torimitsu for bearing with all the administrative hassles during the time she had been in Koseki Laboratory. Thanks also to Dr. Hiroyuki Araki for teaching and helping me during I conducted experiments.

Special thanks to Mr. Kiyoteru Yamamoto for being my tutor when I first came to Japan and patiently dealing with the all the tenuous paper works to start life in Japan.

I would also like to express sincere gratitude to all of my present and former colleagues of Koseki and Kuwano Laboratory for their support and motivation including Mr. Gabriel, Mr. Laddu Indika Nalin De Silva, Mr. Laxmi Prasad Suwal, Mr. Seto Wahyudi, Mr. Wang and Ms. Sato.

I am also sincerely grateful to Ministry of Education, Science and Culture, Japan in providing financial support which enabled me to pursue the Master degree in Tokyo University, Japan smoothly.

Last but not least, special gratitude and thanks to my family who always encourage me and give me their unlimited support and patience.

TABLE OF CONTENTS

LIST OF FIGURES

CHAPTER 1

CHAPTER 2

CHAPTER 4

CHAPTER 1

INTRODUCTION

1.1 General

The concept of soil reinforcement is not a new one. The Ziggurat in Iraq, were constructed by clay bricks reinforced with woven mats of reeds nearly about 3000 years ago. The Great Wall of China is also constructed of a mixture of clay and gravel reinforced with tamarisk branches. Over the past half century a significant progress has been achieved in the research and application of reinforced soil earth structures. From that, the concept of reinforced soil is based on the existence of tensile strength of reinforcement and soil-reinforcement interaction due to frictional, interlocking and adhesion properties. It was first commercially introduced in the construction industry by French architect Henri Vidal in 1965. Since then, this technique has been widely used in geotechnical engineering practice. The reinforcing materials range from stiff metal to flexible geosynthetic materials and can be classified as either extensible reinforcements or inextensible reinforcements.

The main advantages of a reinforced soil structure are in following:

- Lower global cost: the possibility to build with steeper slopes reduces the quantity of the material needed for embankment;
- Moreover, it is possible to use less valuable and then cheaper material;
- Improved stability: the reinforcement guarantees an improvement in the factors of safety;
- It is possible to build directly on low bearing capacity soil;
- A reinforcement on the base allows to build on soft soil, that would normally request a preliminary consolidation and great caution during construction.

A geogrid is defined as a geosynthetic material consisting of connected parallel sets of tensile ribs with apertures of sufficient size to allow strike-through of surrounding soil, stone, or other geotechnical material (Koerner 1998). Their primary functions are reinforcement and separation. Reinforcement refers to the mechanisms by which the engineering properties of the composite soil/aggregates are mechanically improved. Separation refers to the physical isolation of dissimilar materials- for example base course and sub-base.

Geogrids are manufactured as either biaxial or uniaxial. Biaxial geogrids are those that exhibit the same strength in both the machine and cross machine directions while uniaxial geogrids exhibit the primary strength in the machine direction with minimal strength, enough to maintain the aperture structure, in the cross machine direction (**Fig. 1-1**).

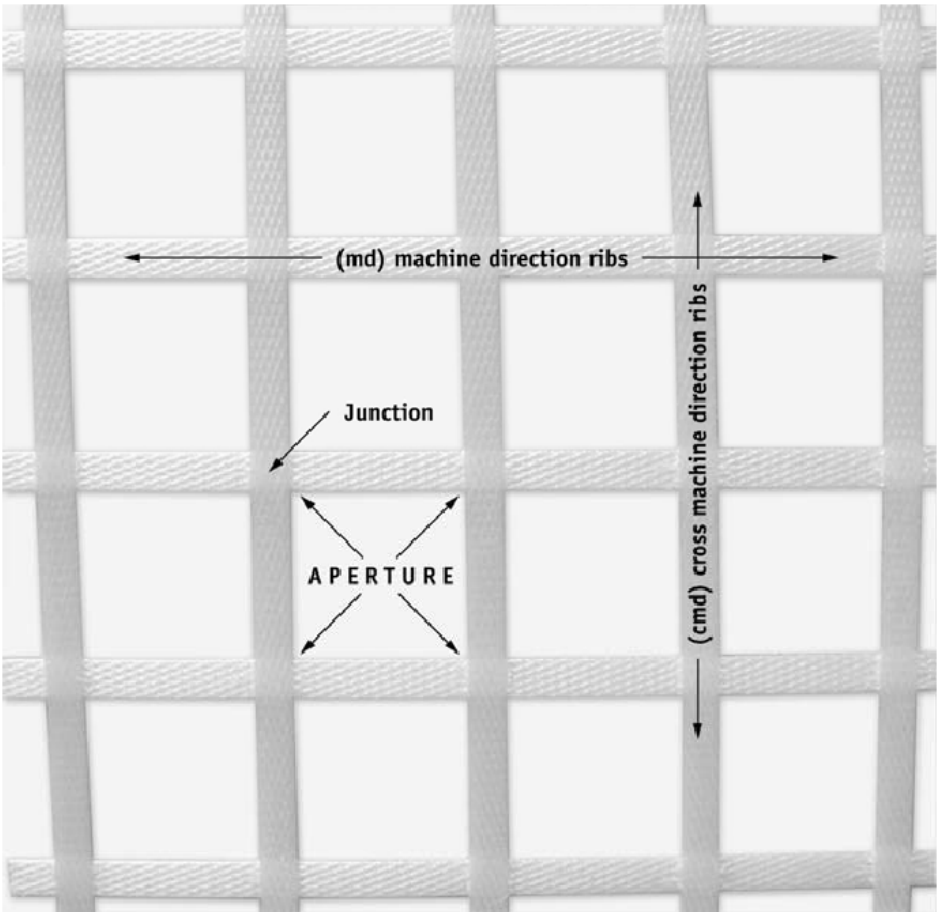

Figure 1-1: Geogrid definition
(K. von Maubeuge and C. Lesny, Mexico 2008)

The applications of geogrids can be listed as followed: base reinforcement, earth retaining wall construction including veneer stabilisation, the segmental retaining wall, embankment reinforcement and pile cap platforms. The applications of biaxial geogrids are mostly in base reinforcement, while the uniaxial geogrids are often used in the other purposes. Geogrids work by interlocking with the granular or soil material placed over them. The apertures allow for strike-through of the cover soil material which then interlocks with the ribs (flat straps/bars) providing confinement of the overlaying granular/soil material due to the stiffness and strength of the ribs (**Fig.1- 2**).

Figure 1-2: Demonstration of the interlock effect with a car standing on a laid and welded geogrid reinforced gravel column (K. von Maubeuge and C. Lesny, Mexico 2008)

Reinforced granular material is a composite material which combines properties resistance of two different materials in such a way to increase its bearing capacity. In this thesis report, a series of tests on unreinforced and reinforced on large true triaxial apparatus were carried out in order to evaluate the potential benefits of using geogrids for reinforcing granular. Three types of biaxial geogrids were used for the purposes of the research. Local deformation on both vertical and horizontal of unreinforced and reinforced tests were measured by sets of Local Deformation Transducers (LDTs) (Goto et al. 1991) and stress distribution was measured by the earth pressure cells.

1.2 Background of Study

1.2.1 Basic principles of reinforced soil

It is a well-known fact that soil is weak in tension and relatively strong in compression and shear. In a reinforced soil, the soil mass is reinforced by incorporating an inclusion (or reinforcement) that is strong in tensile resistance. Through soil-reinforcement interface bonding, the reinforcement restrains lateral deformation of the surrounding soil, increases its confinement, reduces its tendency for dilation, and consequently increases the stiffness and strength of the soil mass.

A simple model helps to explain the principle on which the reinforced soil techniques are based. Let us consider the soil element in **Fig.1-3a**, which is part of an infinite mass of soil: the application of a vertical stress σ_v causes a deformation in the element and the consequent horizontal stress σ_h caused by the lateral compression suffered by the adjacent soil. Horizontally the soil element undergoes a "tensile element" ε_h, which is one of the principle causes of local failure. When a reinforcing element is put in the soil, as in **Fig. 1-3b**, the application of a vertical stress is followed by the deformation of the soil element and the extension of the reinforcement. This extension then generates a tensile force T in reinforcement, which in turn produce a horizontal stress σ_h^* in soil. This stress, which also provide a confinement effect on the soil granules, greatly contributes to resist the horizontal forces and to reduce the horizontal deformations. Therefore the inclusion of a geogrid into the soil mass reduces the stresses and strains apply to the soil; on the other hand, the vertical stress σ_v applied to the soil mass can be increased, compared to the unreinforced soil, at equal deformations.

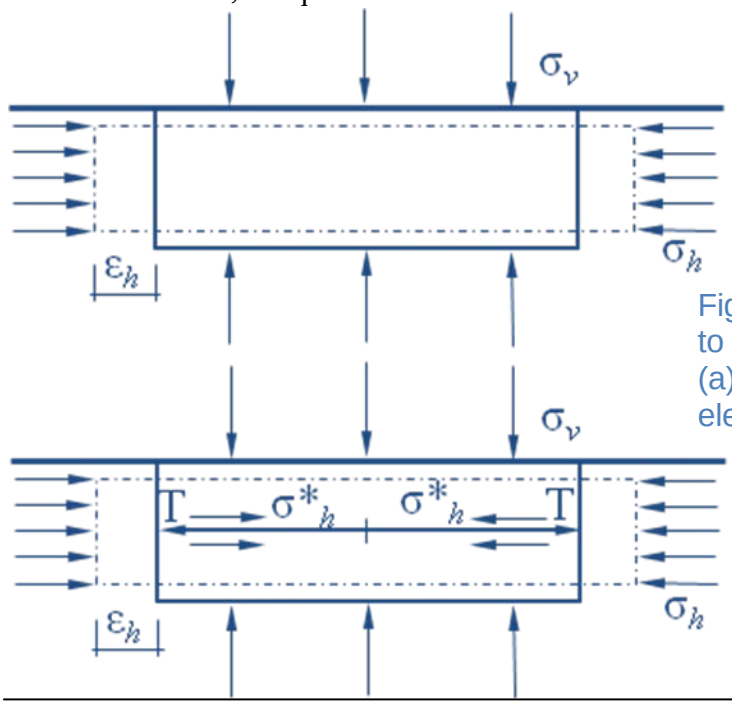

Figure 1-3: Stress and strain due to vertical load in an unreinforced (a) and a reinforced (b) soil element.

1.2.2 Experimental study of geosynthetic-soil behavior

Numerous experimental studies have been conducted to evaluate the interface behavior between geosynthetic and soil, bearing capacities of geosynthetic-reinforced foundations, and permanent deformations of geosynthetic-reinforced bases (Fannin and Sigurdsson 1996; Uchimura et al. 1996; Chang et al. 2000; DeMerchant et al. 2002; Nogami and Yong 2003; Abu-Farsakh et al. 2006; Almohd et al. 2006; Abu-Farsakh et al. 2007; Liu et al. 2009). Different test methods for geosynthetic-soil interaction are briefly reviewed below.

1.2.2.1 Direct shear tests

Abu-Farsakh et al. (2007) found that the interaction coefficient (C_i) from the direct shear tests depended upon soil type, geosynthetic type, and vertical stress. For a coarse-grained soil, they obtained that C_i varied from 0.74 to 0.94 kPa; whereas, for a fine grained soil, it varied from 0.64 to 0.89 kPa. Nakamura et al. (2003) investigated the behavior of the geogrid-sand interface in direct shear tests under two loading conditions: nominal constant pressure (NCP) and constant pressure (CP). This study indicated that the direct shear test apparatus, which provides a constant pressure during the entire test, is adequate for evaluating the interface strengths of geosynthetic and soil.

1.2.2.2 Pull-out tests

The interface properties between geosynthetic and soil are best evaluated by pull-out tests for the applications involving shallow rotational failure of a geosynthetic-reinforced slope where the geosynthetics are subjected to pull-out forces (Mallick et al. 1996). Synthesizing the previous researchers, Farrag et al. (1993) showed that the efficiency factors obtained from pull-out tests are generally larger than those obtained from direct shear tests.

1.2.2.3 Triaxial tests

Triaxial tests are often used to study the geosynthetic-soil reinforcement, probably because the apparatus is commonly available in most research institutes, and these tests allow for the stress controlled conditions. Using two sample sizes: 38-mm and 100-mm in diameter, Haeri et al. (2000) studied the benefits of geotextile reinforcement on sand. The number of geotextile layers placed inside the sample and their proper locations, which can

intercept the failure plane, were crucial for maximizing the benefits. Their study proves that geotextiles provide lateral confinement to the sample. From their experiments, it was observed that the stiffness of the reinforced samples was correlated to the stiffness of the geotextile and was higher than that of the unreinforced sample. Uchimura et al. (1996) conducted a series of large-scale triaxial tests with the specimens were rectangular prism (57 cm in height and 23 cm x 23 cm in cross-section) to investigate the effects of preloading and associated creep deformation on the relaxation in a reinforced soil mass. The results show that the rates of stress relaxation and creep deformation are relatively large in the first relaxation/creep stages. The relaxation rate decrease largely by preloading is consistent well with the behaviors observed in the field tests. The triaxial test results also suggest that for field full-scale Preloaded-Prestressed reinforced soil, prestress may increase with time if a sufficient amount of creep deformation has been allowed to occur during preloading.

The behavior of geosynthetic-soil composites have also been investigated through numerical analysis. Examples of these studies include Zhang et al., 2006; Ketchart and Wu, 2001; and Vulova and Leshchinsky, 2003.

Vulova and Leshchinsky (2003) conducted a series of analyses using a two-dimensional finite difference program FLAC Version 3.40 (1998). From the analysis, it was concluded that reinforcement spacing was a major factor controlling the behavior of geogrid-reinforced soil. Comparisons of the stress distribution in a soil mass with and without reinforcement were made by Ketchart and Wu (2001). It is noted that the presence of the reinforcement layers in the soil mass altered the horizontal and shear stress distributions but not the vertical stress distribution. The horizontal and shear stresses increased significantly near the reinforcement. The largest stresses occurred near the reinforcement and reduced with the increasing distance from the reinforcement. The extent of appreciable influence was only about 0.1~ 0.15 m from the reinforcement. With the increased lateral stress, the stiffness and strength of the soil will become larger. They emphasized the importance of keeping reinforcement spacing to be less than 0.3 m for geogrid-reinforced soil.

1.2.3 Problem Statement

Gravel materials are commonly used in the construction of civil engineering infrastructure ranging from pavements to foundations, embankments or dams. In their design life, these structures are subjected to both monotonic and cyclic loads. Geogrids have been used to improve the performance of these structures in many projects. The properties of geogrids and the interaction between geogrids and gravel materials often govern the extent of improvement. Mechanical properties of geogrid-reinforced gravel include some parameters that affect to its composite behavior. These parameters have been studied by many researchers. Parameters such as moisture content, soil type, geogrid geometry and stiffness, confining pressures and soil density have been the principal ones under their investigations. However, the differences between calculated and measured deformations of geogrid-reinforced structures indicate that the exact behaviour of geogrids in soil is not totally understood yet. That is why the present study will aim to address these issues for a better understanding of the geogrid reinforcement mechanisms. Geogrid-reinforced gravel interaction was studied under a monotonic and small cyclic loading using large-scale triaxial apparatus.

1.3 Objectives and scope of the study

The main objectives of this study are as described in the following

1. To investigate the composite behavior of geogrid-reinforced gravel at different confining pressures.
2. To examine the stress distribution in soil mass with and without reinforcement and the strain distribution along reinforcement.
3. To understand the failure mechanism of reinforced-gravel.
4. To understand the reinforcing mechanism based on the stiffness and the strength on unreinforced and reinforced tests.

To implement objectives of this study, a series of large-scale triaxial tests were conducted on unreinforced and reinforced gravel specimens of 50 cm in height and 23 cm times 23 cm in cross-section, using an apparatus developed at the Institute of Industrial Science, University of Tokyo (Anh Dan et al. 2006). In addition to the variation of the cell pressure, the test series also includes the variation of geogrid types. The experimental study also includes the investigation of the stress distribution in the soil mass with and

without reinforcement and the strain distribution along reinforcement. The vertical and horizontal local stress distribution in the soil were measured by placing earth pressure cells at pre-specified locations/depth within the specimen. The strain distribution along the geogrid was recorded using electrical resistance strain gauges that were instrumented at different locations along the geogrids.

1.4 Organization of the Thesis

This thesis report is divided into five chapters. The brief outline of each chapter is mentioned below.

Chapter 1 is the introductory section of the thesis and consists of the general background of the study.

Chapter 2 consists of description of materials, apparatuses, appurtenances and methodology of conducting the laboratory experiments.

Chapter 3 explains in detail about the parameters that affect to the performance of unreinforced and reinforced specimens.

Chapter 4 delineates the typical test results and discussions on the result in brief.

Chapter 5 summarizes the conclusion of the study along with recommendations for future course of study.

References

Abu-Farsakh, M., Coronel, J., and Tao, M. (2007). "Effect of soil moisture content and dry density on cohesive soil-geosynthetic interactions using large direct shear tests." Journal of Materials in Civil Engineering, 19(7), 540-549.

Almohd, I., Abu-Farsakh, M., and Farrag, K. (2006). "Geosynthetic reinforcement cohesive soil interface during pullout." American Society of Civil Engineers, Reston, VA 20191-4400, United States, Milwaukee, WI, United States, 40-49.

Bhandari, A. (2009).“Micromechanical Analysis of Geosynthetic-Soil Interaction under Cyclic Loading”, Ph.D. Thesis, Dept. of Civil and Environmental Engineering, University of Kansas, 254 pages.

DeMerchant, M. R., Valsangkar, A. J., and Schriver, A. B. (2002). "Plate load tests on geogrid-reinforced expanded shale lightweight aggregate." Geotextiles and Geomembranes, 20(3), 173-190.

Farrag, K., Acar, Y. B., and Juran, I. (1993). "Pull-out resistance of geogrid reinforcements." Geotextiles and Geomembranes, 12(2), 133-159.

Haeri, S. M., Noorzad, R., and Oskoorouchi, A. M. (2000). "Effect of geotextile reinforcement on the mechanical behavior of sand." Geotextiles and Geomembranes, 18, 385-342.

Konietzky, H., te Kamo, L., Groeger, T., and Jenner, C. (2004). "Use of DEM to model the interlocking effect of geogrids under static and cyclic loading." Numerical Modeling in Micromechanics via Particle Methods, Taylor and Francis Group, London, 3-11.

Koseki, J., Watanabe, K., Tateyama, M. and Kojima, K. (2001). “Seismic earth pressures acting on reinforced-soil and conventional type retaining walls.” Swets & Zeitlinger, Landmarks in Earth Reinforcement, (Ochiai et al. eds), Vol 1, pp.393-398.

Ketchart, K., and Wu, J. T. H. (2001). "Performance Test for Geosynthetic Reinforced Soil Including Effects of Preloading." Report FHWA-RD-01-018, Federal Highway Administration, Washington, D.C.

Koerner, R. M. (1998). Designing with Geosynthetics, 4th Ed., Prentice Hall, Upper Saddle River, N.J.

Liu, C.-N., Ho, Y.-H., and Huang, J.-W. (2009). "Large scale direct shear tests of soil/petyarn geogrid interfaces." Geotextiles and Geomembranes, 27(1), 19-30.

Latha, G. M. and Murthy, V. S. (2007). "Effects of reinforcement form on the behavior of geosynthetic reinforced sand." Geotextiles and Geomembranes, 25, 23-32.

Mallick, S. B., Zhai, H., Adanur, S., and Elton, D. J. (1996). "Pullout and direct shear testing of geosynthetic reinforcement: State-of-the-art report." Transportation Research Record, 1534, 80-90.

Nakamura, T., Mitachi, T., and Ikeura, I. (2003). "Estimating method for the in-soil deformation behavior of geogrid based on the results of direct box shear test." Soils and Foundations, 43(1), 47-57.

Nogami, T. and Yong, T. Y. (2003). "Load-settlement analysis of geosynthetic-reinforced soil with a simplified model." Soils and Foundations, 43(3), 33-42.

Thang, P. Q. (2009).“Investigating Composite Behavior of Geosynthetic-Reinforced Soil (GRS) mass”, Ph.D. Thesis, Dept. of Civil and Environmental Engineering, University of Colorado Denver, 378 pages.

Tatsuoka, F., Molenkamp, F., Torii, T., and Hino, T. (1997). "Preloaded and Prestressed Reinforced Soil." Soil and Foundations, Japan, 37(3), 79-94.

Uchimura, T., Shinoda, M., Siddiquee, M.S.A., and Tatsuoka, F. (2001). “Deformation analysis of PLPS GRS bridge pier during construction and in service.” Swets & Zeitlinger, Landmarks in Earth Reinforcement, (Ochiai et al. eds), Vol 1, pp.293-298.

Uchimura, T., Tatsuoka, F., Sato, T., Tateyama, M. and Tamura,Y. (1996). “Performance of preloaded and prestressed geosynthetic-reinforced soil.” Balkema, Int. Symp. on Earth Reinforcement, Fukuoka, Japan, (Ochiai et al., eds), Vol. 1, pp.537-542.

Vulova, C. and Leshchinsky, D. (2003). “Effect of Geosynthetic Reinforcement Spacing on the Performance of Mechanically Stabilized Earth Walls.” Publication No. FHWA-RD-03-048, Federal Highway Administration, McLean, VA, USA.

Zhang, M.X., Javadi, A.A., Lai, Y.M., and Sun, J. (2006). “Analysis of Geosynthetic Reinforced Soil Structures with Orthogonal Anisotropy.” Geotechnical and Geological Engineering, 24, 903-917.

CHAPTER 2

MATERIALS, APPARATUSES AND TESTING PROCEDURES

2.1 Testing Material

Chiba gravel

There are two batches of Tochigi gravel used in this study. Though both batches were originated from same area in Tochigi prefecture in Japan, they had been retrieved at different times. As test results from two different batches are used in this study for comparison, the author names them as old batch and new batch, respectively.

The material was crushed sand stone from Kuzuu mountain area, Tochigi prefecture, and could be categorized as sandy gravel. The raw material was thoroughly mixed and brought to the laboratory from Chiba experimental station of IIS, and was kept in plastic containers with it′s natural moisture content. The reconstituted specimens were prepared by molding and compacting manually, layer by layer, so as to obtain specimens with desired initial dry densities with almost a uniform moisture content. In order to study the degree of particle breakage due to heavy compaction, sieve analysis was carried out before testing and in one case after finishing testing. **Fig. 2.1** shows the particle size distribution of Tochigi gravel. From the figures it is clear that the particle breakage is not significant. The amount of fines content varies slightly in the old batch and the new batch. The old batch contains slightly higher percentage of fines than the new batch.

2.2 Large-scale True Triaxial Apparatuse

2.2.1 Description of apparatus

The large-scale true triaxial apparatus with specimen size of 23x23 cm^2 in cross-section and 50 cm in height, that has been recently developed in geotechnical laboratory at IIS, University of Tokyo was used for the present study. In this apparatus, all three-principle stresses can be controlled independently. In order to improve the accuracy of loading and

measurement systems, several modifications are made on the true triaxial apparatus employed in this study (AnhDan, 2001). The apparatus and its controlling system are shown in **Figs. 2-2** through **2-4**, respectively. The apparatus consists of a triaxial cell, axial and lateral loading device and a cell-pressure controlling device, while the lateral loading device was not used in the present study. The definition of x, y, z coordinates are presented in **Fig.2-4**. The vertical (axial) normal stress is σ_z; σ_y is the horizontal (lateral) stress controlled by the lateral loading device; and σ_x is the other horizontal stress, which is equal to the cell pressure. The axial load is measured with a load cell placed inside the large triaxial cell in order to eliminate the effects of piston friction (Tatsuoka, 1988). The pressure cell and the top and bottom plates of the triaxial cell are made of stainless-steel. The triaxial cell has a capacity of 2.94 MPa for the cell pressure and 490 kN for the axial load. Four observation windows were installed on the cell. The axial loading device consists of an electro-hydraulic actuator, having a capacity of 490 kN with a stroke of 200 mm, and a device called "zero-balance system" which controls a target axial displacement very accurately, including an application of cyclic axial loading with a strain amplitude of about 0.001%. The latter device (zero balance system) is driven by an AC servo-motor, which is connected to a series of reduction gears, electro-magnetic brakes and clutches (Santucci de Magistris, et al., 1999). This control system employs a multi-channel parallel sampling system together with 32-bit high-speed processors, achieving high-speed digital control, and being capable of highly accurate and stable control. It also employs a personal computer connected to the main processors with GPIB interface as well as portable operation console. The personal computer is capable of various operations including setting of test conditions, actual testing, recording of data and processing of data. Furthermore, the portable operation console, which is composed of a display, functional keys, and a rotary knob, allows simple manual operations. When there occurs any trouble, the controller can stop functioning automatically, which improved the safety in operating the large triaxial apparatus.

The cell pressure controlling device to apply the minor principle stress is similar to the one employed by Hayano et al. (1999). An original pneumatic pressure of about 1 MPa is amplified by an air-driven pump up to 3 MPa and is regulated by an electro-pneumatic servo valve to a specified value. At a cell pressure not exceeding 1 MPa, a volume booster is also employed to increase the volume of supplied air.

To reduce the mechanical errors (e.g. backlash) in the axial loading system, the gear system employed a special technique called “rotating only in one direction”. In this technique, the rotation direction of the motor rod is fixed so that the spur gear (numbered as 2 in **Fig.2-5**) connected to the motor does not change its rotation direction. Two different bevel gears (numbered as 3 and 4) are set at upper and lower positions to the spur gear (**Fig.2-5**). These two gear rotate in different directions; one is clockwise and the other is anti-clockwise. Each of these two gears is connected to an electro-magnetic clutch system (numbered as 6 and 7). When an electric current activates the system, it will be connected to the shaft to transfer the rotation. During loading or unloading; one clutch system is connected to the shaft, while the other is set free. When no loading is applied, both clutch systems are set free, while the shaft is fixed by an electro-magnetic brake (numbered as 8). Calibration curve of the load cell is shown in **Fig.2-6**.

The axial and lateral deformations that are free from the effects of bedding error and membrane penetration are measured directly on the lateral surface of specimen by using local deformation transducers (LDTs), developed by Goto et al. (1991).

2.2.2 Operation of system for stress control and strain control in triaxial test

2.2.2.1 Stress controlled test

The output from the internal load cell, which is denoted as LC, was defined as zero when the deviator load at the top of the specimen was zero. The axial stress σ_v is evaluated as:

$$\sigma_V = \sigma_h + \frac{LC}{A_s} \qquad (2\text{-}1)$$

where A_s is the current cross sectional area of the specimen, and σ_h is the lateral stress measured with differential pressure transducers. In the automated system, any required stress path is achieved by controlling the values of σ_v and σ_h in the desired manner. Since the response of the internal load cell, which is free from bearing friction of the loading piston, is referred throughout the test, the measured σ_v value by Eq. (2-1) does not need any correction. Equation 2-1 is valid whether or not σ_v is greater than or less than σ_h so that compression or extension could be measured correctly.

The axial load P acting on the top of the loading piston is related to the value of LC as:

$$P = LC - W + a_{lp}.\sigma_h \qquad (2\text{-}2)$$

where W is the weight of the loading piston and the specimen cap and "a_{lp}" is the cross-sectional area of the loading piston. Therefore, we have:

$$\sigma_V = \frac{P+W}{A_s} + \sigma_h(1 - \frac{a_{lp}}{A_s}) \qquad (2\text{-}3)$$

It implies that the vertical stress σ_v is dependent of σ_h and LC. Therefore, the working principle of automation is that a stress path with varying σ_h needs both σ_v and σ_h to be controlled simultaneously, which is traced by imposing many small steps of loading (or unloading). In each step, a very small incremental feedback to the deviator load is applied until the stress state returns to the intended stress path (Hoque, 1996).

The stress paths employed in this study is isotropic consolidation stress path at constant stress increment ratio K = $\Delta\sigma_v/\Delta\sigma_h$ = 1 (high confining pressure tests), vertical small cyclic loading stress path with $\Delta\sigma_h$ = 0 and then apply loading until the specimen fail.

2.2.2.2 Strain controlled test

In the case of strain control loading , the axial strain rate was set to be the desired value. The external diplacement transducer having a capacity of 200 mm was used to evaluate the feedback strain, resulting into relatively rough resolution because its full stroke of 200 mm was controlled by an AC current of ± 5V, which means 1 mV corresponds to 0.02 mm (axial strain of about 0.003% with the 500 mm high specimen).

2.2.2.3 Principle of zero-balance system

Zero-balance system is the system that was developed to improve the resolution of axial loading system. With this system shown in **Fig. 2-7**, axial loading is controlled in such a way that the vertical location of the loading piston is equal to that of a small target rod to an accuracy of less than 0.5 μm as detected by the small-range displacement transducer with a stroke of ±3mm which is in turn controlled by a precise motor-gear system. The motor gear system is free from backlash when reversing the loading direction (Tatsuoka et al., 1994). Using this set-up, the loading system has a large stroke equal ±100 mm in this case, with a fixed resolution equal to 0.5 μm.

It consists of two different parts. One part is connected rigidly with loading piston, while another part consist of a small target rod that is connected with the motor-gear system in order to control its location very accurately. An AC servo-motor, which can change the rotational speed in the range of maximum 3000 times is connected to target rod through a series of reduction gear. Second part link with the first part by magnetic foil.

Principle of zero-balance system is as follows. When tests are started, the condition will be called as 0 state and the stroke measured with the small-range displacement transducer is set at 0 mm. The motor runs and makes the first movement of target rod (part 1 unit) downward (or upward), then the measured value of stroke will not be zero because there occurs a relative movement from the 0 state to the current position, called as "gap". At the same time, the part 2 unit is still in the same position as the 0 state. The system will detect this gap by magnetic field and feed-back will be made to actuator to move the loading piston (connected with part 2 unit) for recovering this gap and restoring to the 0 state. According to the feedback control system introduced for this purpose, the small-range displacement transducer detects the gap (Fb), which is compared with the initial signal at the 0 state (S); thereby the flow rate of hydraulic oil is controlled by the servo-value based on the deviation signal E= S-Fb (**Fig.2-8**). The nearer the displacement of the loading piston gets close to that of target rod, the nearer the deviation signal (E) moves to 0. Zero-balance system makes loading piston move down or up continuously at a constant rate.

2.2.2.4 Local Deformation Transducers (LDTs)

The small strain behavior of soils is of great importance in various geotechnical-engineering problems where pre-failure ground deformation is of major concern. In particular for cases with relatively stiff soils (e.g., dense sands, gravels and hard clays) and soft rocks, typical strain levels in the ground under working load conditions are less than about 0.1% (e.g., Burland 1989; Jardine et al. 1991; Tatsouka et al. 1995). On the other hand, precise determination of soil stiffness at strain level lesser than about 0.1% is difficult to achieve in the conventional laboratory triaxial tests. The conventional external measurements of specimen deformation of hard soils and soft rocks can include large effects of the compliance of the loading system and load measuring systems as well as the so called bedding error at both longitudinal ends of the specimen, resulting in the

overestimation of strain or in other words, underestimation of stiffness. A number of local strain measuring devices have been developed in the past two decades, such as electro-level gauge by Burland and Symes (1982) and Jardine et al. (1984), Hall effect transducer by Clayton et al. (1987), non-contact type proximeter by El-Horsi et al. (1981) and Hird and Yung (1987), local deformation transducer (LDT) by Goto et al. (1991). In many laboratories nowadays, it is possible to measure with confidence axial strains smaller than 0.01% or even lesser than 0.001%.

LDTs have been widely used since their development by Goto et al. (1991). The advent of LDTs has allowed geotechnical engineers to measure deformation properties of geomaterials for a wide range of strains, from very small strain up to those at the peak failure condition (Tatsouka and Kohata, 1995), which is very important for proper modeling and design of geomaterials. Detailed facts about LDTs could be found in Hoque (1996).

In this study, several LDTs with different length were used and the calibration curves for all LDTs used in this study are shown in **Figs 2-9a** through **2-9q**. They were installed vertically and horizontally facing the opposite sides of the specimen. Each LDT was held at their ends by a pair of pseudo hinges attached on the membrane of the specimen along a vertical alignment. The hinges were attached to the membrane in such a way that the distance between them was slightly shorter than the free, unstressed length of the LDT so that it can support itself on its own elastic force when pinned against the hinges.

LDTs are made of a thin, flexible, heat-treated phosphor bronze strip on which two electronic-resistant strain gauges are placed, one each on the compression and the tension side and forming a Wheatstone bridge when combined with the resistors present in the pin connectors. When the LDT is subjected to any bending deformation associated with axial compression between both ends, a consistent change in the voltage by strain gauges is obtained, which provides the basis for developing relationship between the deformation and the response voltage. The LDTs were calibrated by incremental displacement method, where in each step an axial compression of 0.1mm was applied using a micrometer having a capacity of 4mm.

2.2.2.5 High Capacity Differential Pressure Transducer (HCDPT)

A high capacity differential pressure transducer (HCDPT) as shown in **Fig. 2-10**, was used to measure effective lateral stress acting on the specimen. The positive terminal of the HCDPT is connected to the inside of the triaxial cell chamber while the negative terminal is connected to the inside of the specimen via the top and bottom drainage of the specimen. In all of the tests, the cell pressure was controlled by the electro-pneumatic (E/P) transducer and the back pressure was kept constant throughout. The calibration chart of the HCDPT is shown in **Fig. 2-11**.

2.2.2.6 External Displacement Transducer (LVDT)

A displacement transducer called Linear Variable Differential Transducer (LVDT), also called External Displacement Transducer (EDT) is the conventional type of transducer used to measure the axial displacement of the sample by measuring the displacement of a horizontal plate clamped to the loading piston. **Fig. 2-12** shows the picture of the EDT employed in this study. In this study, EDT was used to calculate the final height of the specimen after it is fixed to the loading system. The EDT was calibrated by adding and removing blocks with known standard heights and measuring the output voltage. The calibration chart for the EDT is given in **Fig. 2-13**.

2.3 Earth Pressure Cells

Six earth pressure cells were employed in this study in recent last tests as can be seen in **Fig. 2-14**. These pressure cells were made of stainless steel, had a thickness of 11.3 mm, an outer diameter of 50 mm with the sensing area diameter of 46 mm, and total weight of 160 g. Their primary functions were to monitor the change in the stress state and also measured the increase in vertical and horizontal pressure due to loading conditions. The maximum stress to be applied on these pressure cells is 2 MPa.

2.4 Testing Procedure

2.4.1 Specimen Preparation

The reconstituted Tochigi gravel specimens were prepared by manual compaction in the laboratory. The mold was made up of four plates, which can be fixed together with

screws to make a rectangular prism. The inner dimensions can be adjusted by attaching additional thin plates to the main frame internally. For a tolerance, four additional plates with a thickness of 8 mm were attached to the top of vertical plates of the mold. A 2 mm-thick membrane was used for all tests. The circumference of the pedestal was applied with a uniform thin layer of grease (30μm), to ensure a proper seal to the specimen after preparation and the membrane. Lubrication layer including one uniform layer of grease about 30 μm thick and double layers of 2 mm thick membrane equal in size of the top surface of pedestal but having a small hole at the center equal in size of the porous stone was put on the upper surface of pedestal to reduce friction between the specimen and pedestal. Then the membrane was placed and the bottom of membrane was well tied to the pedestal and the mold. The verticality of the mold was checked with respect to some reference vertical columns. A piece of filter paper slightly larger in size than the hole in the lubrication membrane was on the lubrication membrane to avoid entry of small particle of specimen inside the porous stone which can block the pores. After fixing the mold and membrane, vacuum was applied to the space between the mold and membrane to remove the trapped air and to fasten the membrane to the inside of the mold.

Before preparing the specimen by compaction, the raw material was mixed well for making the particle size distribution uniform. The current moisture content was evaluated by taking specimen including fine and coarse particles. According to the initial moisture content and the required dry density, the amounts of material and water to be added, were calculated assuming a specific gravity of 2.68 for the material. The optimum moisture content and the maximum dry density were defined by modified Proctor compaction test as w_{opt}=4.0 % and ρ_d=2.168 g/cm^3, respectively.

Dense specimens were prepared by manual compaction at nearly optimum moisture content. The compaction was done layer by layer. The whole process was done for altogether 10 layers of thickness of around 5 cm each, which was sufficient enough to accommodate the maximum particle size. Before placing the material for the next layer, the surface of the previously compacted layer was scrapped to a depth of about 2 cm to ensure a good interlocking between vertically adjacent layers.

The compaction was done using a metal block with a weight of 2 kg and a handle, which is 3 kg in total as shown in **Figs. 2-15** and **2-16**. A metal square plate, with a dimension

little smaller than that of the inner cross section of the mold, was placed on top of the material to give a uniform compaction. An electro-magnetic rod was used to place the plate inside the mold, and then to take out, without damaging the membrane. The compaction technique was rather simple but needed much more physical effort to get efficient results. The compaction was applied with an aim to reach dry density of specimen as close as possible to the one defined by the modified Proctor test. Compaction was given until the desired density was reached, by referring to the depth of compacted material. Several measurements were taken for depth from various points and averaged at each time.

Special care was taken to avoid damage to the membrane by the sharp edges of the particles or the edge of the compacting block during such heavy compaction. The blows were given with relatively low frequency to make sure perfect vertical blows at center without hitting the sides of the mold. Before compaction, for minimizing the problem with the sharp edges of particles, the material for each layer was placed step by step in smaller amounts, and large particles having sharp edges were positioned closed to the center of specimen. For avoiding similar problems with the sharp edges of the plates of the mold, four pieces of plastic block were placed in between the sharp portion of mold plate and membrane, when fixing the mold.

Vacuum pressure was applied throughout the compaction process in order to keep the membrane fastened to the mold properly. The top layer of specimen was smoothened with using a finer material, making a flat surface to reduce the bedding error. Filter paper was placed on the top of specimen for facilitating drainage during testing. As there was a high possibility of membrane damage during the compaction of the last sub-layer, additional care was taken in compaction of the last layer. In reinforced tests, two geogrid layers have been placed in the reinforced specimens leading to a vertical reinforcement spacing of nearly 0.3 m. Test results presented in this paper are obtained from specimen reinforced with a biaxial polypropylene and biaxial combi-polypropylene geogrids with a nominal strength of 40kN/m and welded, pre-stretched flat bars. The aperture size of the grid was 31mm x 31mm and the tensile force at 2% strain was 16kN/m, as given by the manufacturer. They are shown in **Fig.2-17**. One more test was perfomed using the biaxial polypropylene from a Japanese manufacturer with a nominal strength of 12x22 kN/m, the aperture size of the grid was 28mm x 40mm as given by the manufacturer.

In some recent tests, earth pressure cells were put inside specimens to measure the stress distribution in both vertical and horizontal direction. The schematic of position of earth pressure cell is shown in **Fig.2-18**.

2.4.2 Specimen Setting

Lubrication layer consisting of two layers of 2mm thick membrane stick over the 30 μm thick grease layer was used underneath the top cap before placing it at the specimen. A small hole inside equal with porous stone fixed inside the top cap was made in the lubrication membrane to provide proper drainage. Similarly, while applying grease over the top cap it was also tried to avoid application of grease over the porous stone. After fixing the lubrication layer at the top cap, the top part of triaxial cell, consisting of the top platen of the triaxial cell, the loading piston, the load cell and the specimen cap, all in one unit, was assembled above the specimen. Once the specimen preparation was over, the top cap of the triaxial apparatus was lifted to be vertically above the specimen. Then the top cap of the apparatus was gradually brought down in order to place it on the top of the specimen, while keeping a clearance between the top surface of sample and the bottom surface of top cap. After fixing the top cap to the two vertical supporting columns with nuts by simultaneously tightening both sides, the piston was balanced by vertical lifting with two small scale pneumatic pressure cylinders, and then unclamped without allowing the top cap to strike on specimen.

The terminals of the channels for inner load cell were then connected and the analogue-to-digital reading of load cell was set to a voltage range according to the calibration of the inner load cell with respect to zero reading at neutral position. Keeping the neutral position with zero reading, the piston was brought down very gently until it touches the top surface of sample, which was realized by the positive change in the voltage reading load cell. After this setting, the piston was clamped with the top cap again. A homogeneous thin layer of high quality grease was applied along the side surface of the top cap to ensure a proper seal from air leakage. The membrane was firmly tied with the top cap using 0.8 mm thick and 20 mm wide membrane strips. After that the tolerance plates of 8 mm thick, four in number, were removed from the top of the mould. The purpose of these plates was to get an additional dimension of around 8 mm on the height of the specimen, for providing a possibility of consolidation and to make a good contact

between the specimen and top cap. After that a vacuum pressure of around 25 kPa was applied to the interior of sample to keep the structure of the specimen unchanged when removing the mould plates. Note that at this point the piston can move freely in vertical direction with its self weight was balanced by the small scale pneumatic pressure. This allowed the specimen to be freely consolidated during vacuum pressure application. The vacuum pressure was applied through the top and bottom side of the specimen. The system was left for about 15 minutes for stabilizing. After applying vacuum pressure interior to the sample, the vacuum pressure being applied in between metal mold and membrane was released, and then the mould plates were disassembled.

The surface of the sample was checked for any possible damage or holes and ensured for proper air seal. The height, width, and breath of the sample were taken at several points and averaged.

2.4.3 Setting of Local Deformation Transducers (LDTs)

The membrane surface was then cleaned by using ethanol, and the desired points for the hinges of LDTs were marked. For unreinforced tests, axial strain (ε_1) was measured by three pairs of vertical local deformation transducers (V-LDTs). Lateral strains in two directions (ε_3) were measured by another three pairs of horizontal local deformation transducers (H-LDTs). For in the reinforced tests, axial strain (ε_1) and lateral strains (ε_3) were measured by four pairs of vertical and horizontal local deformation transducers in each side of the specimen, respectively. The schematic diagrams showing the location of all LDTs over the specimen for both types of tests are shown in **Figs.2-19** and **2-20**. The mean of data measured with three or four pairs LDTs was used for each direction of local strain measurement for the analysis of test results.

The hinges for those devices were cleaned and fastened with membrane at appropriate points. A high quality bonding material was used to paste the hinges with the membrane. Fixing the hinges to membrane was done very carefully to make a firm bond of hinges in order to eliminate the possible errors in strain measurements due to improper bond of hinges. The typical dimensions of hinges used for vertical and horizontal LDTs are shown in **Fig. 2-21.**

The terminals were connected, and digital reading of LDTs was initially set for specified balanced positions, with respect to zero reading at neutral position. For vertical LDTs this was done by hanging the LDT vertically with strain free condition. In the case of horizontal LDTs, the LDT was kept horizontally with its surface in vertical plane. In case of necessity, the initial reading, which had been set to zero, was shifted to some value (e.g. shift from zero to -5V in the case of vertical and horizontal LDTs) depending on the expected behavior of specimen during testing and the performance characteristics of the particular devices. This depends also on the condition during the calibration of the device. It should be ensured that the initial setting of voltage be the same as that of during calibration. Firstly, one hinge was fixed and after allowing it to get firmly fastened, the LDT was placed by adjusting the other hinge position until desired position of LDT was reached. Then the hinge position was marked and hinge was fastened at that point. Then again the LDT was placed on both hinges and checked. The position of second hinge may vary depending on the requirement during the test. If the test is expected to undergo large compression then the LDT must be set to accommodate much of compression. If it is the case with large extension then the LDT must be set with initial bent so that it can be used to measure large extension. If the voltage went out of range (over ± 5 volt) during setting or even during testing, then the voltage can be shifted to be within the workable range. The amount of shift in voltage must be recorded and considered during calculation as the behavior of LDT is non-linear.

Once the LDT was set, some provision was made to safely remove the LDTs from the hinge during testing, for avoiding damage to the LDTs that occurs when the strain values go beyond the allowable limit at high strain levels close to failure states. This situation may occur when large amount of compression occurs. In the case of large amount of extension, the LDT would be released from the hinges automatically.

After setting LDTs to appropriate positions, the entire set up was left under the same condition for about one day so as to allow for possible creep due to stiffness of the devices and hinges. During all these process, a vacuum pressure of 25 kPa was being applied to the specimen. After this process, the vertical and horizontal dimensions of the sample were measured using measuring tape and Vernier-calipers at several points and averaged. During this process, the vertical piston movement was free and the self-weight was counter-balanced.

For the tests under low confining pressure (e.g 25 kPa or 70 kPa), the vacuum was applied during preparing of specimen till the end of the test without applying any cell pressure. In case of high confining pressure tests, positive cell pressure was applied. The large cylindrical cell was then lifted by the pulley arrangement and gently brought down to cover the specimen set up. A homogeneous thin layer of grease was applied at bottom plate surface and top cap surface to ensure proper sealing to eliminate air leakage from the cell. The cell and the top cover were fixed firmly. The vacuum pressure, being applied to the sample, was slowly reduced to zero while a positive pressure in the cell was slowly increased from zero to 25 kPa. This was done very gently in small steps of decreasing vacuum pressure and increasing cell pressure simultaneously to avoid disturbance due to sudden pressure transfer. Then the operating system of the actuator unit was swiched on and the loading ram was moved up. Then the triaxial cell was placed into the frame, and the loading ram was brought down slowly until it reaches very close to the top of the piston from triaxial cell. The triaxial cell was set in alignment of the loading ram by adjusting the position of the triaxial cell. Once the alignment was ensured then the triaxial cell was firmly clamped with the bottom of the frame to avoid any up-lift of cell due to high pressure. The ram was then moved downwards very gently until it touched the top of the piston of the triaxial cell. The moment of touching was realized by noticing the digital voltage signal of the outer load cell. The loading ram and the piston were then clamped, and the counter balance pressure for the self weight of piston was released.

2.4.4 Testing process and stress path applied

All samples initially underwent cyclic isotropic consolidation. After that, the specimen was sheared in triaxial compression with large unload-reload cycles. At various stress levels, small vertical unload-reload cyclics were applied in order to evaluate the elastic Young's moduli in vertical direction. The amplitude of these small strain should be ideally less than about 0.001%, which are considered as the elastic limit strain.

Once the pre-peak testing program was over, The specimens were sheared up to failure in triaxial compression with constant confining pressure. This last shearing was monotonic loading and was carried out in strain control mode with an axial strain rate of around 0.06 % per minute.

During last shearing when the strain level was reached to the allowable limit of LDTs, the corresponding LDTs were removed from the hinges by pulling the connecting string or by hand (in case of low confining pressure tests), to protect LDTs from breaking. External LVDT measurement was continuously done until the end of the test. During the strain control tests the voltage of inner load cell could also be adjusted to keep it in the allowable range of ± 5 volts.

Table 2-1 shows the initial properties of specimen and testing program for this study.

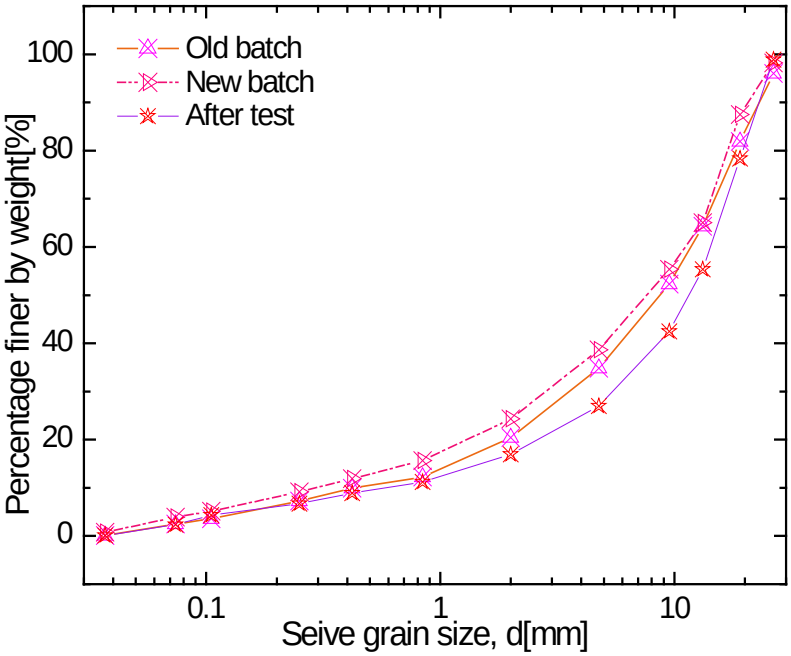

Figure 2-1: Grain size distribution of Tochigi gravel

Figure 2-2: Photo of Large-scale True Triaxial Apparatus employed in this study

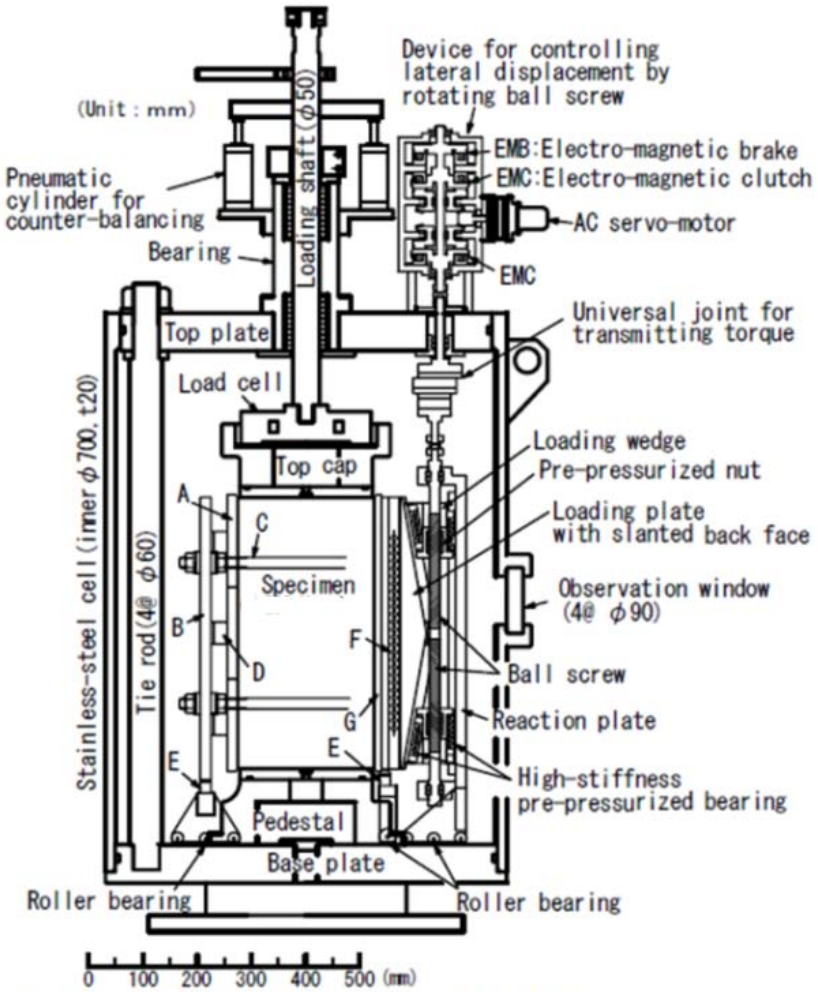

Figure 2-3: Schematic figure of Large-scale True Triaxial Apparatus

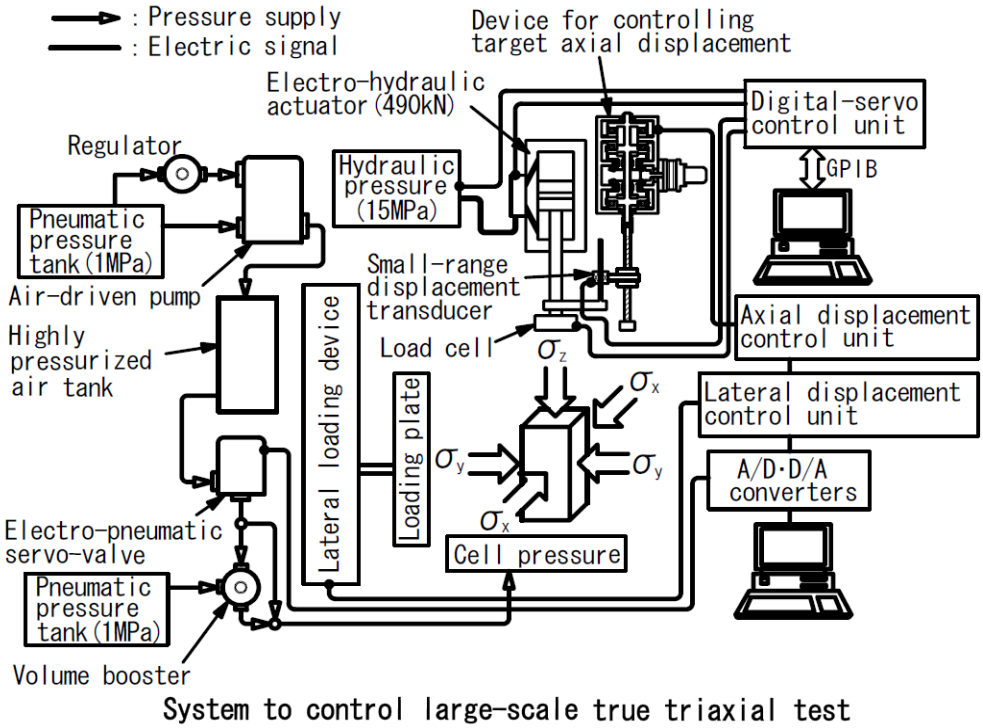

Figure 2-4: System to control the apparatus

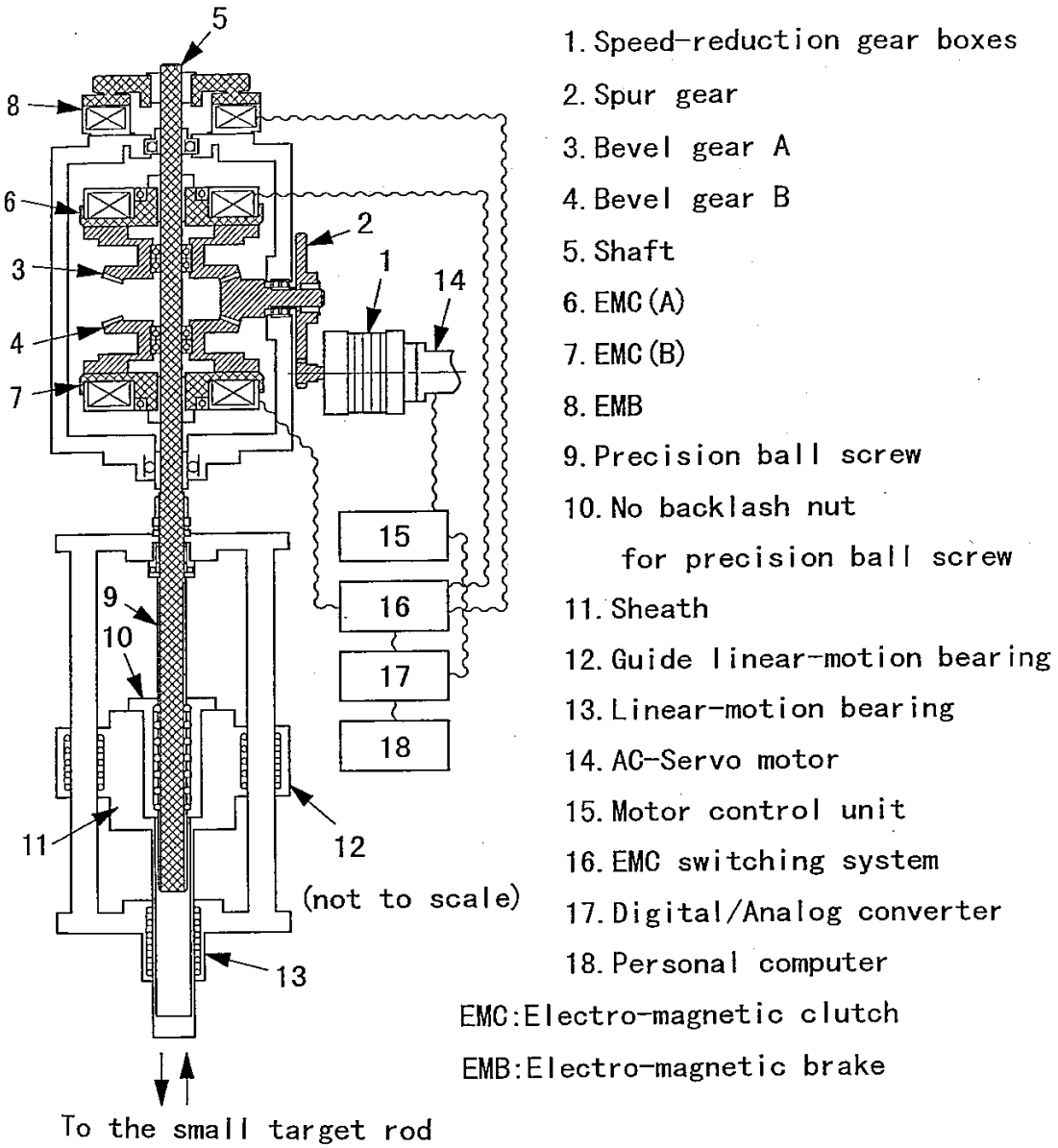

Figure 2-5: Gear Loading System in True Triaxial Test

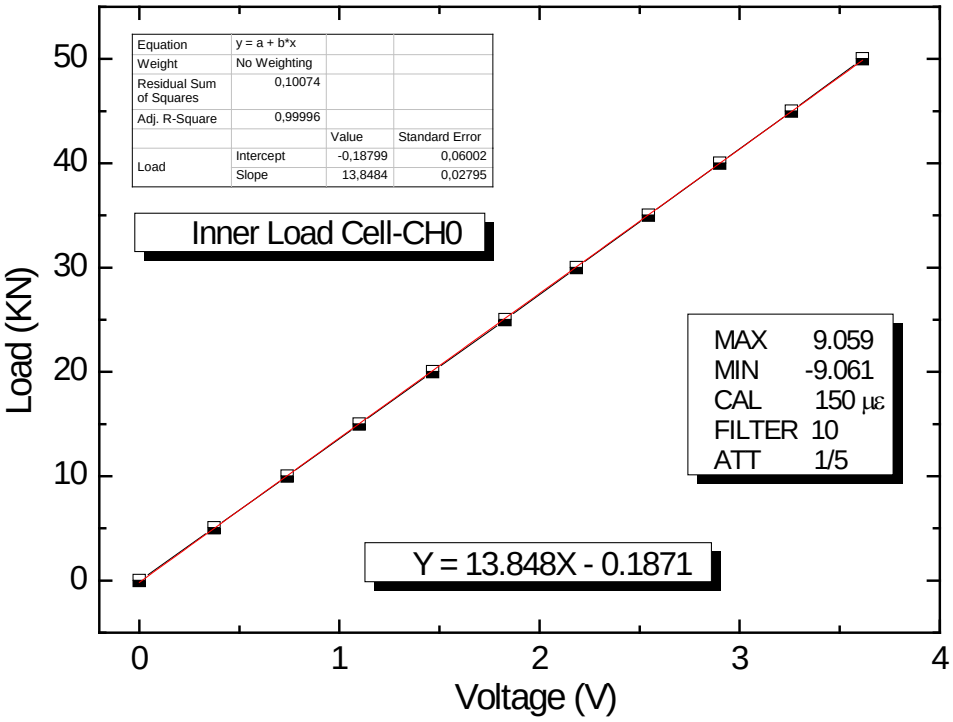

Figure 2-6: Calibration of inner load cell

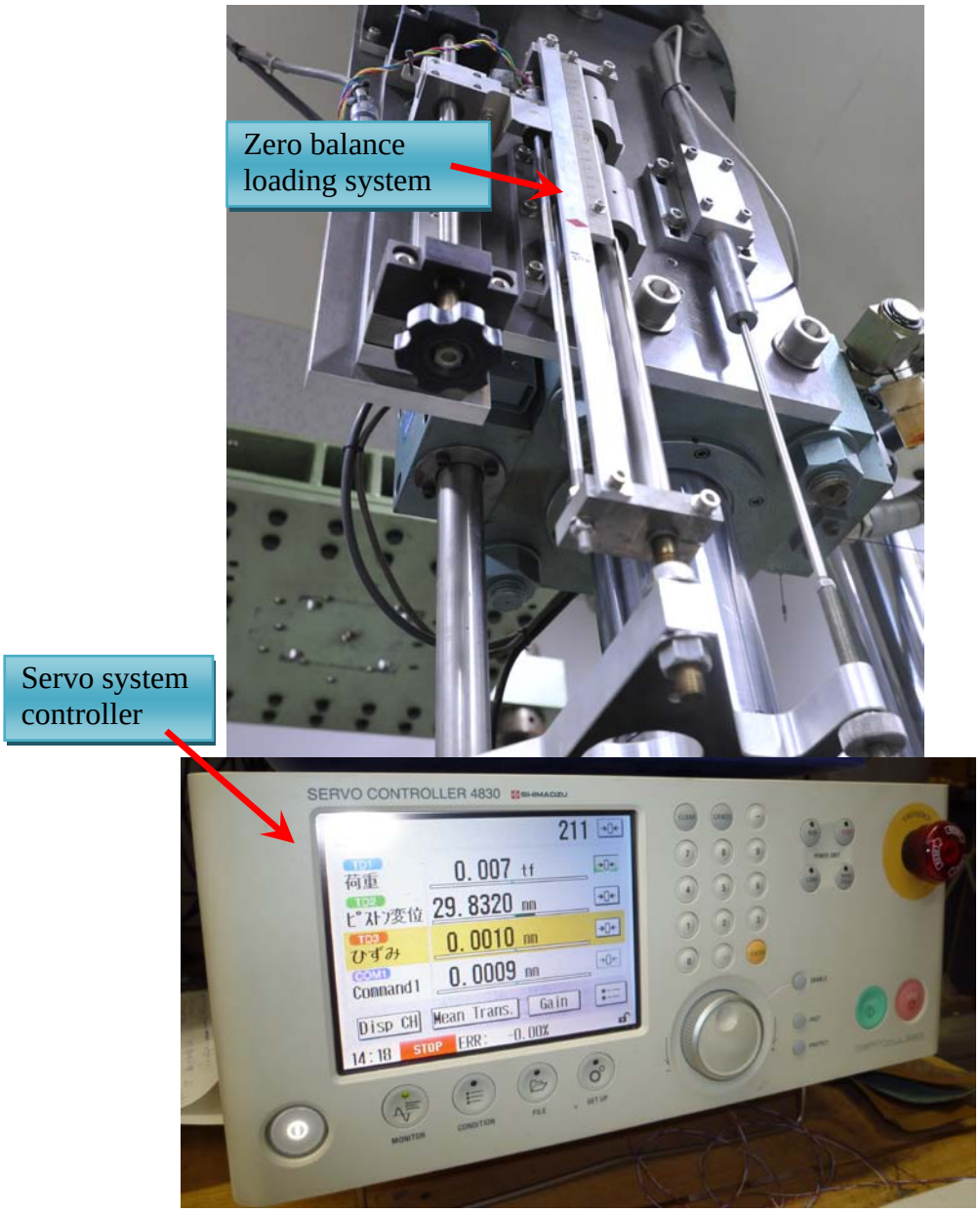

Figure 2-7: Servo system loading control devices and zero-balance loading system

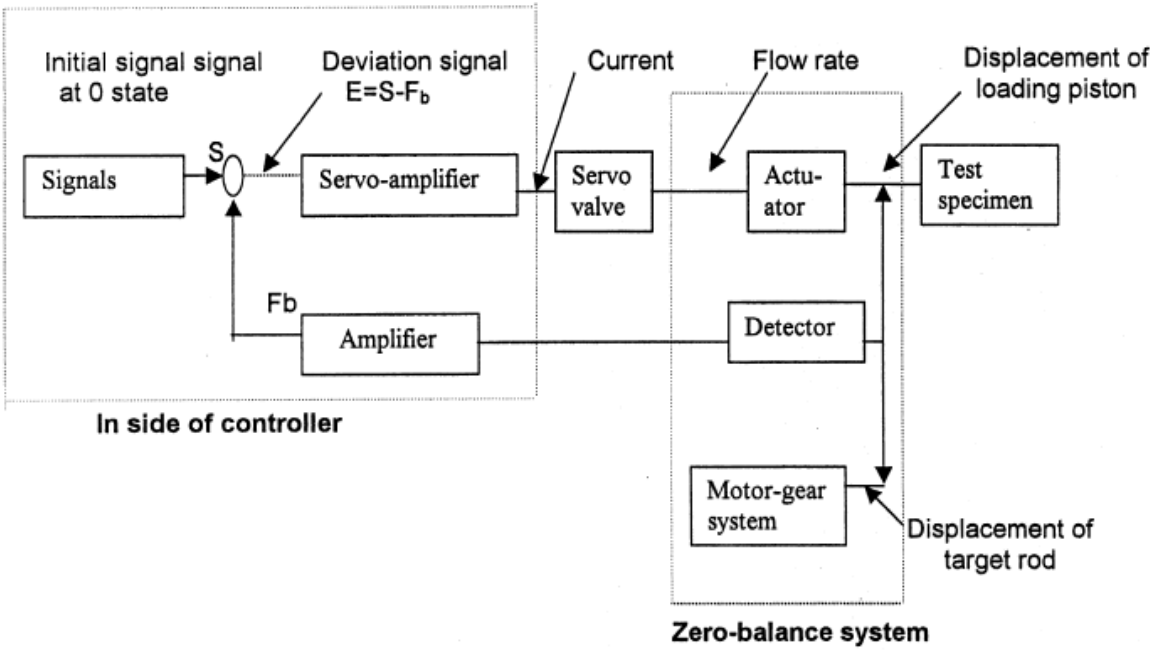

Figure 2-8: Working principle of loading system

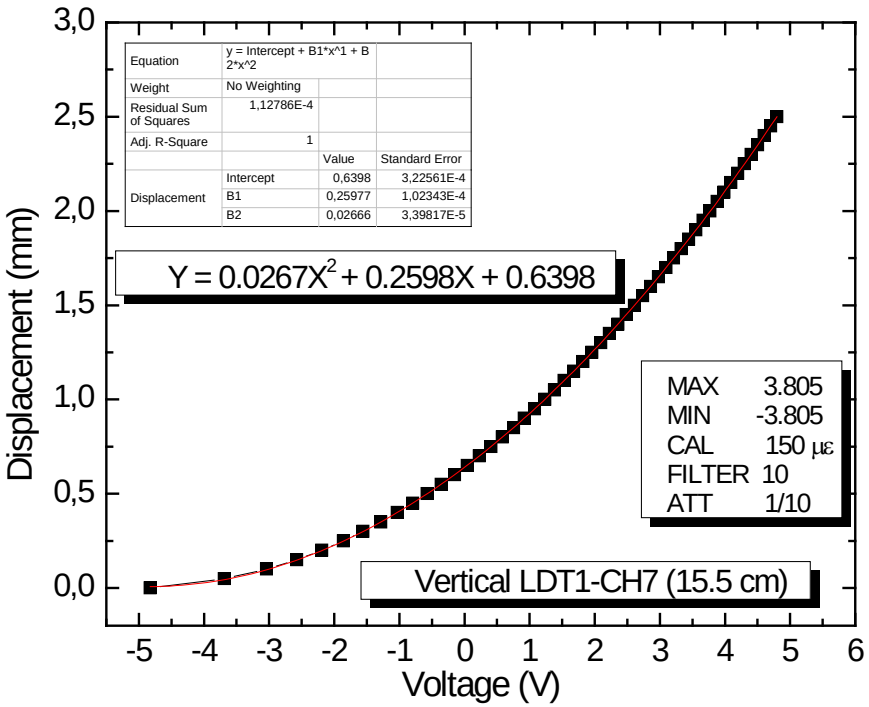

Figure 2-9a: Calibration curve for vertical LDT-1

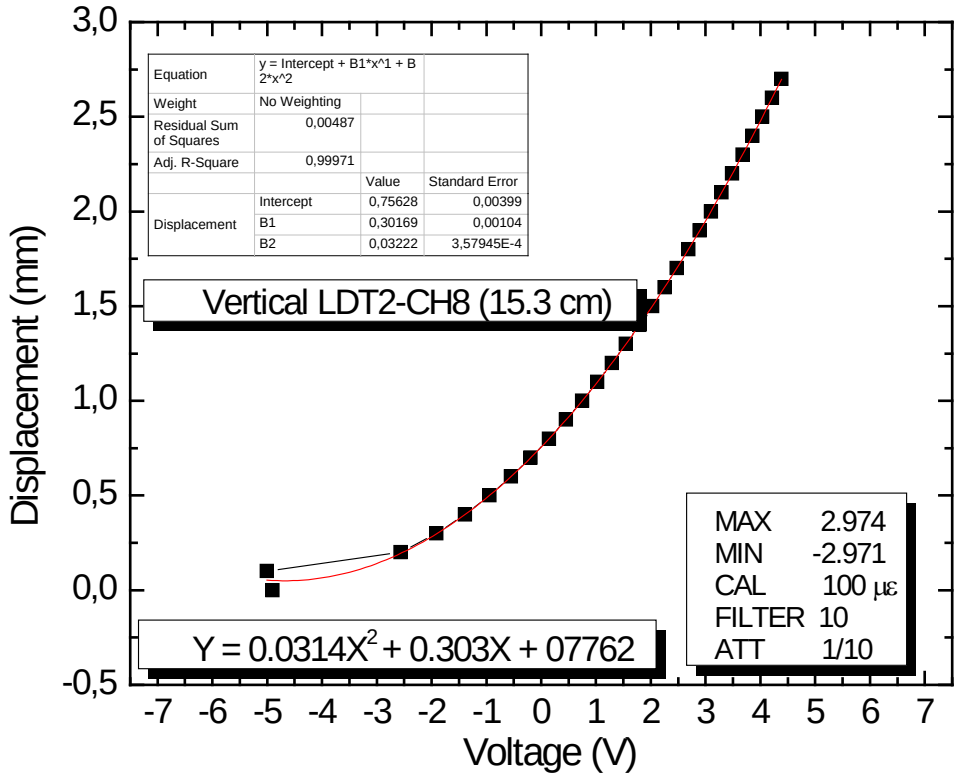

Figure 2-9b: Calibration curve for vertical LDT-2

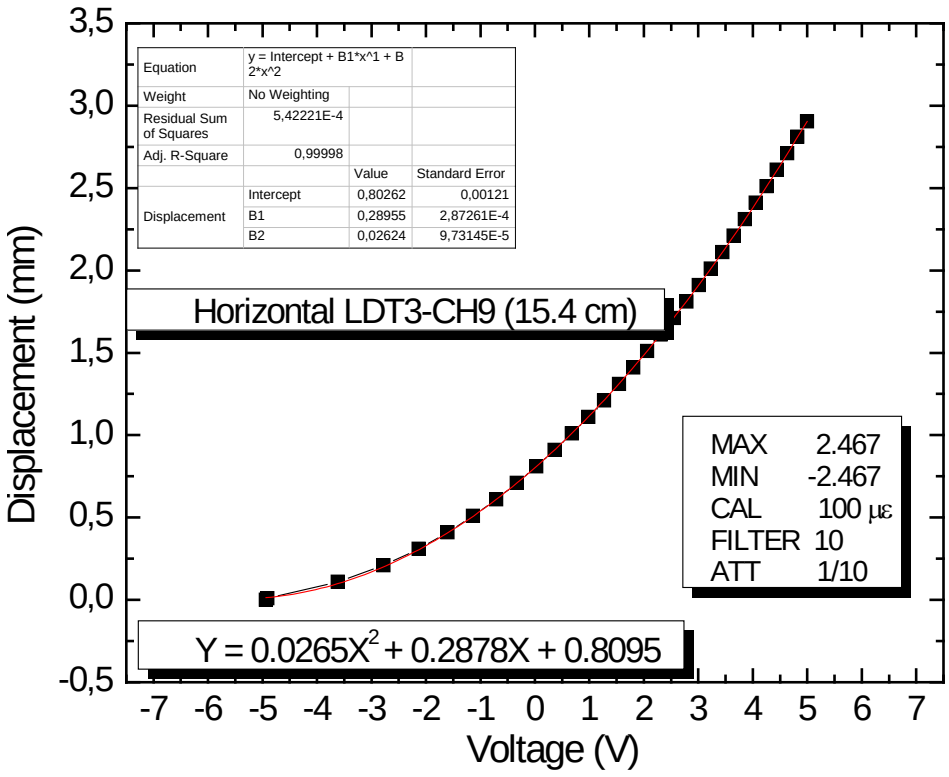

Figure 2-9c: Calibration curve for horizontal LDT-3

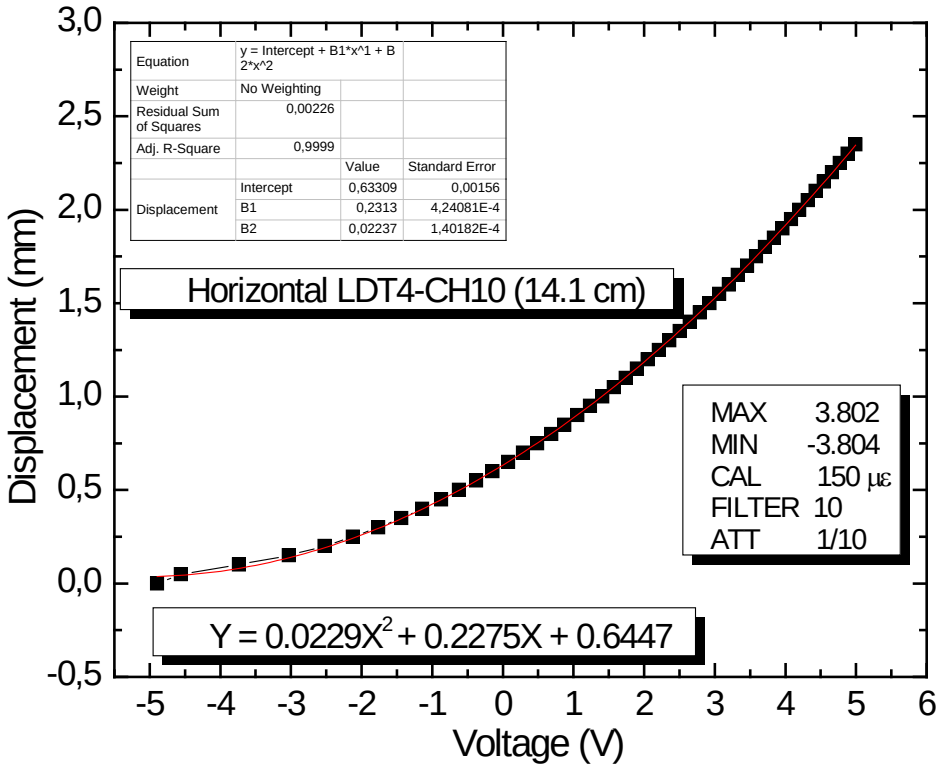

Figure 2-9d: Calibration curve for horizontal LDT-4

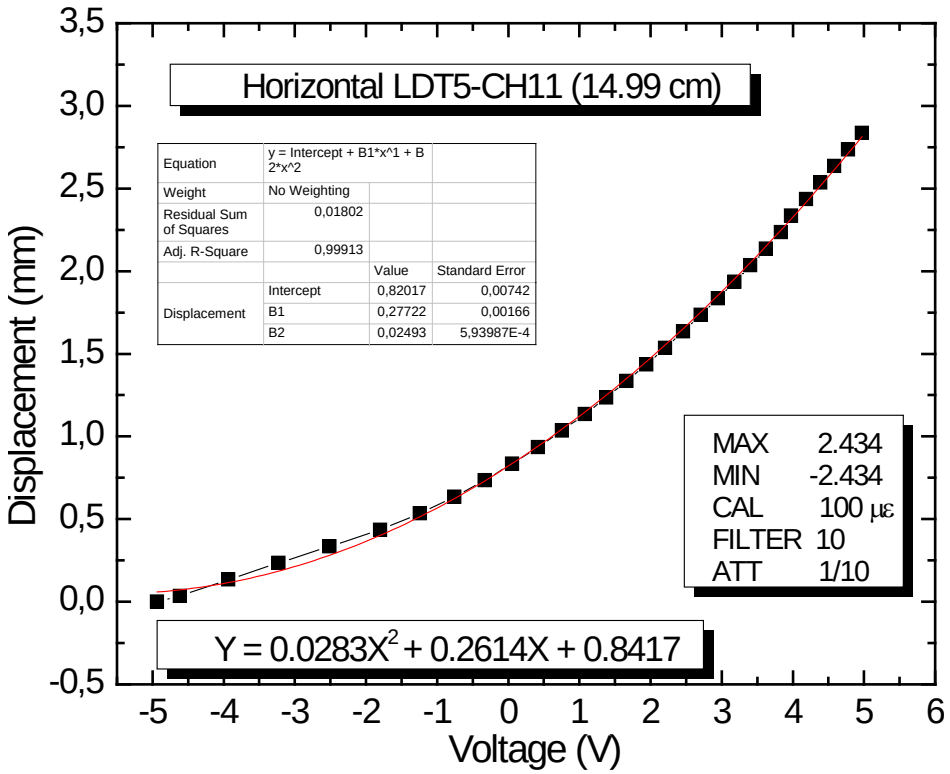

Figure 2-9e: Calibration curve for horizontal LDT-5

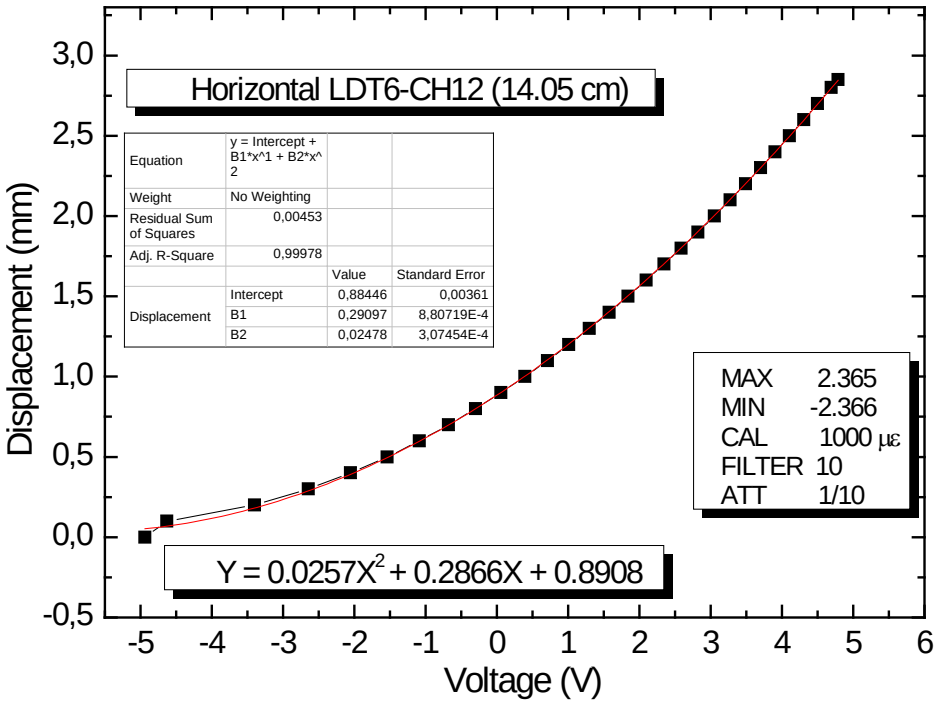

Figure 2-9f: Calibration curve for horizontal LDT-6

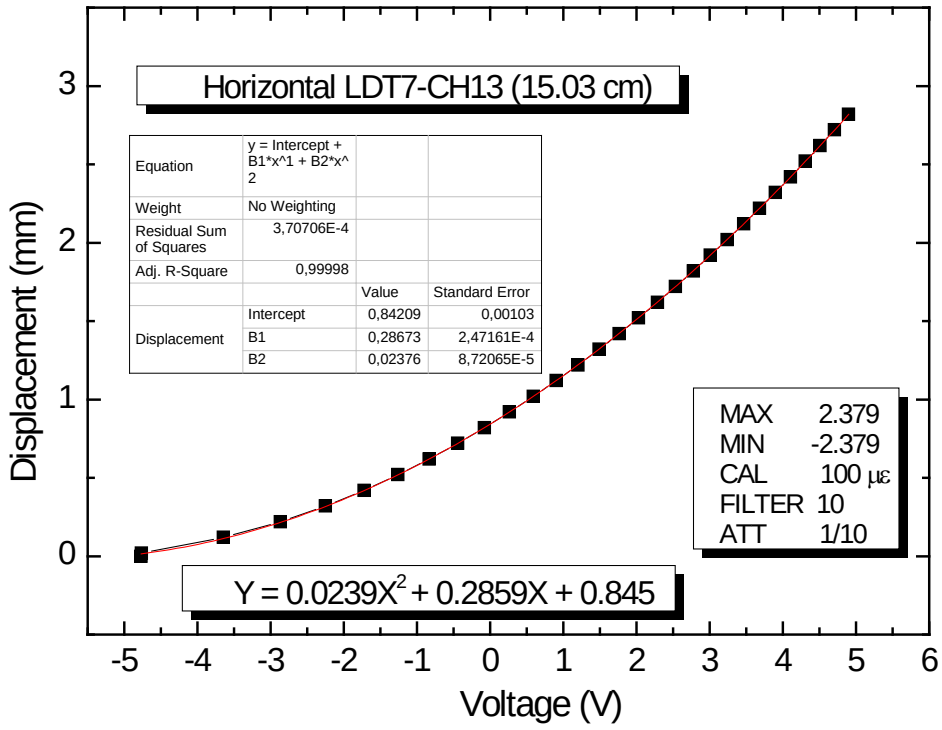

Figure 2-9g: Calibration curve for horizontal LDT-7

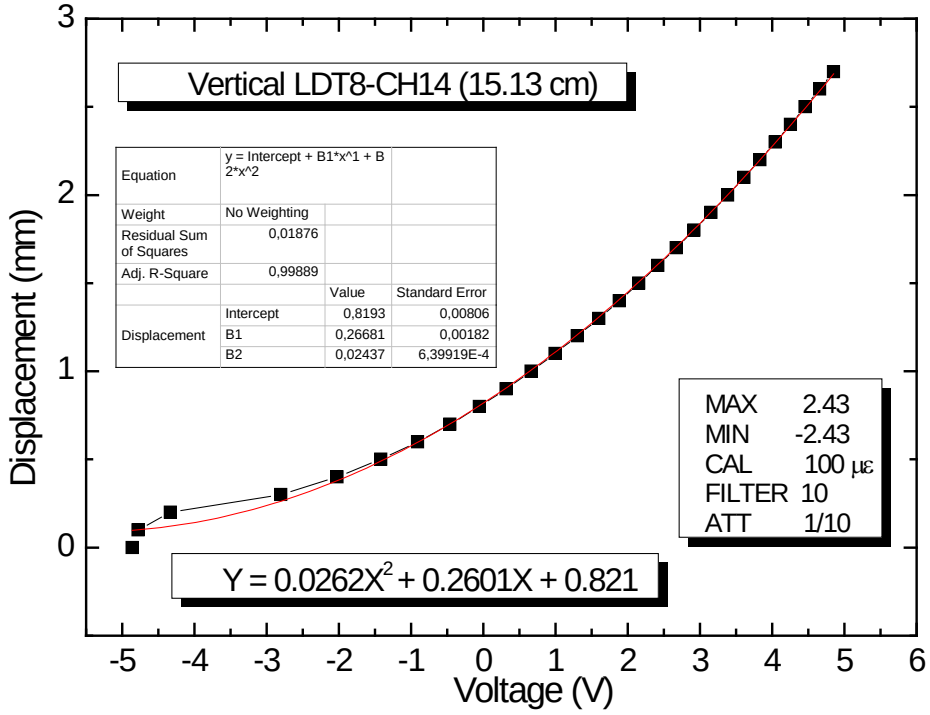

Figure 2-9h: Calibration curve for vertical LDT-8

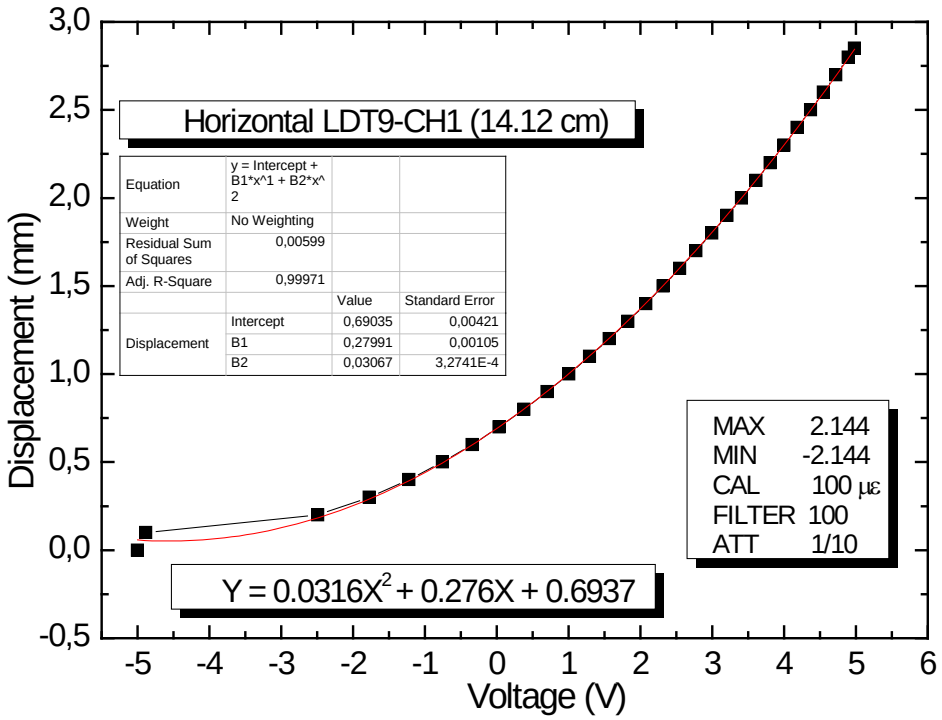

Figure 2-9i: Calibration curve for horizontal LDT-9

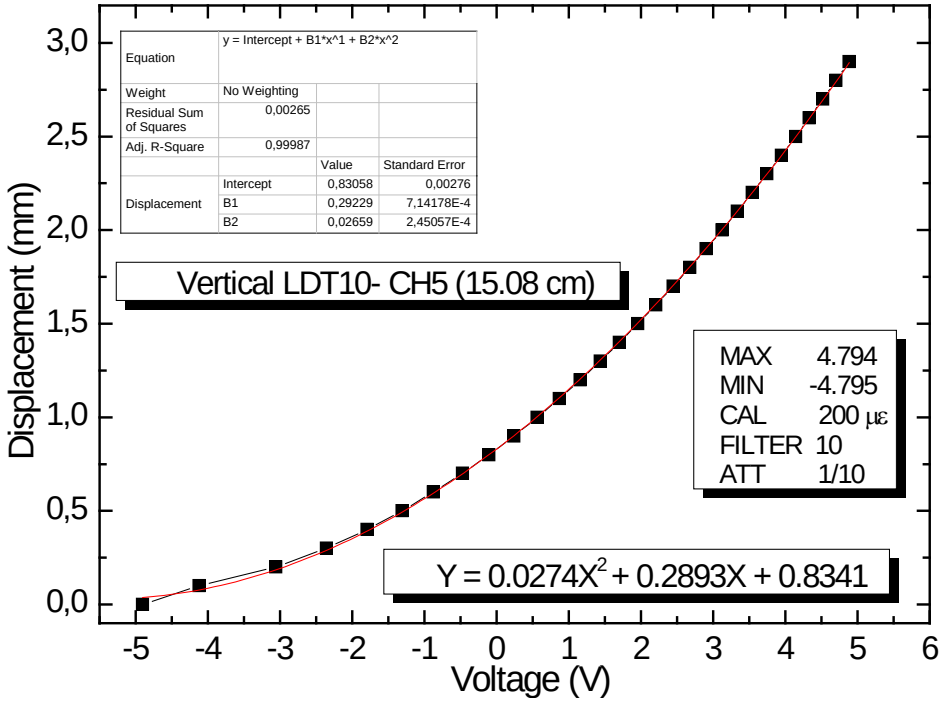

Figure 2-9j: Calibration curve for vertical LDT-10

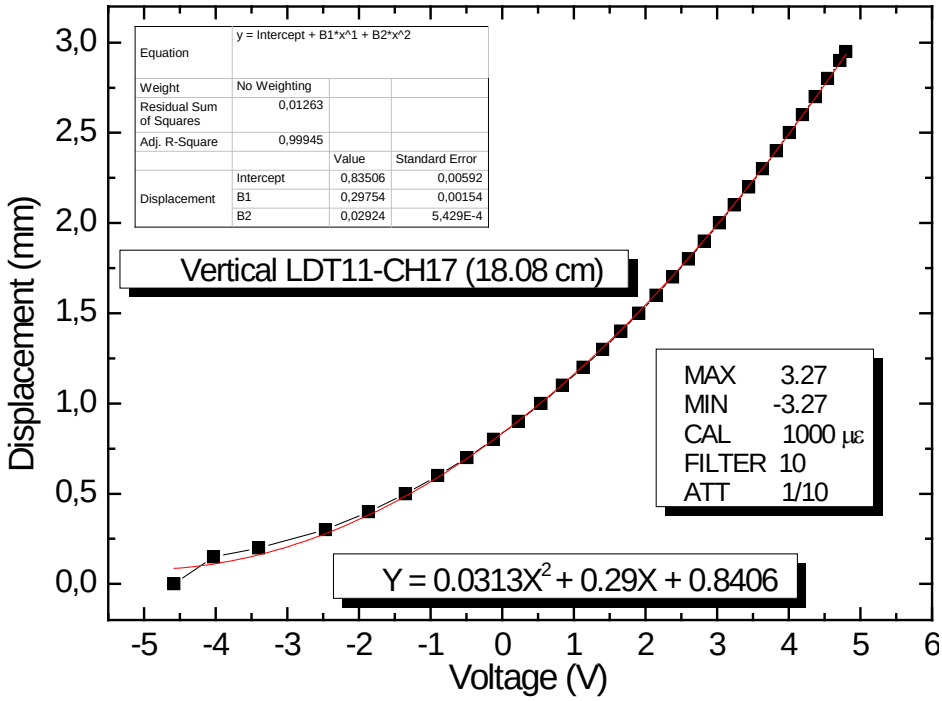

Figure 2-9k: Calibration curve for vertical LDT-11

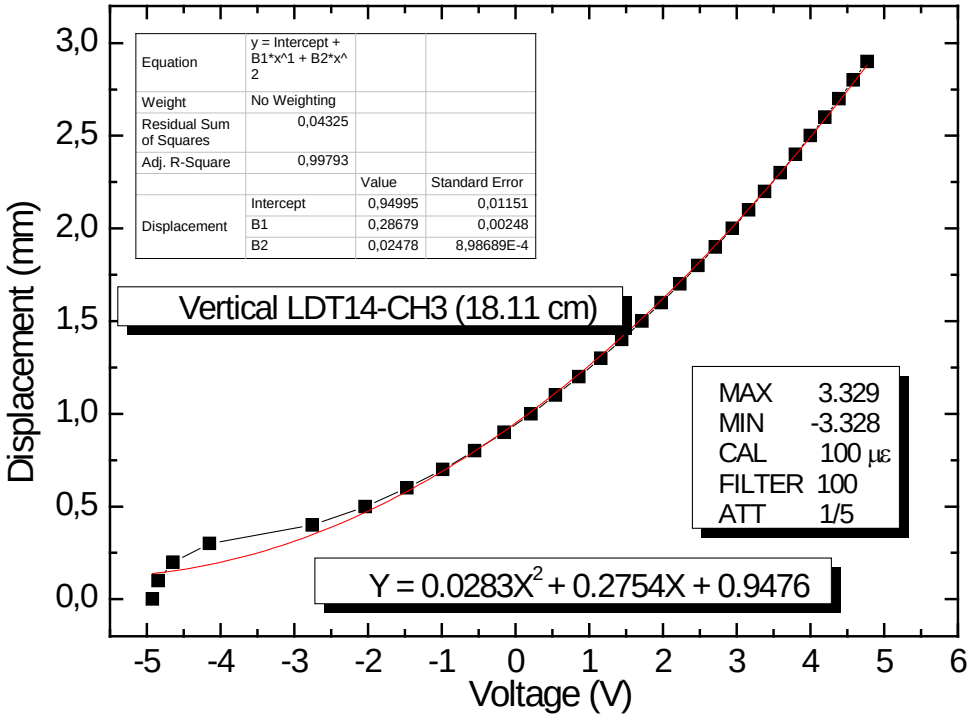

Figure 2-9l: Calibration curve for vertical LDT-14

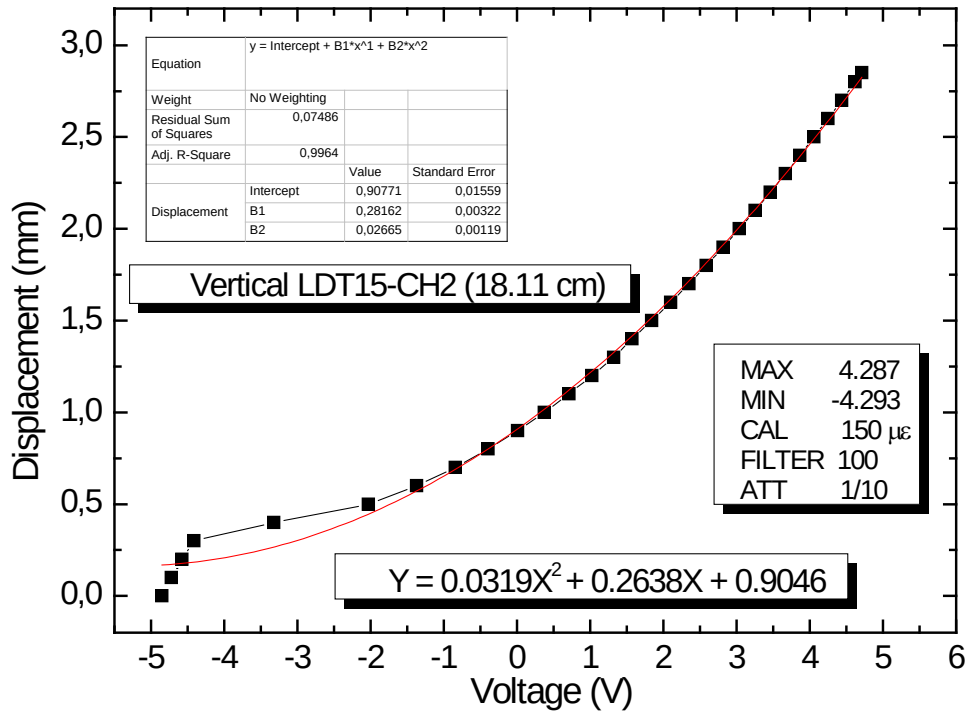

Figure 2-9m: Calibration curve for vertical LDT-15

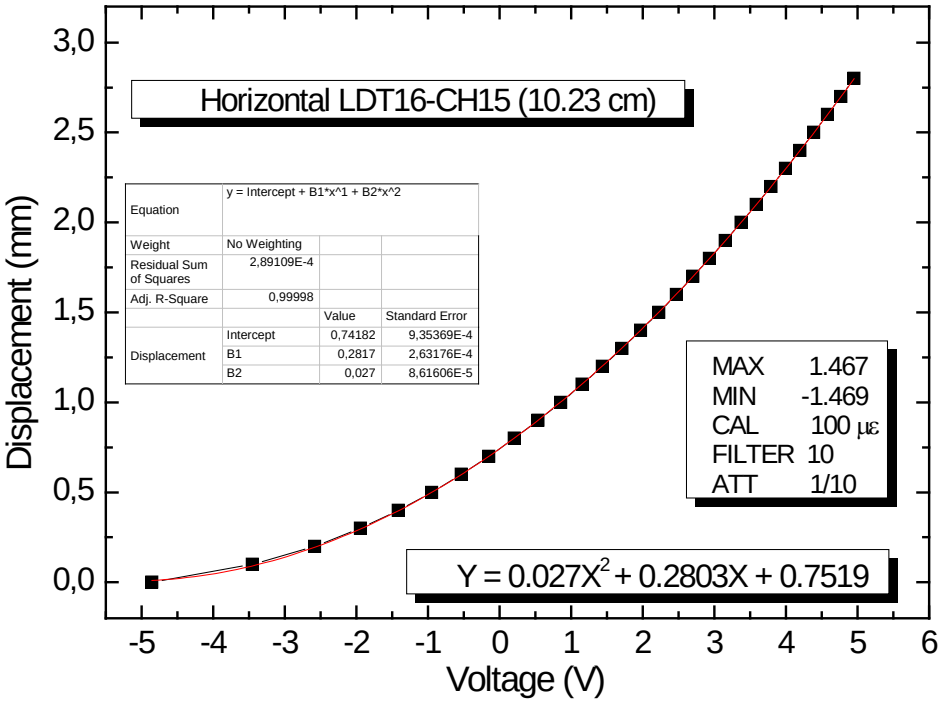

Figure 2-9n: Calibration curve for horizontal LDT-16

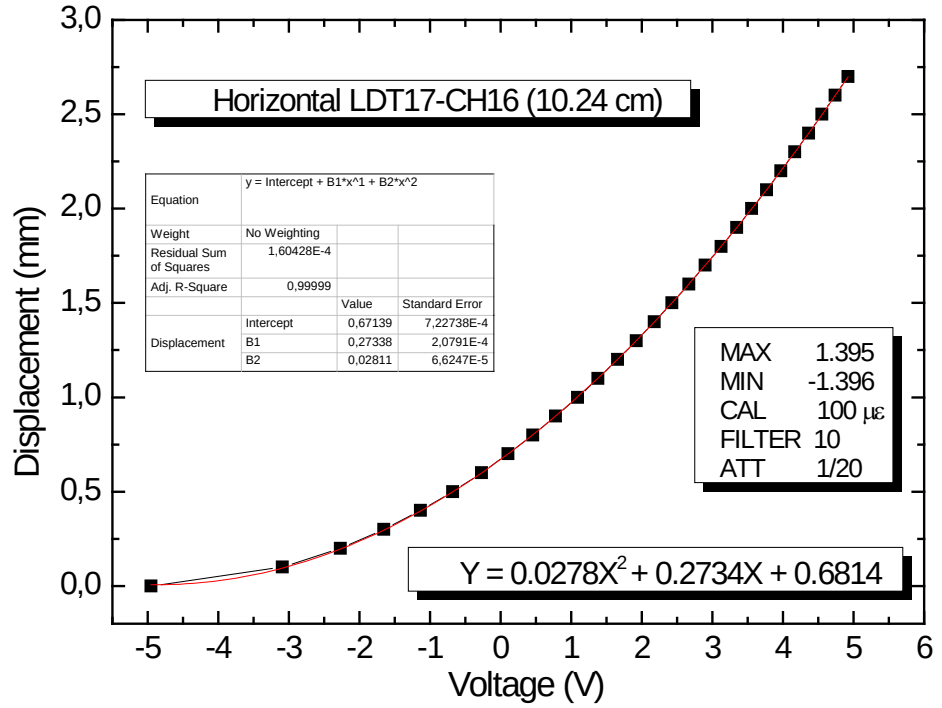

Figure 2-9o: Calibration curve for horizontal LDT-17

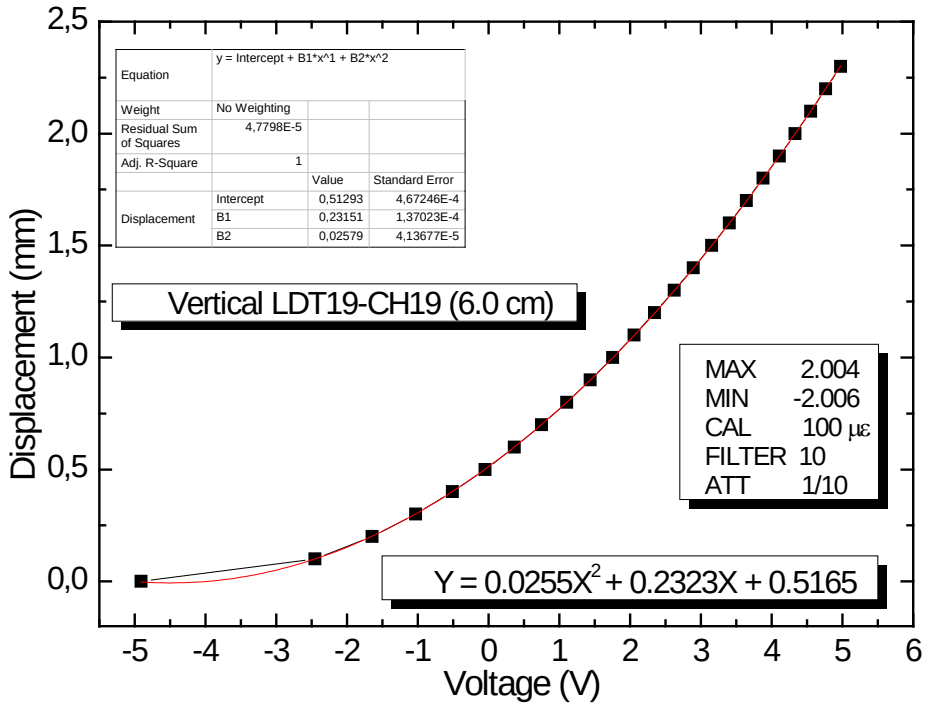

Figure 2-9p: Calibration curve for vertical LDT-19

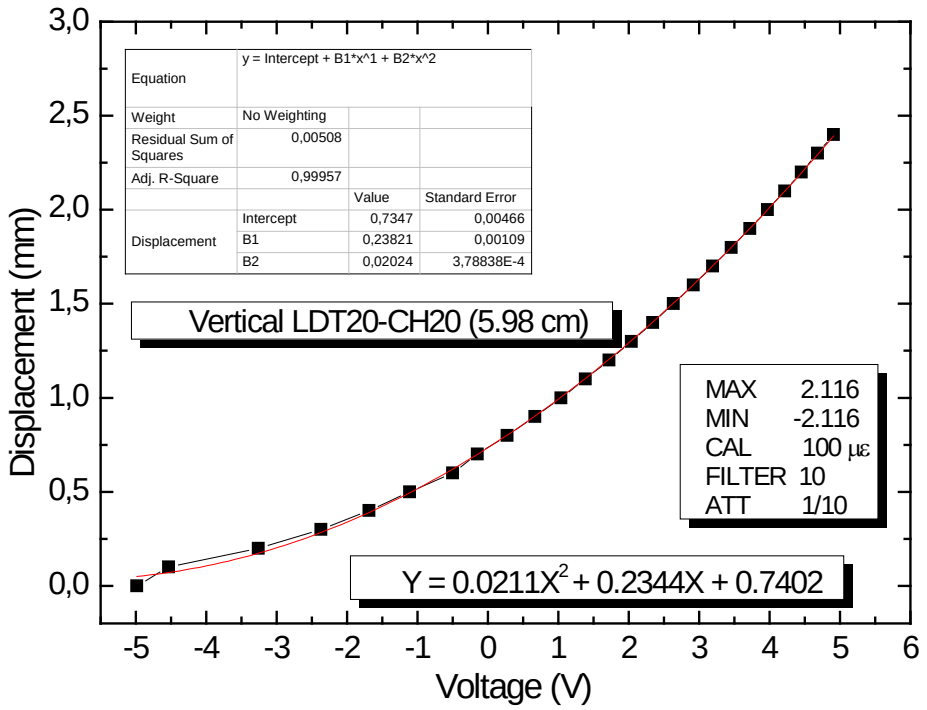

Figure 2-9q: Calibration curve for vertical LDT-20

Figure 2-10: Picture of HCDPT

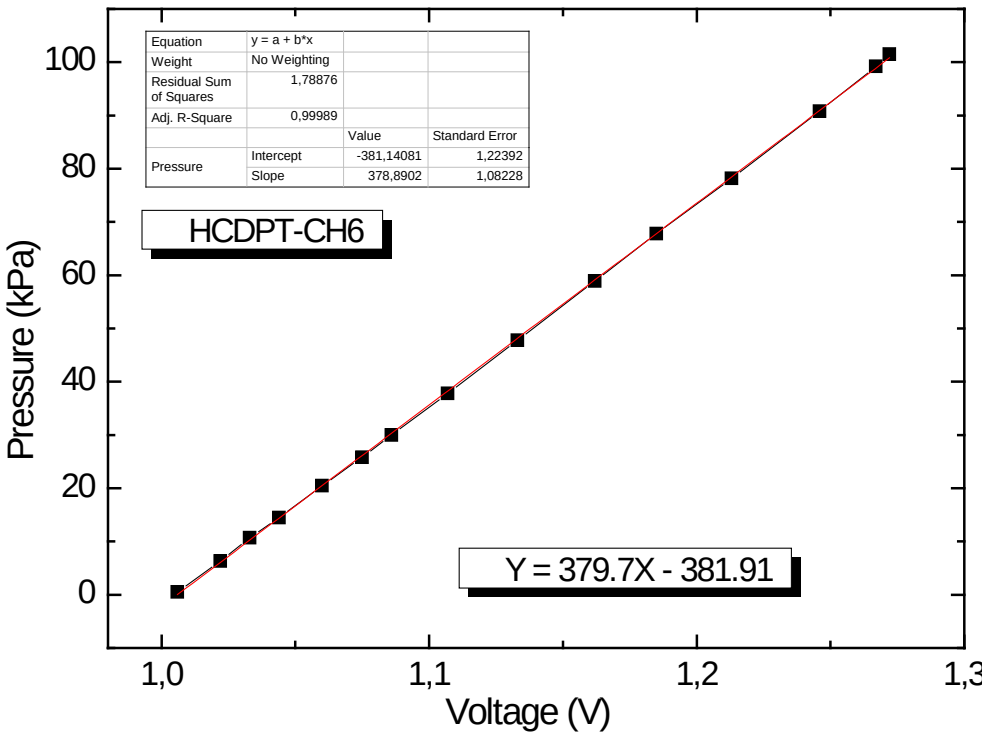

Figure 2-11: Calibration of HCDPT

Figure 2-12: Picture of LVDT

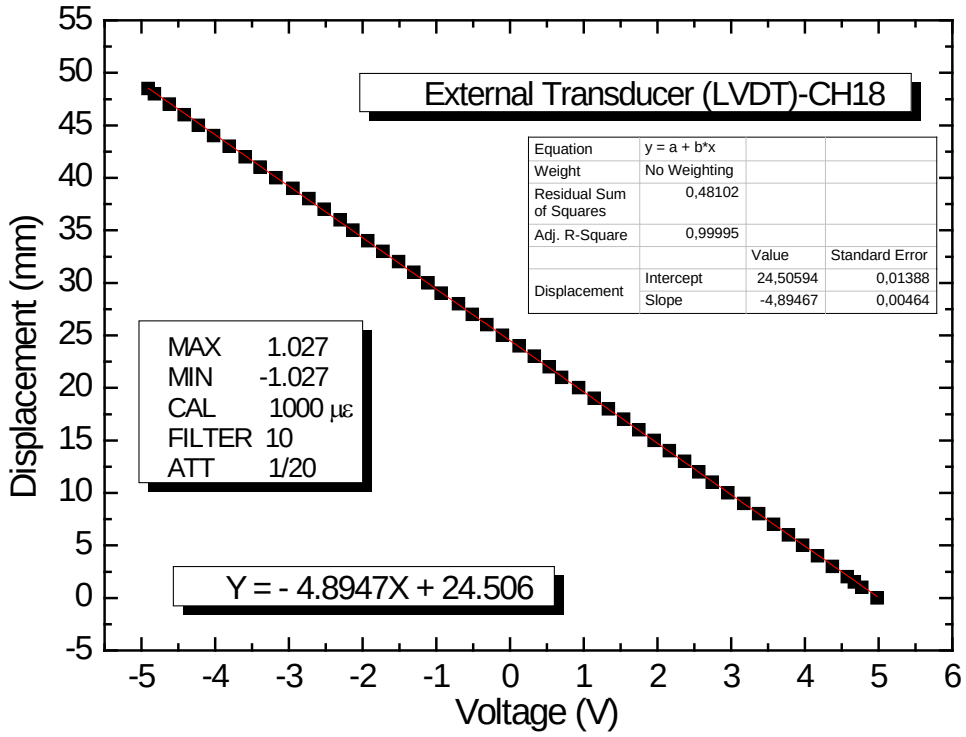

Figure 2-13: Calibration of LVDT

Figure 2-14: Picture of Earth Pressure Cell

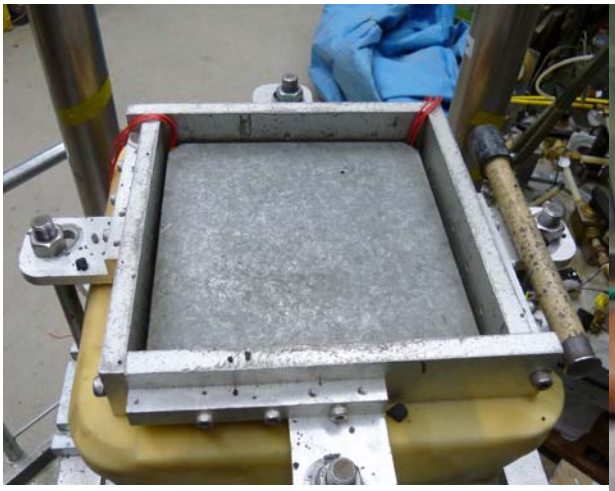

Figure 2-15: Compaction rod, plate, mold and specimen after compaction

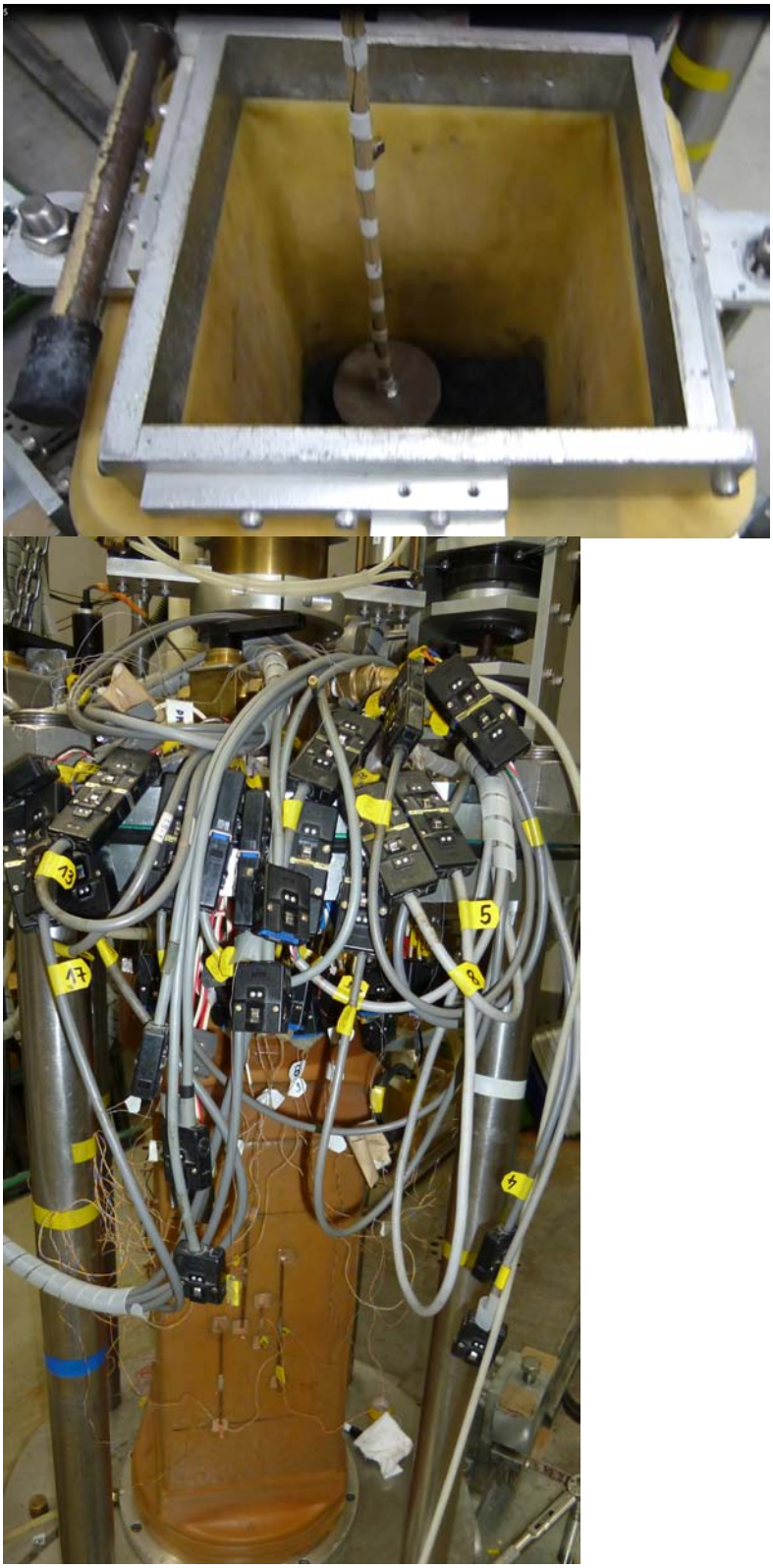

Figure 2-16: During and after compaction and preparing specimen

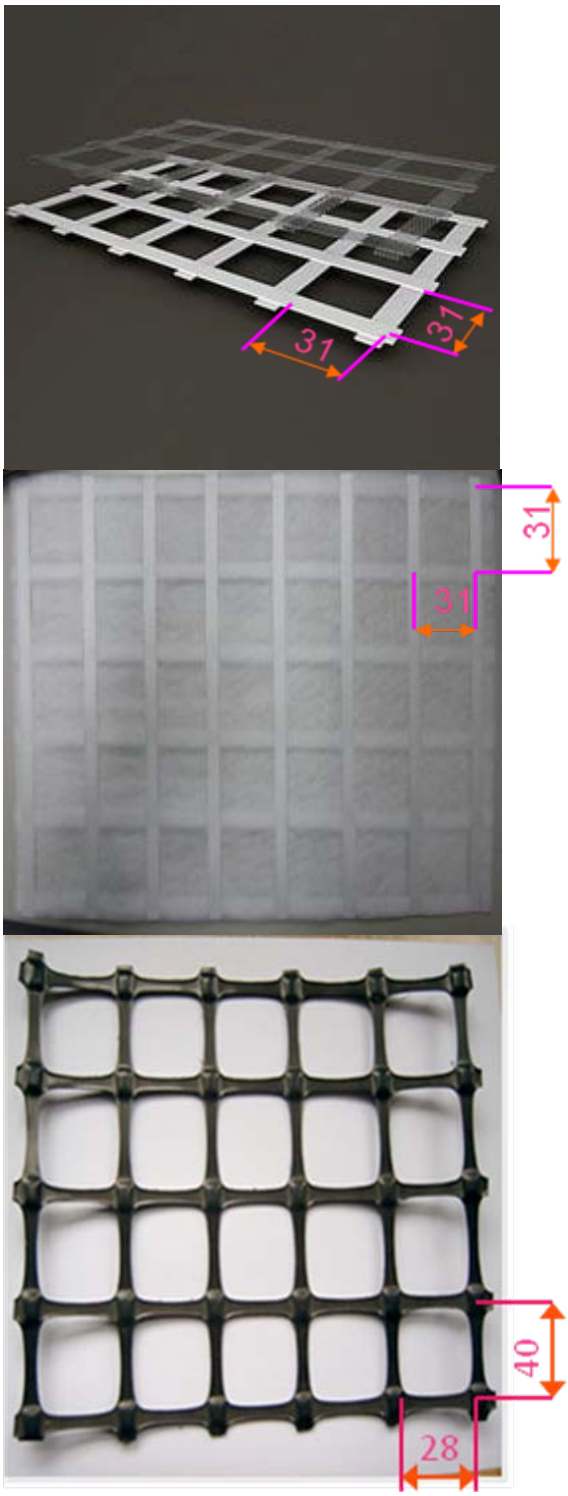

Figure 2-17: a) Polypropylen geogrid; b) Combi-polypropylen geogrid; c) Polypropylen geogrid (Japanese manufacturer) (unit in mm)

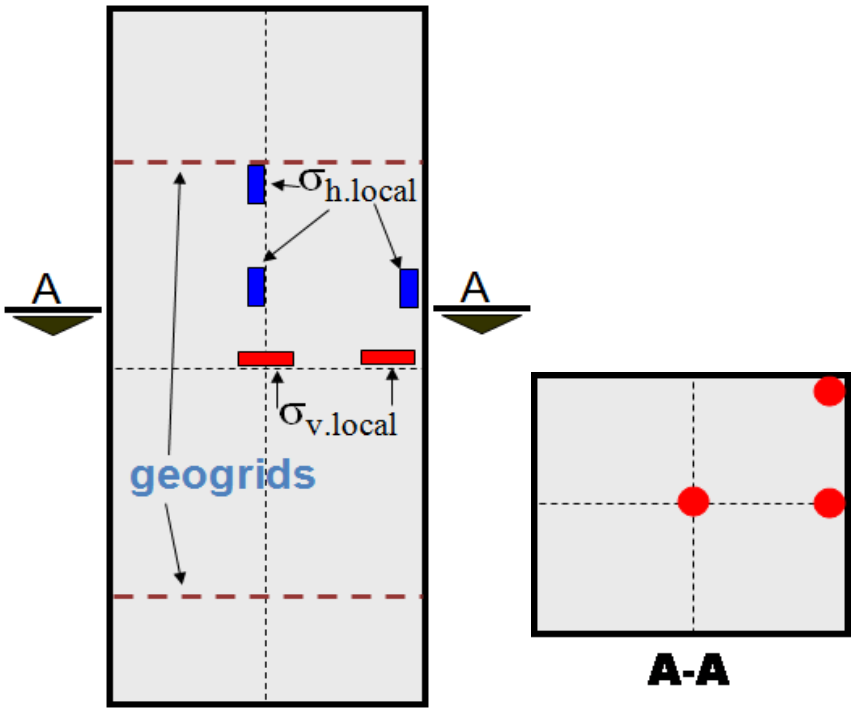

Figure 2-18: Schematic figure of position of earth pressure cell

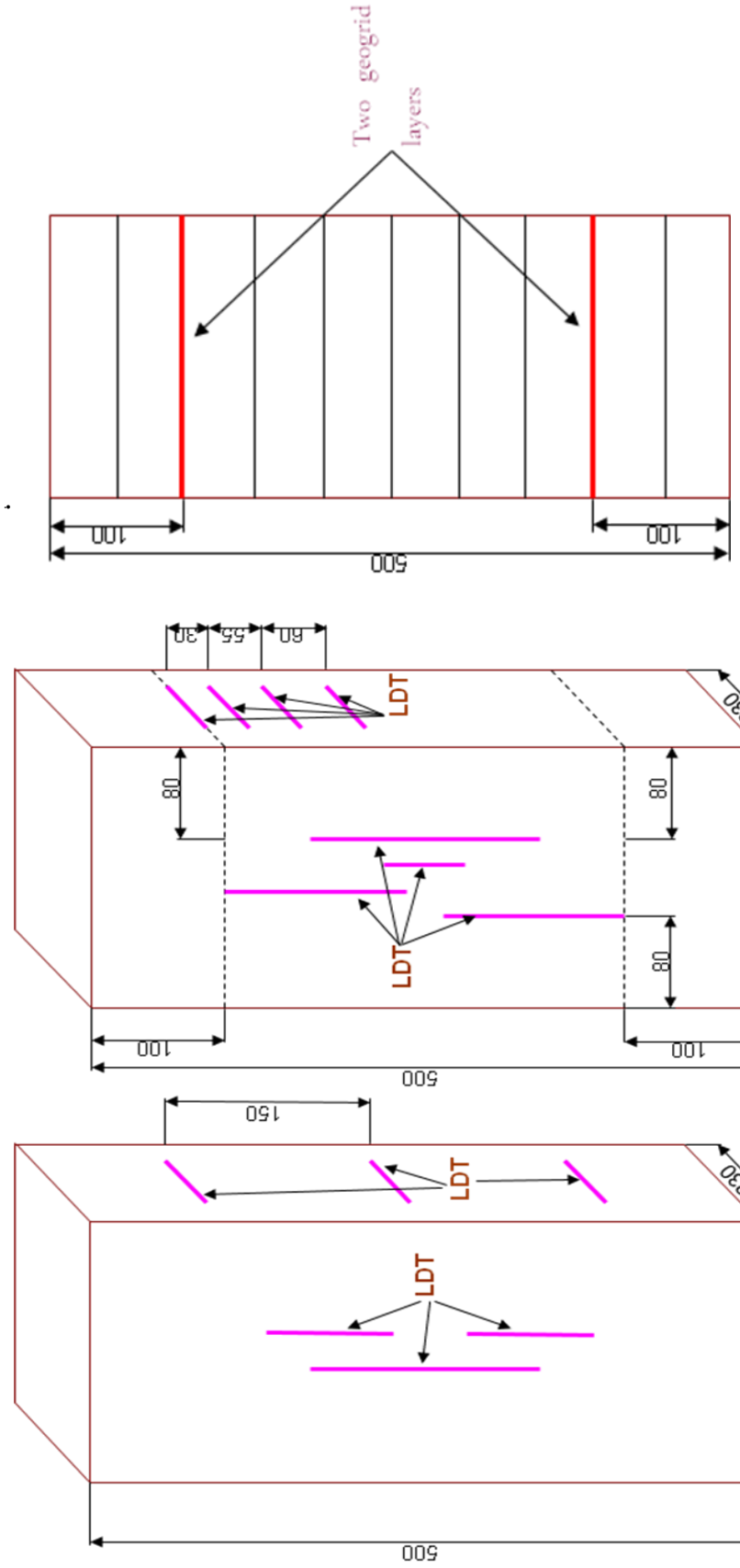

Figure 2-19: Positioning of LDTs in case of a) unreinforced and b) reinforced tests (unit in mm)

Figure 2-20: The compaction was perfomed in 10 layers with a compacted thickness of about 5 cm per layer (unit in mm)

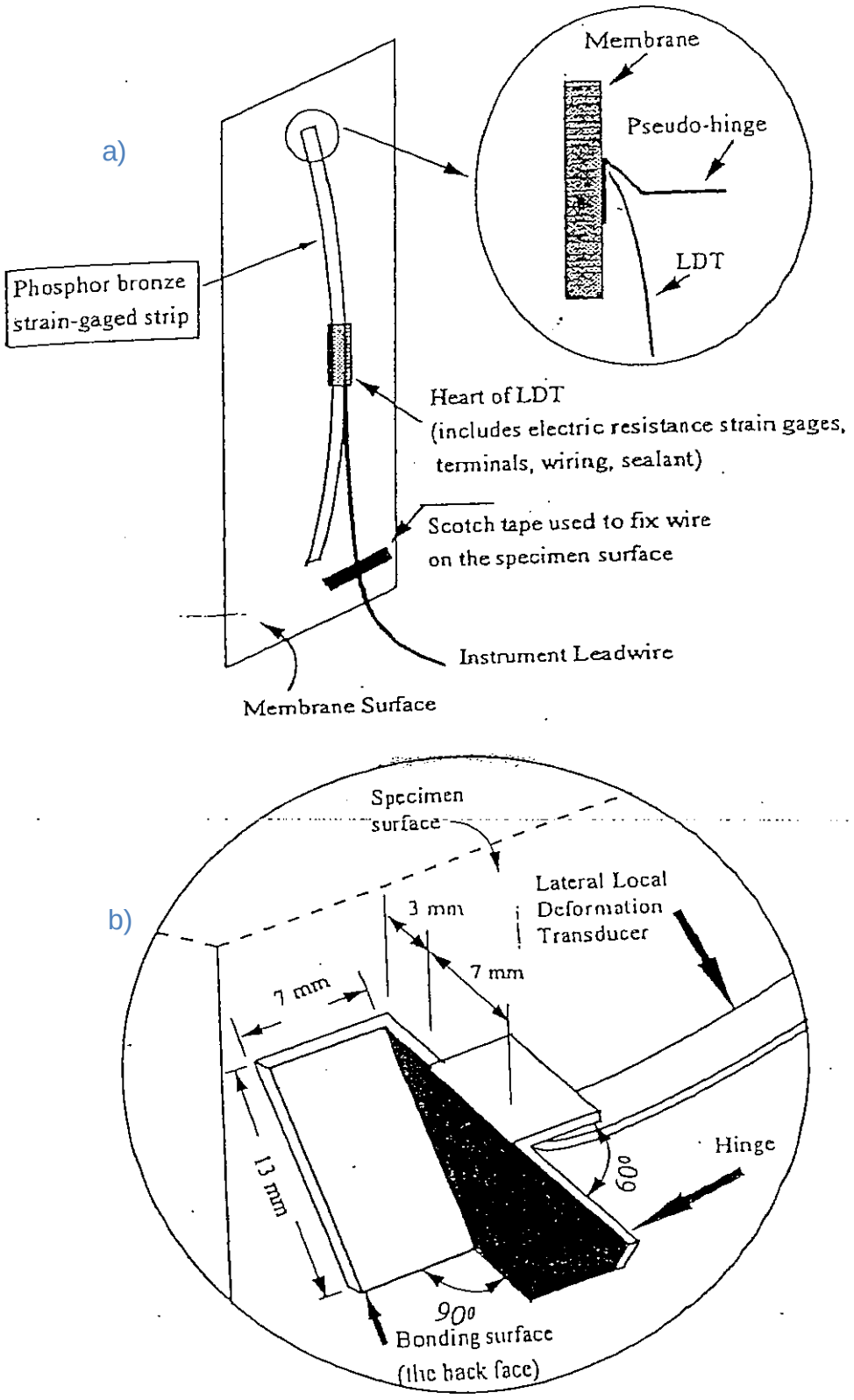

Figure 2-21: Detail of setting of Local Deformation Transducers, LDTs (Hoque et al., 1996)

a) Vertical LDTs

b) Horizontal LDTs

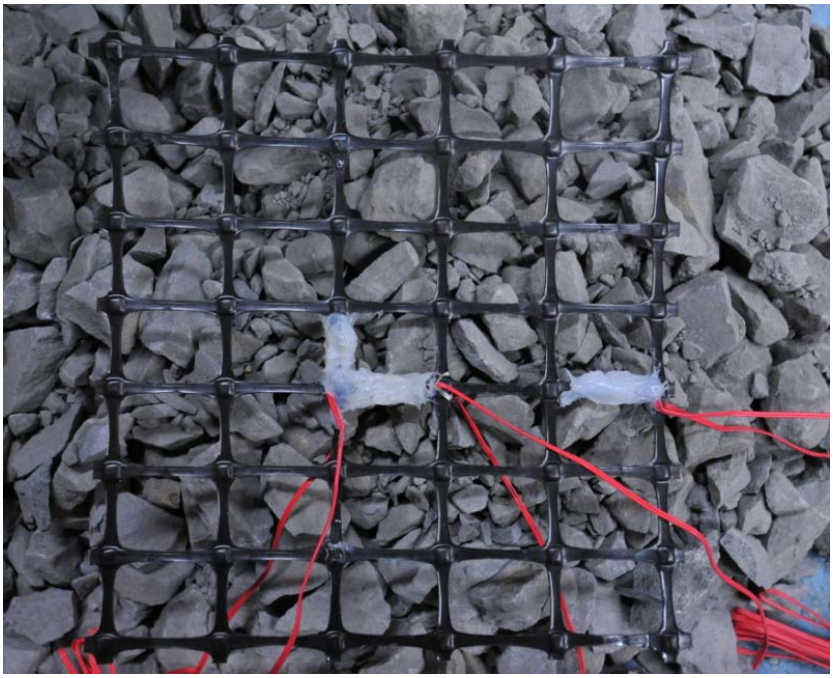

Figure 2-22: Detail of position of strain gauges attached on geogrid

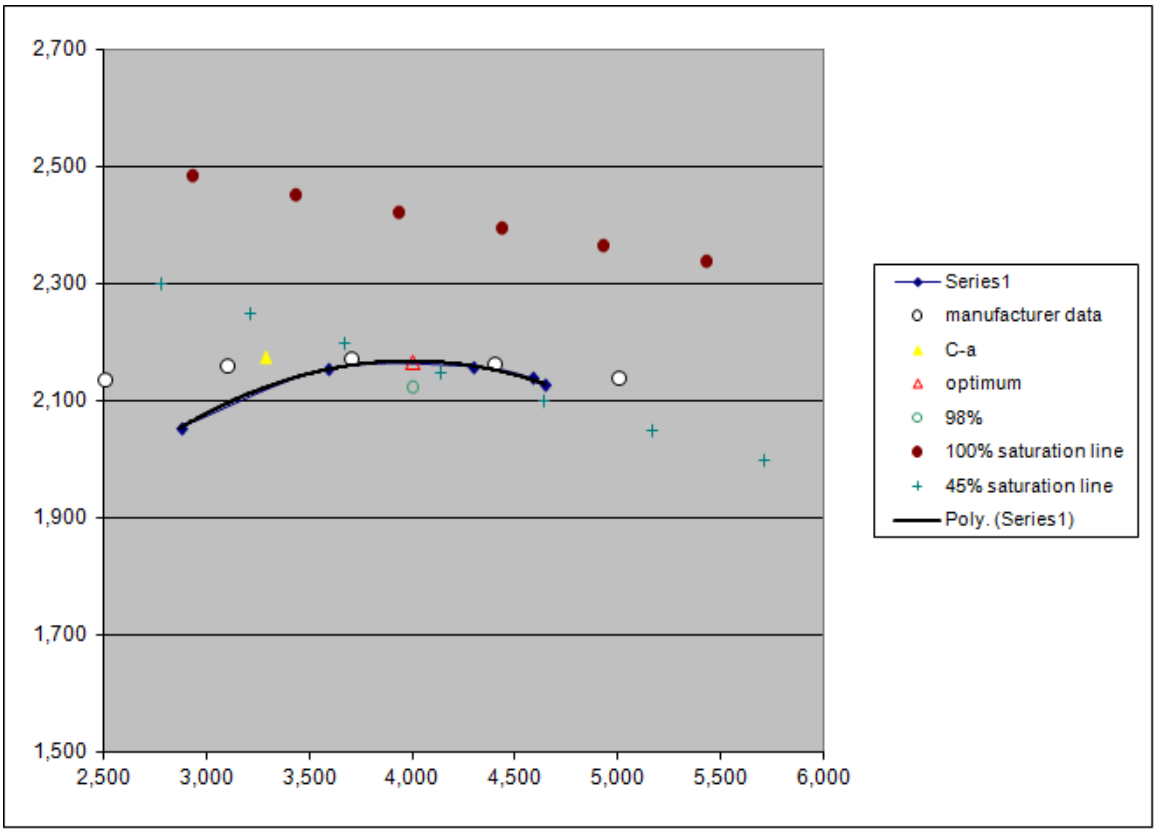

Figure 2-23: Compaction curve of Tochigi gravel

Table 2-1: Test conditions

Test name	**Reinforcement**	**σ'_3 (kPa)**	**ρ_d (g/cm^3)**	**e**	**ω (%)**
IIS-0E	Unreinf	25	2.053	0.310	3.73
IIS-0G	Unreinf	150	2.096	0.280	2.41
IIS-0H	Unreinf	70	2.098	0.280	2.78
IIS-2D	PP Geogrid	150	2.089	0.280	3.81
IIS-2E	PP Geogrid	25	2.066	0.300	2.53
IIS-JG	Japanese PP Geogrid	25	2.085	0.290	2.27
IIS-COM-C	Combi-grid	25	2.112	0.270	2.25
IIS-COM-D	Combi-grid	150	2.080	0.290	2.11
IIS-COM-E	Combi-grid	70	2.069	0.300	2.15

CHAPTER 3

CALCULATION OF ELASTIC DEFORMATION AND PARAMETERS

3.1 Introduction

When the deformation is fully recoverable with a negligible damping value and the deformation is essentially independent of strain rate, it is considered as the elastic deformation. Many existing data of the deformation properties from cyclic loading tests on soils, soft rocks and hard rocks (intact cores) reported in the literature show that the behavior at strains less than about 0.001% is nearly elastic.

Over some region of stress level, the strain responds linearly. If the stress is reduced and the strain decreases reversibly and upon the removal of stress, the strain goes to zero, the material is said to be behaving elastically. On the other hand, plastic deformation is accompanied with slippage between particles and re-arrangement and crushing of particles. In the framework of elasto-plasticity, strain increments of soil are composed of elastic and plastic components. Elastic strain may be or may not be very small when compared to the total strains. In many cases, the elastic strain is one of the essential components to describe the mechanical behavior of geomaterial. Hence their measurement is very important for many engineering problems.

Mindlin (1949) obtained an elastic solution for two elastic spheres subject to both normal and tangential contact forces. He found that, without slippage at the contact point, the circumferential shear stress is infinite. Therefore, slippage must occur even for the smallest tangential force. Hence, it is difficult to measure any essentially elastic property by using the conventional laboratory test apparatus unless very small strains and stresses can be measured. It has been found that elastic strain can be isolated in static loading tests by applying small cyclic strains with axial strain amplitudes less than 0.001% (Hardin, 1978).

Tatsuoka and Shibuya (1992) reported a large amount of data which showed that the deformation of geomaterials measured at strains smaller than about 0.001% in monotonic loading tests is essentially strain rate-independent and recoverable (i.e., elastic), and the initial stiffness values at very small strains determined by static monotonic loading tests are essentially the same with those determined by the corresponding static cyclic loading tests and dynamic loading tests.

For the triaxial test, we often use and study into Young's modulus E and Poisson's ratio ν. The ratio between the stress and the strain is called the Young's modulus. In addition to the elongating (or contracting) in the direction of axially applied stress, the sample simultaneously narrows (or widens) in the lateral direction. The change in the dimension in the direction perpendicular to the direction of the applied stress develops from an interaction of the strain components that are generated within the material as a consequence of being stressed, principally, as a volume converse strain. Poisson's ratio which is defined as the ratio of change on dimension in the lateral direction to the change in length is needed to describe this behavior.

However the deformation of most soil are not isotropic even at very small strains in many respects. Most geotechnical problems are 3-D, for which elasto-plastic analyses are getting popular. For these analyses both plasticity and elasticity should be properly dealt with and anisotropy must be properly accounted for. Anisotropy of soil can be classified into the following two categories:

a. Inherent anisotropy, due to the initial anisotropic macro or micro fabric, which persists even when the stress state changes, which lead to anisotropic stiffness at isotropic states.

b. Stress-state induced anisotropy, developed by current anisotropic stress states, which may be modified easily by stress changes. However, stress changes that cause large strains can in turn alter the soil fabric, and hence modified its inherent anisotropy; so the two aspects can be difficult to separate.

In this study, we use the following formula for elastic modulus:

$$\frac{E_{eq}}{f(e)} = E_0\left(\frac{\sigma}{\sigma_0}\right)^m \qquad (3\text{-}1)$$

Where E_{eq} is the equivalent elastic Young's modulus at current stress state σ and E_0 is the reference Young's modulus when $\sigma = \sigma_0 = 1$ kPa.

The above relationship was examined in the case of isotropic consolidation with monotonic/large cyclic loading as well as anisotropic stress condition during shearing. The elastic moduli obtained during isotropic consolidation were assumed to be undamaged properties.

Equation 3-1 becomes more invalid as the stress σ= 0 (Jiang, 1998). On the other hand, Eq. (3-1) becomes more relevant as the stress σ increases. As the pressure level dealt with in the present study are relatively high, errors resulting from the approximate nature of this equation can be considered to be negligible.

From Eq. (3-1) we can obtain elastic vertical strain:

$$\varepsilon_v = \int_{\sigma_1}^{\sigma_v} \frac{d\sigma_v}{E_{eqv}} \qquad (3\text{-}2)$$

From Eq. (3-1) and (3-2), we obtain:

$$\varepsilon_v = \frac{(\sigma_0)^m}{E_0 f(e)} \int_{\sigma_1}^{\sigma_v} \frac{d\sigma_v}{(\sigma_v)^m} \qquad (3\text{-}3)$$

$$= \frac{(\sigma_0)^m}{E_0 f(e)(1-m)}[(\sigma_v)^{1-m} - (\sigma_1)^{1-m}]$$

Where σ_1 is the initial stress.

3.2 Theoretical background on elasticity

For a linear elastic body, strain ε_{ij} defined from a stress-free condition are related uniquely to stresses σ_{kl}; that means that, strains are stress-path independent. A general anisotropic body has 36 independent elastic constants. Such linear elasticity is called "hyper-elasticity", where there exists a potential energy function, such as:

$$W = \int \sigma_{ij} d\varepsilon_{ij} = \int \sigma_{ij} C_{ijkl} d\sigma_{kl} \qquad (3\text{-}4)$$

Then the compliance matrix C_{ijkl} becomes symmetric (i.e., $C_{ijkl}=C_{klij}$). This is because:

$$\varepsilon_{kl} = \partial W / \partial \sigma_{kl} \text{ ; and } C_{ijkl} = \partial \varepsilon_{kl} / \partial \sigma_{ij} = \partial^2 W / \partial \sigma_{ij} \partial \sigma_{kl} \qquad (3\text{-}5)$$

$$\varepsilon_{ij} = \partial W / \partial \sigma_{ij} \text{ ; and } C_{klij} = \partial \varepsilon_{ij} / \partial \sigma_{kl} = \partial^2 W / \partial \sigma_{kl} \partial \sigma_{ij} \qquad (3\text{-}6)$$

Such kind of material is called a hyper-elastic body, which has 21 independent elastic constants, because of symmetry of the compliance matrix. On the other hand, when strain increments $d\varepsilon_{ij}$ are uniquely related to stress increments $d\sigma_{kl}$; that is, $d\varepsilon_{ij}$ are independent of the path of stress increment, $d\varepsilon_{ij}$ are directly related to $d\sigma_{kl}$ as,

$$d\varepsilon_{ij} = C_{ijkl} d\sigma_{kl} \qquad (3\text{-}7)$$

This kind of material is defined as hypo-elastic body. Generally, C_{ijkl} is a function of current stress state σ_{kl}. When strains ε_{ij} which were obtained by integrating $d\varepsilon_{ij}$, becomes stress path-independent, the hypo-elastic body is an ordinary elastic body. In general, the strains ε_{ij} are stress path-dependent for most soils. In this case, $d\varepsilon_{ij} = C_{ijkl} \bullet d\sigma_{kl}$ is not a total differential, which means that $d\varepsilon_{ij}$ can be integrated partially only when a stress path is defined. This is the case with granular materials such as sands and gravels. Yasin (1998) reported that the deformation characteristics of Toyoura sand are stress-path dependent based on test results under plane strain condition. Anh Dan (1999) also investigated to some extent with dense gravel under triaxial condition and reported the same tendency of stress path-dependent behavior.

In general, most of the granular materials being as natural or man-made deposits, or compacted vertically exhibit cross-anisotropic deformation properties, which are symmetric about the vertical axis. Cross-anisotropy requires only six elastic parameters for the characterization. The incremental relationship between stress and strain (Hooke's law) is:

$$\begin{bmatrix} \delta\varepsilon_{xx} \\ \delta\varepsilon_{yy} \\ \delta\varepsilon_{zz} \\ \delta\gamma_{yz} \\ \delta\gamma_{zx} \\ \delta\gamma_{xy} \end{bmatrix} = \begin{bmatrix} \frac{1}{E_h} & \frac{-\nu_{hh}}{E_h} & \frac{-\nu_{vh}}{E_v} & 0 & 0 & 0 \\ \frac{-\nu_{hh}}{E_h} & \frac{1}{E_h} & \frac{-\nu_{vh}}{E_v} & 0 & 0 & 0 \\ \frac{-\nu_{hv}}{E_h} & \frac{-\nu_{hv}}{E_h} & \frac{1}{E_v} & 0 & 0 & 0 \\ 0 & 0 & 0 & \frac{1}{G_{vh}} & 0 & 0 \\ 0 & 0 & 0 & 0 & \frac{1}{G_{vh}} & 0 \\ 0 & 0 & 0 & 0 & 0 & \frac{2(1+\nu_{hh})}{E_h} \end{bmatrix} \begin{bmatrix} \delta\sigma_{xx} \\ \delta\sigma_{yy} \\ \delta\sigma_{zz} \\ \delta\tau_{yz} \\ \delta\tau_{zx} \\ \delta\tau_{xy} \end{bmatrix} \qquad (3\text{-}8)$$

where, the stress and strain increments are referred to rectangular Cartesian axes x (≡h), y(≡v), and z(≡v) with the x, y axis in horizontal plane and z axis as vertical axis; E_v, E_h are the elastic Young's moduli in vertical and horizontal directions respectively; ν_{vh}, ν_{hh}, ν_{hv} are Poisson's ratios; G_{vh} is the shear modulus.

When we can assume that for small stress increments $\Delta\sigma_{ij}$, the potential strain energy increment $\Delta W = \int \Delta\sigma_{ij}\, d(\Delta\varepsilon_{ij})$ exists, then the compliance matrix becomes symmetric, which requires $\nu_{vh}/E_v = \nu_{hv}/E_h$. At this point the compliance matrix becomes with only five individual elements to be determined. The ever existence of function ΔW, however, is not verified yet for a given soil element under a given stress-strain condition. Furthermore, even if the function ΔW exists for a given small stress increments $\Delta\sigma_{ij}$, this does not mean that a potential strain energy function $\Delta W'$ also exists for larger stress increments $\Delta\sigma'_{ij}$.

The quasi-elastic Young's moduli of an un-cemented soil, E_v and E_h , within the quasi-elastic threshold strain, depend on the following factors:

- the soil state, expressed by a combination of the current void ratio (e) and the current stress state (σ_{ij}).
- the soil fabric reflecting the depositional environment and post-depositional processes such as aging, cementation etc.

Considering all these aspects, for a 3-D analysis of the stress -strain characteristics of soils, it requires a clear understanding of the inherent and induced anisotropy of deposited materials. In the case of convensional triaxial compression or extension, the stress conditions are identical in horizontal plane, with vertical axis of symmetry. In addition, if

the specimens are prepared by air-pluviation or vertically compacted then the properties in two horizontal directions can be assumed isotropic. Then the Eq.(3-8) becomes well simplified as;

$$\begin{bmatrix} \delta\varepsilon_h \\ \delta\varepsilon_v \end{bmatrix} = \begin{bmatrix} (1-\nu_{hh})/E_h & -\nu_{vh}/E_v \\ -2\nu_{hv}/E_h & 1/E_v \end{bmatrix} \begin{bmatrix} \delta\sigma_h \\ \delta\sigma_v \end{bmatrix} \qquad (3\text{-}9)$$

The matrix in Eq. (3-9) is not symmetric, because the stress and strain vectors used in Eq. (3-9) have not been chosen in such a way that the product of the corresponding stress and strain increments give the input work increment.

In this study, elastic parameters could be obtained by static triaxial cyclic loading tests with a single amplitude principal strain $(d\varepsilon)_{SA}$ less than the threshold value of about 0.001% (Hoque, 1996; Jiang, 1996). The quasi-elastic properties evaluated within this small strain range are almost free from the influence of stress-strain histories that are small enough to maintain the initial fabric, type of loading (monotonic or cyclic), wave-form during cyclic loading and rate of shearing (dynamic or static) (Tatsuoka and Kohata, 1995). For small vertical cyclic tests at constant lateral stress (i.e., $\Delta\sigma_h = 0$ and $\Delta\sigma_v \neq 0$);

$$E_v = \Delta\sigma_v / \Delta\varepsilon_v, \quad \text{and} \quad \nu_{vh} = -\Delta\varepsilon_h / \Delta\varepsilon_v \qquad (3\text{-}10)$$

where, E_v is the equivalent quasi-elastic Young's modulus in vertical. The parameters E_v and ν_{vh} (Eq. 3-10) could be evaluated from small vertical cyclic loadings. In this thesis, only the elastic Young's modulus in vertical direction and it's stress state dependency is reported.

3.3 Effect of specimen density

The linear elastic stiffness of gravel increases systematically as the dry density increases or as the void ratio decreases. Several alternative expressions exist which link the value of

E_{max} or G_{max} to void ratio, e. One example is the normalizing function f(e) proposed by Hardin and Richart (1963) for clean granular materials tested under similar conditions:

$$f(e) = (2.17 - e)^2 / (1 + e) \tag{3-11}$$

Jamiolkowski et al. (1991) also suggested that another expression is applicable to a wider range of geomaterial:

$$f_1(e) = 1/(e^{1/3}) \tag{3-12}$$

Note that $f_1(e)$ varies more steeply with void ratio than f(e) until e around 0.8, and f(e) tends to be zero when e>2. In the present study, E_{max} values have been normalized by diving this function f(e) in order to exclude the effects of variations in the void ratio among different specimens.

3.4 Calculation of void ratio

If the soil is assumed to be composed of solid grains and voids occupied by air or water,

void ratio

$$e = \frac{V_V}{V_S} = \frac{V - V_S}{V_S} \tag{3-13}$$

where, V_v, V_s and V are volume of voids, volume of solids and total volume respectively.

$$\Rightarrow \frac{V}{V_S} = 1 + e$$

$$de = \frac{dV_V}{V_S};$$

As the soil particles itself is assumed to be incompressible,

$$dV_S = 0$$

$$dV_V = dV;$$

$$de = \frac{dV}{V_S} = \frac{(1+e)dV}{V};$$

$$de = (1+e)\ d\varepsilon_{vol}$$

$$\frac{de}{(1+e)} = d\varepsilon_{vol}$$

The integrated form will implies that,

$$\int_{e_o}^{e} \frac{de}{(1+e)} = \int_{0}^{\varepsilon_{vol}} d\varepsilon_{vol}$$

$$\Rightarrow \varepsilon_{vol} = \ln\left(\frac{1+e_o}{1+e}\right)$$

$$\Rightarrow e = \frac{(1+e_o)}{\exp(\varepsilon_{vol})} - 1 \qquad (3\text{-}14)$$

3.5 Calculation of stresses

Vertical stresses were calculated from the voltage response of the inner load cell. The instantaneous load Q could be evaluated by using the calibration factor of the load cell and the voltage increment. This load is the deviator load, i.e., the load excess in vertical direction to horizontal direction. The deviator stress q can be obtained using this deviator load and the cross sectional area of the specimen.

$$q = Q/A \qquad (3\text{-}15)$$

where, A is the corresponding cross sectional area.

From the operating principle given in Eq. 2.1,

$$q = \sigma_v - \sigma_h \qquad (3\text{-}16)$$

Instantaneous horizontal stress σ_h was obtained from the response of either direct pressure transducer or high capacity differential pressure transducer (HCDPT). The vertical stress was then obtained from,

$$\sigma_v = \sigma_h + Q/A \qquad (3\text{-}17)$$

3.6 Calculation of strains

In this study, the strains were determined by conventional way; that is, the incremental strain was evaluated by taking the initial dimension as the reference. For example, suppose, the instantaneous length was L, and the initial length of that portion was L_O, the strain, by conventional method is given as,

$$\varepsilon = (L - L_O) / L_O \qquad (3\text{-}18)$$

According to soil mechanics sign convention, compression is taken as positive.

Then, the compressive strain is given as,

$$\varepsilon = - (L - L_O) / L_O \quad = (L_O - L) / L_O \qquad (3\text{-}19)$$

Strains were evaluated considering the deformation in axial direction and lateral direction. The axial strains were calculated locally by the results from LDTs and externally by the results from LVDT. The average of the individual strain values of the vertical LDTs were used. Horizontal strains were evaluated by the results from lateral LDTs and then averaged.

Volumetric strain was evaluated as,

$$\varepsilon_{vol} = \varepsilon_a + 2\varepsilon_h \qquad (3\text{-}20)$$

where ε_a and ε_h are axial (vertical) strain and lateral (horizontal) strain, respectively.

References

Anh Dan, L. Q. (1998): "Effects of stress history and time on the deformation of gravelly soil", Master thesis, University of Tokyo, Japan.

Balakrishnaiyer, K., Koseki, J., Modoni, G., Anh Dan,.L.Q & Tatsuoka, F. (1998): "Deformation Characeristics at Small Strain Levels of Dense Gravel", Italy: Proc. of the 2nd Int. Symp. on Hard Soils-Soft Rocks, Balkema, Vol. I, pp. 423-430.

Balakrishnaiyer, K. (1997): "Deformation characteristics of gravelly soils with stress state dependency", Master thesis, University of Tokyo, Japan.

Bellotti, R., Jamiolkowski, M., Lo Presti, D.C.F. and O'Neill, D.A. (1996): "Anisotropy of small strain stiffness in Ticino sand", Geotechnique 46-1, pp. 115-131.

Flora, A., Jiang, G.L., Kohata, Y., & Tatsuoka, F. (1994): "Small strain behavior of a gravel along some triaxial stress paths", Proc. Int. Symp. on Pre-failure Deformation Characteristics of Geomaterials, IS-Hokkaido, Balkema, Vol.I, pp.279-285.

Hoque, E., (1996): "Elastic Deformation of Sands in Triaxial Tests", Doctoral thesis, University of Tokyo.

Jiang, G.L., (1996): "Small Strain Behavior and Deformation and Strength Characteristics of Gravel by Large Triaxial Tests", Doctoral thesis, University of Tokyo (In Japanese).

Jamiolkowski, M., Lerouell, S., and Lo Presti, D.C.F. (1991): "Design parameters from theory to practice", Theme lecture, Geo-Coast 1991, Yokohama, pp.917-977.

Mindlin, R.D (1949): "Compliance of elastic bodies in contact", Journal of applied mechanics, ASME, Vol 71, pp. A-259-268.

Kohata, Y., Tatsuoka, F., Dong, J., Teachvorasinskun, S. and Mizumoto, K. (1994): "Stress States Affecting Elastic Deformation Moduli of Geomaterials", Proc., IS-Hokkaido, Balkema, Vol. I, pp. 3-11.

Tatsuoka, F., Uchimura, T., Hayano, K., Di Benedetto, H., Koseki, J. and Siddiquee, M.S.A., (1999): "Time-dependent deformation characteristics of stiff geomaterials in

engineering practice", Keynote lecture for 2nd IS on Pre-failure deformation characteristics of Geomaterials, Torino-Italy.

Tatsuoka, F. and Shibuya, S. (1992): "Deformation characteristics of soils and rocks from field and laboratory tests", Keynote lecture, 9th Asian Regional Conf. on SMFE, Bangkok, Vol.2, 1992, pp.101-170.

CHAPTER 4

TEST RESULTS AND DISCUSSIONS

4.1 General behavior

The peak or maximum deviator stress generally corresponds to the failure state of the specimen. A positive sign of the volumetric strain represents specimen dilation; whereas, a negative sign represents specimen contraction. **Figures 4-1** through **4-4** show the stress-strain curves of tests with unreinforced and reinforced specimens compacted to 95% proctor density for three types of geogrid at some different confining pressures. The specimen was initially loaded to a prescribed load level, then unloaded. As typically shown in **Fig. 4-5** almost recoverable deformation occured when the specimen was unloaded. The recoverable deformation was due to the elastic deformation of individual grains. The deviator stress increased with the axial strain until failure occurred. The increase of the peak strength due to the reinforcements can be seen clearly. The tests using PP geogrid show the highest peak strength in both low and high confining pressures.

This is in accordance with the volumetric strains calculated from the horizontal and vertical strains. **Figure 4-6** shows the comparison in volumetric strain between the unreinforced and reinforced (Japanese geogrid) test at 25 kPa. The reinforced test experienced negative dilatancy at larger axial strain than the unreforced test. The unreinforced specimens initially contracted during unloading-reloading stage and started dilating at axial strains of about 0.3%. At the beginning of shearing stage, the unreinforced test almost reached the positive dilatancy side. During that, as shown in **Fig. 4-7**, the PP geogrid did not show any dilative behavior at confining pressure of 150 kPa. This is consistent with the above description regarding in **Fig. 4-4**. In addition, **Fig. 4-7** shows that even at very low confining pressure of 25 kPa, the reinforced test using PP geogrid started dilating at vertical strain as nearly as the vertical strain at which the unreinforced test at 150 kPa started dilating. The geogrid can increase the peak strength

of the specimen without making the specimen expand laterally during its mobilisation. That means the geogrid can increase the stiffness of the specimen.

For the reinforced tests using Combi-grid, the increase of stiffness due to reinforcement can be seen clearly in **Fig. 4-8** at three different confining pressures. However, the stiffness of both unreinforced and reinforced specimens at 150 kPa seems to be similar to each other for vertical strains up to 1%. This can be explained by considering that at high confining pressure, as in case of large depths, the effect of reinforcement is not as significant as in case of low confining pressure.

Figure 4-9 shows that most of the tests start showing dilative behavior when they finish the unloading-reloading stage except the unreinforced test IIS-0E. All the tests indicate almost pure compaction at the beginning of the tests. This can be explained by considering that as the beginning of the test, the vertical loading was still small enough which did not make the specimen extend in lateral direction. As soon as the specimen starts to extend radially, the geogrids are increasingly mobilised, which subsequently leads to an increase of the stiffness and the peak strength. The mobilisation of tension in the geogrid is accompanied with reduced dilatancy effects.

Effects of reinforcement on shear strength of gravel are examined by a means of Mohr-Coulomb shear strength parameters (i.e., internal friction angle and cohesion). The shear strength parameters are determined from the s-t diagram at failure and Mohr circles as shown in **Fig. 4-10** and **4-11**. As can be seen, in unreinforced tests, the cohesion and internal friction angle are less than that of in case of reinforced tests. It has shown that the geogrids lead to an increase of the shear strength and the stiffness of the soil. This is consistent for all stress levels tested.

Furthermore, as indicated in **Fig. 4-12**, the lateral strains measured by horizontal LDTs in reinforced tests are reduced significantly compared to the results of the unreinforced tests at confining pressure of 25 and 70 kPa. Similar observations were made by Ziegler et al. (2008), who carried out unreinforced and reinforced triaxial tests too. They observed clearly a reduction of deformations due to the reinforcement. In the present tests, on the other hand, at the high confining pressure of 150kPa, there was almost no effect of reinforcement. It indicates that the influence of the reinforcement at low confining

pressures, as it is the case at small depths, is significantly higher than at higher confining pressures.

The stiffness of the specimens derived from small cyclic loading is shown in **Fig. 4-13**. As can be seen, the reinforcement does not largely affect the small strain stiffness of the specimens under both low or high confining pressures except the reinforced test using Japanese geogrid (IIS-JG). This test showed the highest stiffness even at very low confining pressure of 25 kPa.

The strain distribution within the geogrid reinforcement obtained from strain gauge measurements is given in the **Fig. 4-14** for the geogrid located near the top cap. Geogrid strains increase from the free end towards the center, where the maximum strain is mobilised, and correspond directly with the tensile force acting in the geogrid. Maximum strains are mobilised in the center of the specimen, because at this point the maximum anchorage length of 11.5 cm is provided in each direction. Similar results were obtained by Ketchart & Wu (2001) for the strain distribution in the geogrid, from laboratory testing as well as from calculations. There are two principle mechanisms in corresponding for transferring the load from the soil into the geogrid as described in Ziegler & Timmers (2004). One mechanism is the constant induction of shear forces from the soil into the geogrid, which depends on friction on the grid's surface. The other mechanism is the accumulation of soil particles in front of the cross members, leading to a jump of the drag force in the longitudinal member when induced from the cross member through the junction.

The development of reinforcement strains $\varepsilon_{reinf.}$ with increasing vertical compression of the specimen is given in **Fig. 4-15**. It is plotted for the strains measured at the center of the cross section, i.e. the maximum reinforcement strain. The strain gauge distribution inside the Japanese geogrid shows the highest performance than the other results.

4.2 Mechanical model

The mechanical model shown in **Fig. 4-16** has been derived from the large triaxial test results on the reinforced gravel. Due to the vertical loading the specimen expands radially. As mentioned above, this is accompanied by the mobilization of the geogrids, leads to which the deformation is reduced and the peak strength is increased.

With progressive deformation of the specimen, the confining forces of the geogrids increase. As a simplifed assumption, this can be considered as an equivalent, additional confining pressure $\Delta\sigma_3$ acting homogeneously over the whole height of the specimen (**Fig. 4-16**), it can be applied only in case that the vertical spacings between the reinforcement layers are small enough.

In **Fig. 4-17** the stress paths of an unreinforced and a reinforced specimen are drawn qualitatively. The scale of the axis in the diagram is changed in order to show up the details. Therefore, the straight line $\sigma_1 = \sigma_3$, which usually be the bisecting line is less inclined. In both tests the specimens are being consolidated under isotropic conditions before loading. The stress path of the unreinforced specimen (continuous line) shows an increase of σ_1 until failure while the cell pressure σ_3 is kept constant. At a reinforced test, an increase of σ_1 beyond the critical limit of the unreinforced soil can be observed, during that the cell pressure is the same as it was for the unreinforced test. The stress condition at failure for "case I" is therefore $\{\sigma_1 + \Delta\sigma_1;\ \sigma_{3,cell}\}$. However, due to the deformation caused by the mobilization of the geogrids and based on the model described above, the effective stress path of a reinforced specimen (dashed line) shows actually an increase of the confining pressure by $\Delta\sigma_{3,reinf.}$ during loading. When failure occurs, the stress condition will reach the failure criterion as in case of the unreinforced soil (case II), but at a much higher stress level $\{\sigma_1 + \Delta\sigma_1;\ \sigma_{3,cell} + \Delta\sigma_{3,reinf.}\}$.

4.3 Stress distribution in gravelly soil

Based on the above test results, the author decided to use the earth pressure cells for measuring the stress distribution in the specimen. This measurement can be used as a part of explaination how to calculate the additional confining pressure $\Delta\sigma_3$ in the reinforced tests. Two laboratory tests were conducted to evaluate the stress distributions in the specimen with and without reinforcement. They are IIS-COM-E and IIS-0H. Pressure cells were placed at specified locations/depth for this purpose. **Fig. 4-18** and **4-19** show the vertical and horizontal stress distribution in test IIS-COM-E. In this test, there were some unexpected results. For the pressure cells which measure the vertical stresses, the pressure cell named 2D should show the higher value than the pressure cell named 3D. The same problems were found in the horizontal distribution results. The pressure cell named 2U was in the negative side instead of positive side. For the unreinforced test IIS-

0H, even the author tried to prepare the specimen much more carefully, the result has shown the same problems as shown in **Fig. 4-20**. The reason might be caused by the bending of the gauge measurement inside the pressure cells during compaction.

4.4 Evaluating the additional confining pressure $\Delta\sigma_3$

Figure 4-21 compares the real strain distribution in the grid in analogy to **Fig. 4-14** and a simplified model. This simplified model has been taken to pick the corresponding load out of the characteristic load-strain relationship of the geogrid. Dividing the load by the number of longitudinal members per metre width, the drag force of a single longitudinal member $F_{i,Z}$ is obtained. A linear relation between load and strain can be assumed as follows:

$$F_{i,Z} = \frac{N}{n} \qquad (4\text{-}1)$$

Where $F_{i,Z}$: drag force (kN/member)
N: average tensile force in the geogrid (kN/m)
n: the number of longitudinal members per metre width (member/m)

The resistance of the geogrid is supporting the soil mass from the outside towards the centre and can therefore be considered as an addition of the confining pressure σ_3. In terms of the geometry the width of effectiveness for one longitudinal member $b_{e,Z}$ is the same as the aperture width plus the width of the member b_Z (**Fig. 4-22a**). With this assumption and by dividing the members drag force by the width of influence $b_{e,Z}$ and by the vertical spacing between the geogrid layers l_v (**Fig. 4-22b**) the mobilised tensile force of geogrid can be expressed by an equivalent confining pressure. Therefore, the influence of the reinforcement can be considered as an additional confining pressure $\Delta\sigma_3$, activated independent of the deformation.

$$\Delta\sigma_3 = \frac{F_{i,Z}}{b_e . l_v} \qquad (4\text{-}2)$$

Where:
$F_{i,Z}$: drag force (kN/member)
b_e: the width of influence for one longitudinal member $b_{e,Z}$ (m/member)
l_v: the vertical spacing between the geogrid layers (m)

The results based on these assumption were shown in **Fig. 4-23** and **4-24**. Based on the **Fig. 4-17**, the failure criteria of both unreinforced and reinforced tests should be in the same line. However, in **Fig. 4-23** it showed in different line. This is caused by the overestimation of $\Delta\sigma_3$ in the simplified model employed in this study, including overestimation of the failure stress state. **Fig. 4-24** again proves that the influence of geogrid at low confining pressure is higher than at high confining pressure.

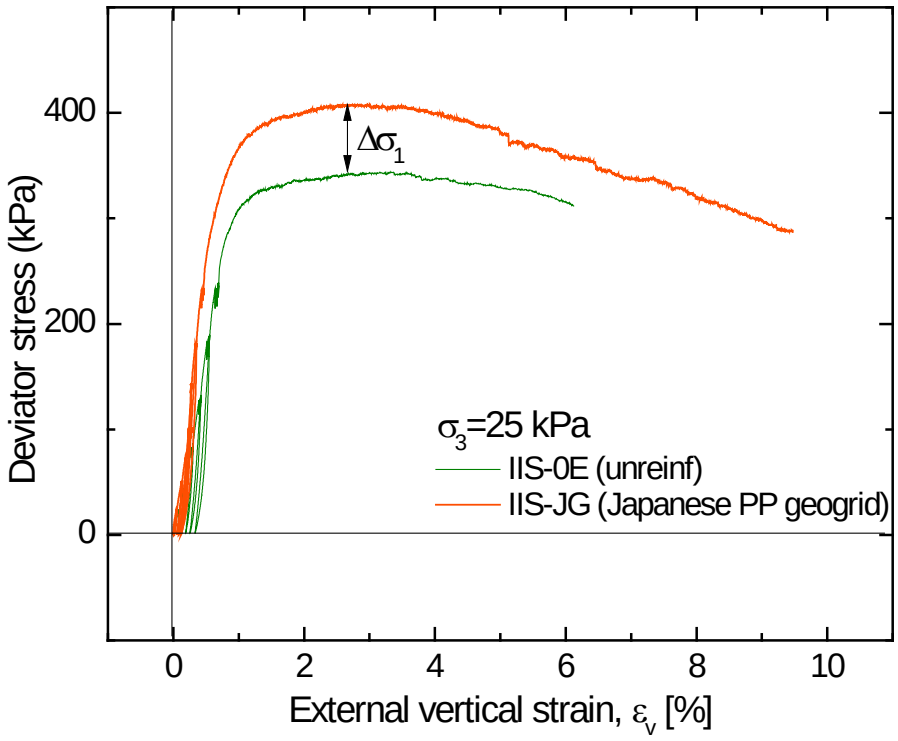

Figure 4-1: Stress-strain curve of unreinforced and reinforced tests at 25 kPa

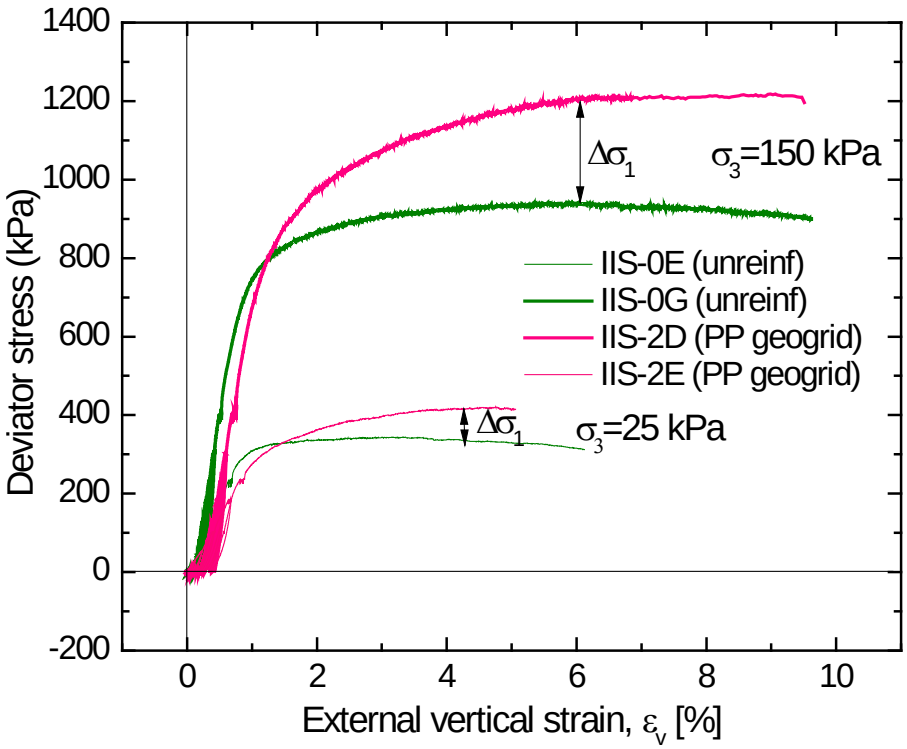

Figure 4-2: Stress-strain curve of unreinforced and reinforced tests at 25 kPa and 150 kPa

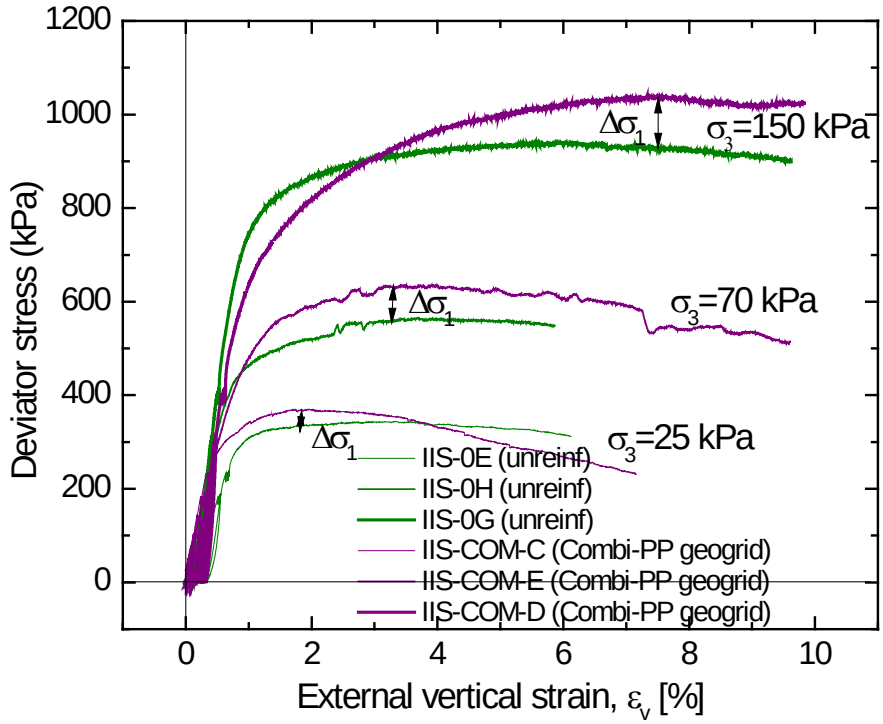

Figure 4-3: Stress-strain curve of unreinforced and reinforced tests at 25, 70 and 150 kPa

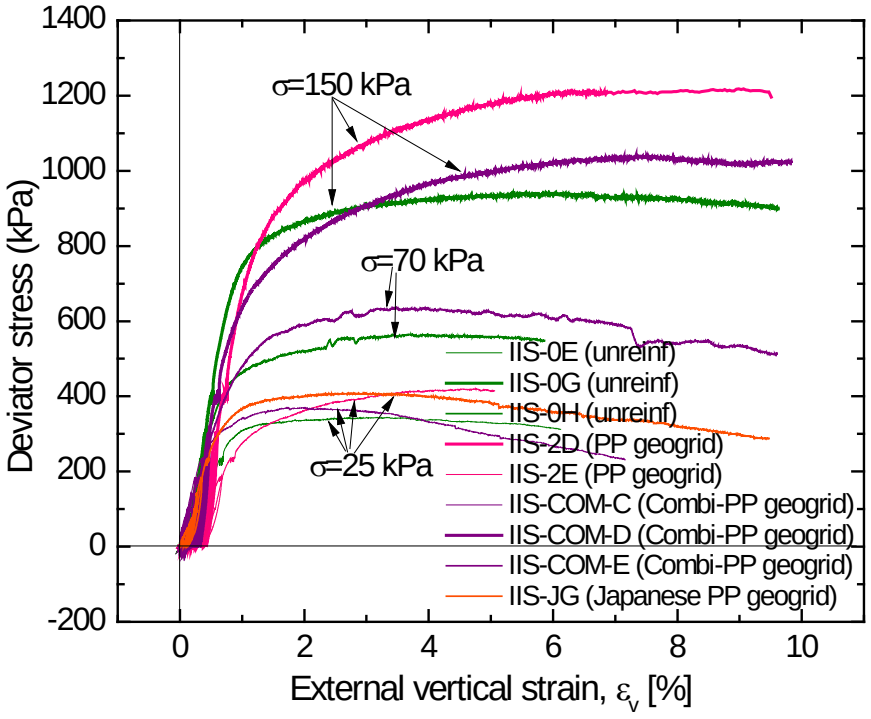

Figure 4-4: Stress-strain curve of unreinforced and reinforced tests in combination

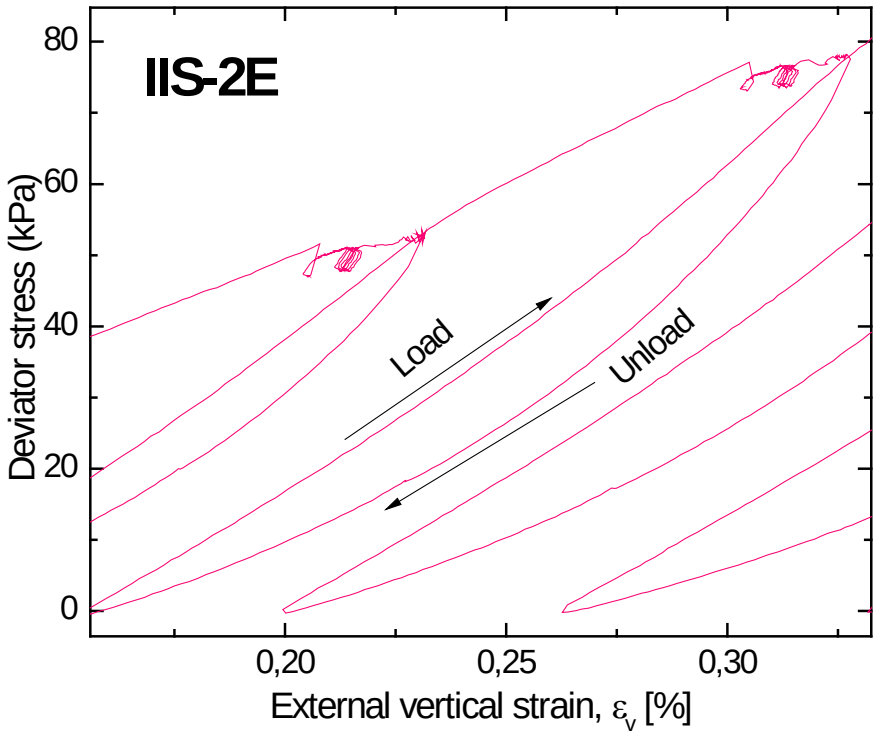

Figure 4-5: Unloading-reloading stage

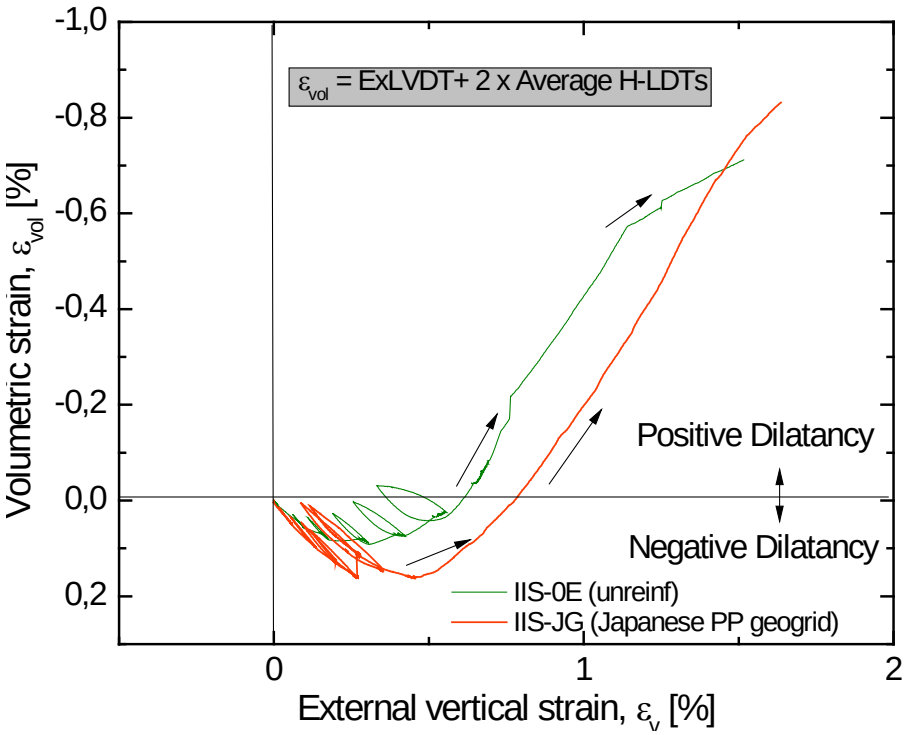

Figure 4-6: Volumetric strain of unreinforced and reinforced tests at 25 kPa

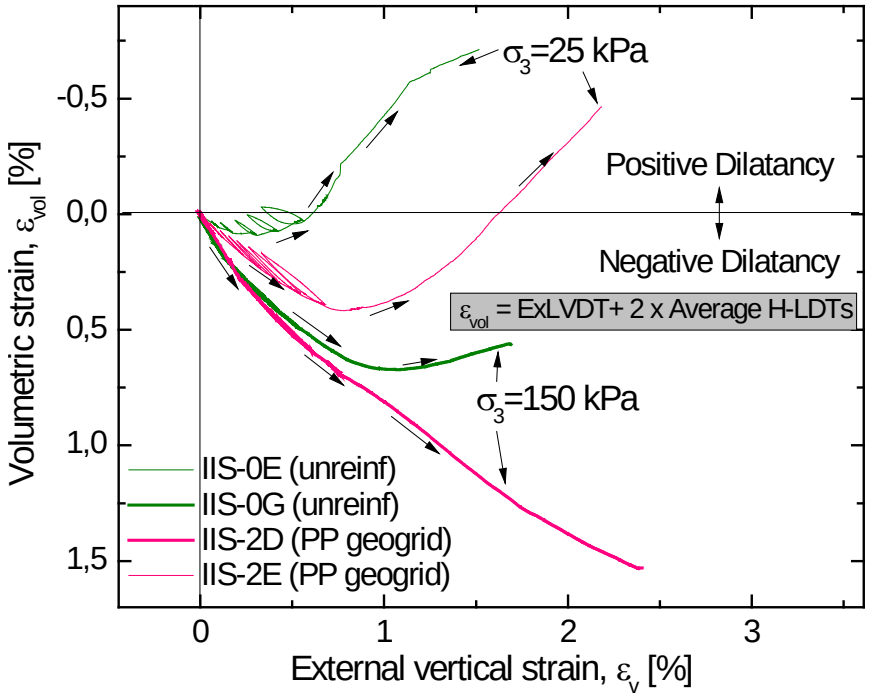

Figure 4-7: Volumetric strain of unreinforced and reinforced tests at 25 and 150 kPa

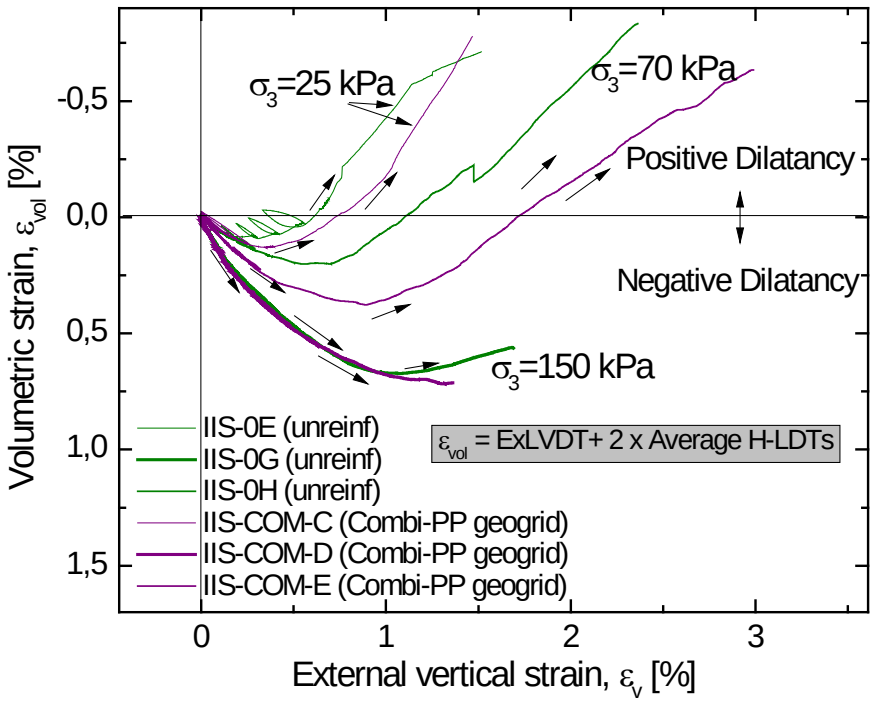

Figure 4-8: Volumetric strain of unreinforced and reinforced tests at 25, 70 and 150 kPa

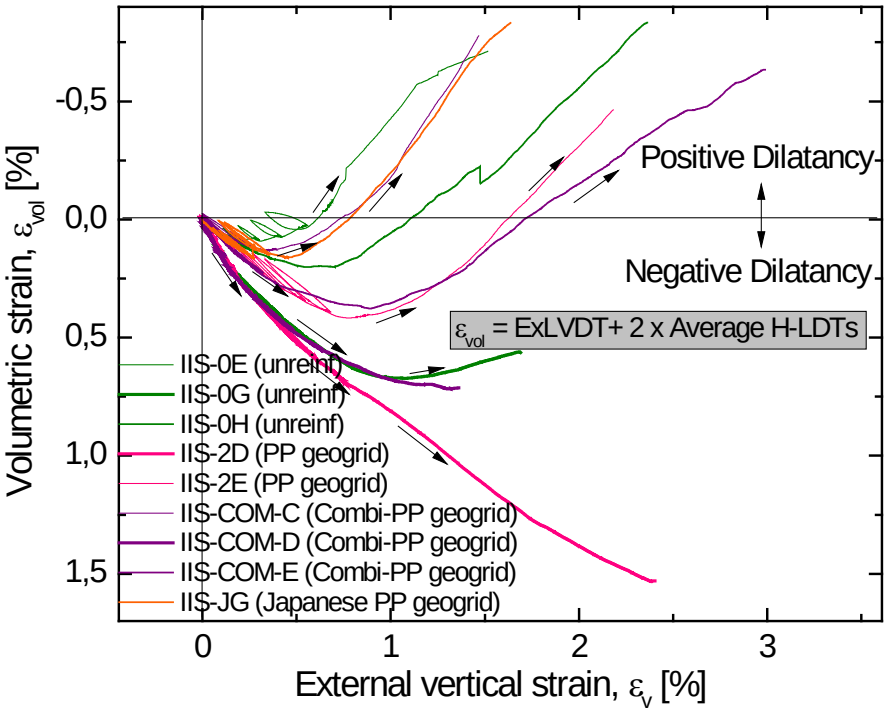

Figure 4-9: Volumetric strain of unreinforced and reinforced tests in combination

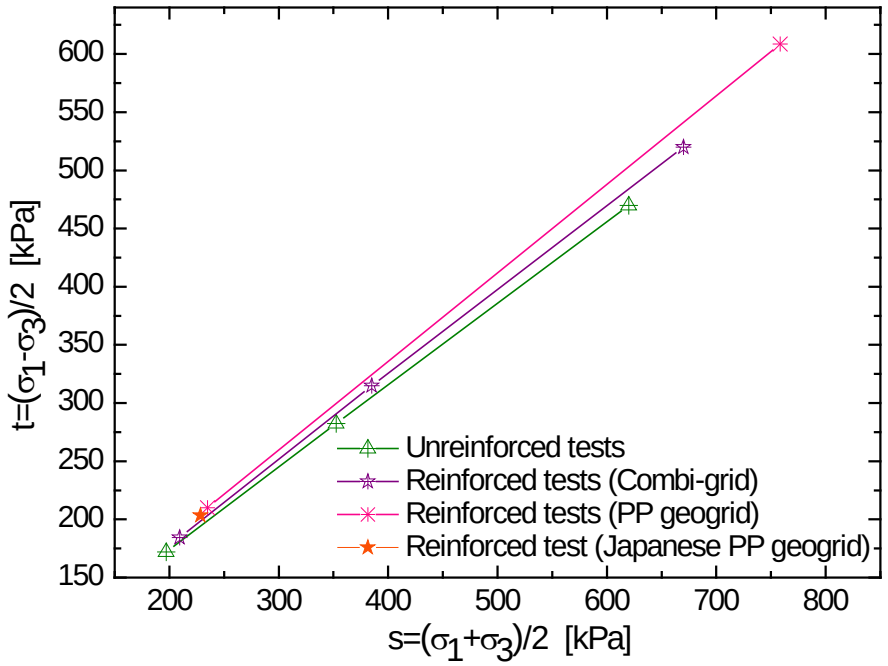

Figure 4-10: p-q Diagram at failure of unreinforced and reinforced tests in combination

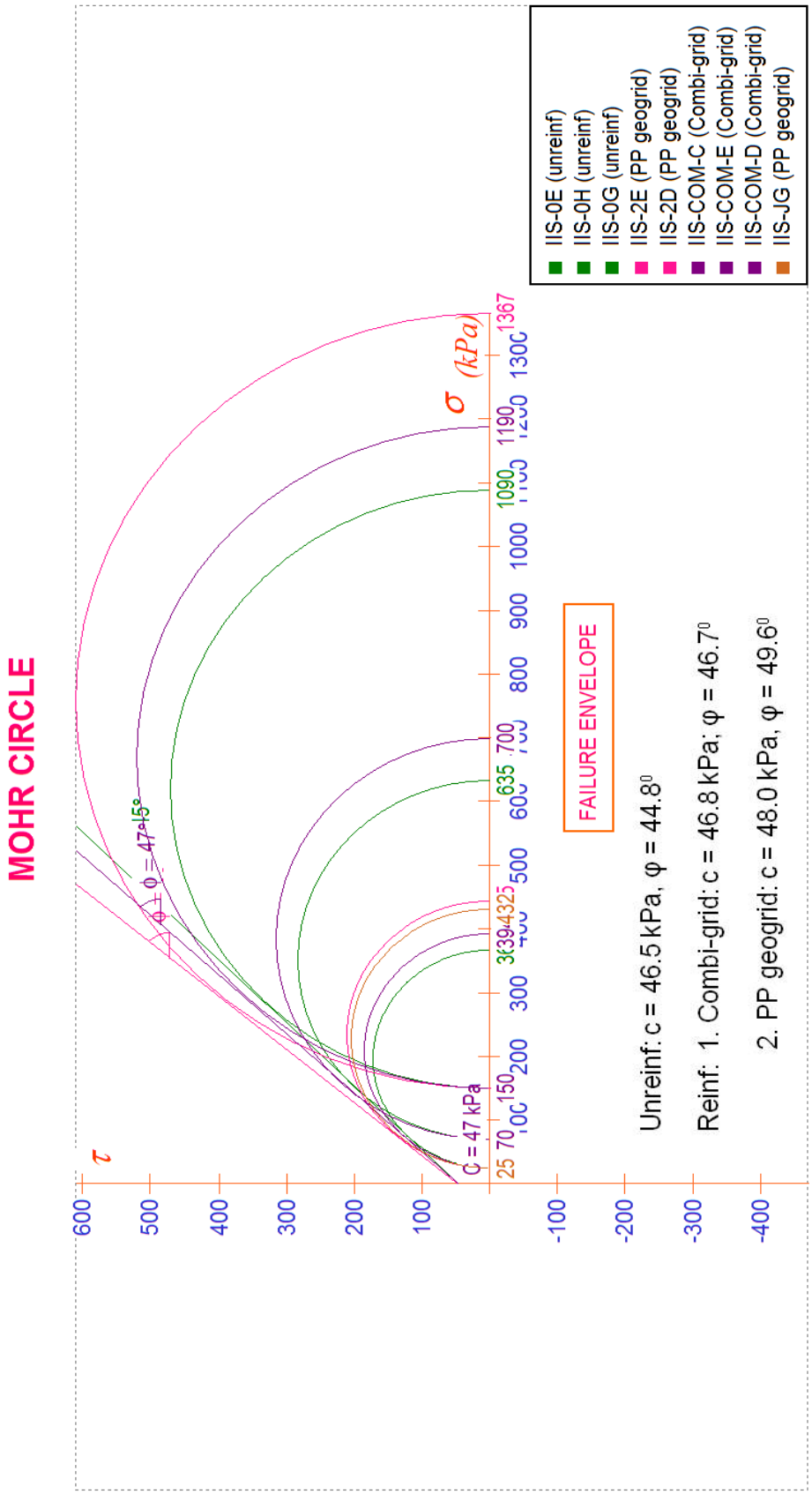

Figure 4-11: Mohr circle of unreinforced and reinforced tests

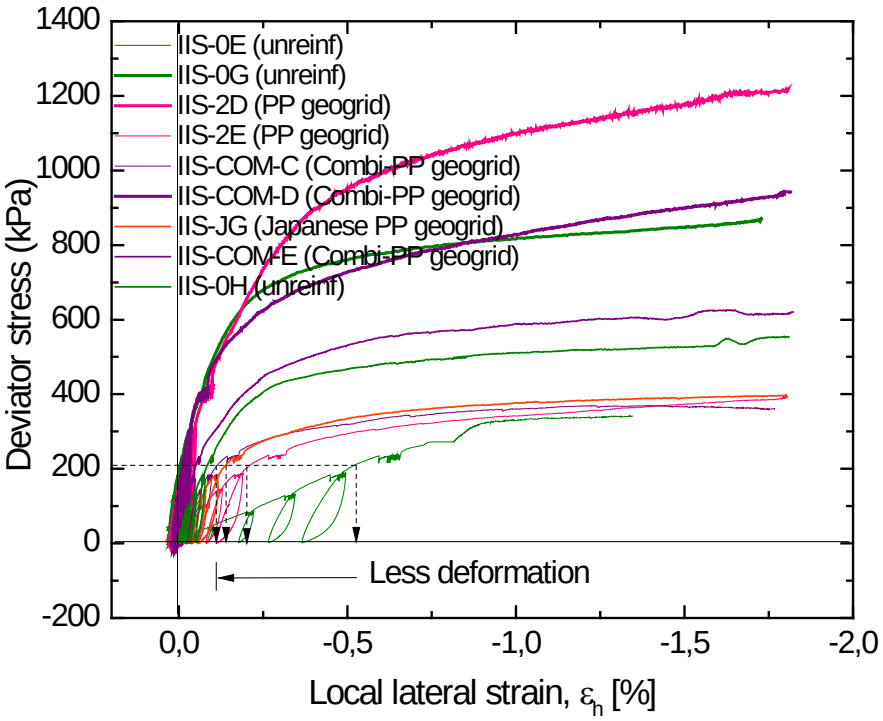

Figure 4-12: Reduction of deformation due to mobilization of reinforcement

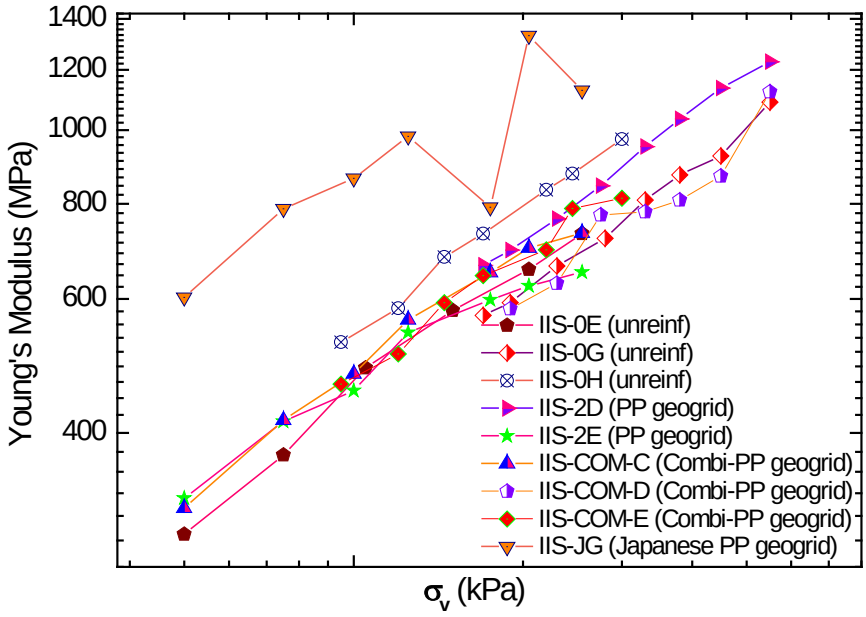

Figure 4-13: Small strain stiffness of unreinforced and reinforced tests

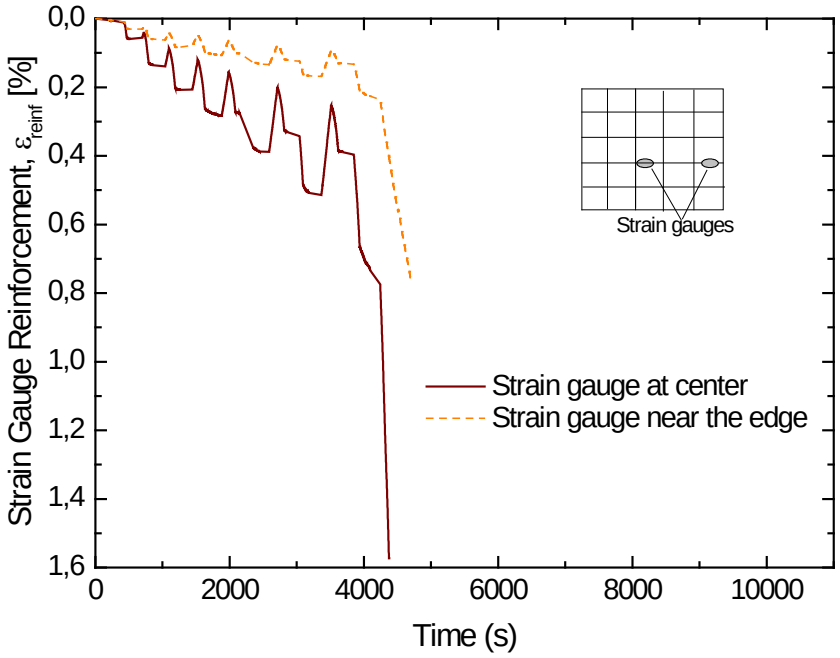

Figure 4-14: Strain gauge distribution in the geogrid

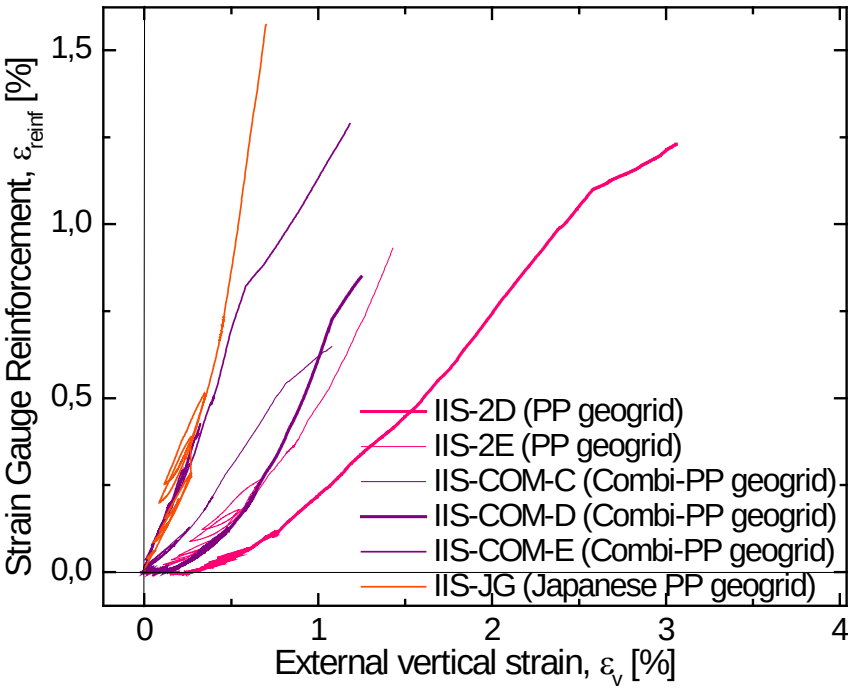

Figure 4-15: Comparison of strain gauge distribution in the geogrid

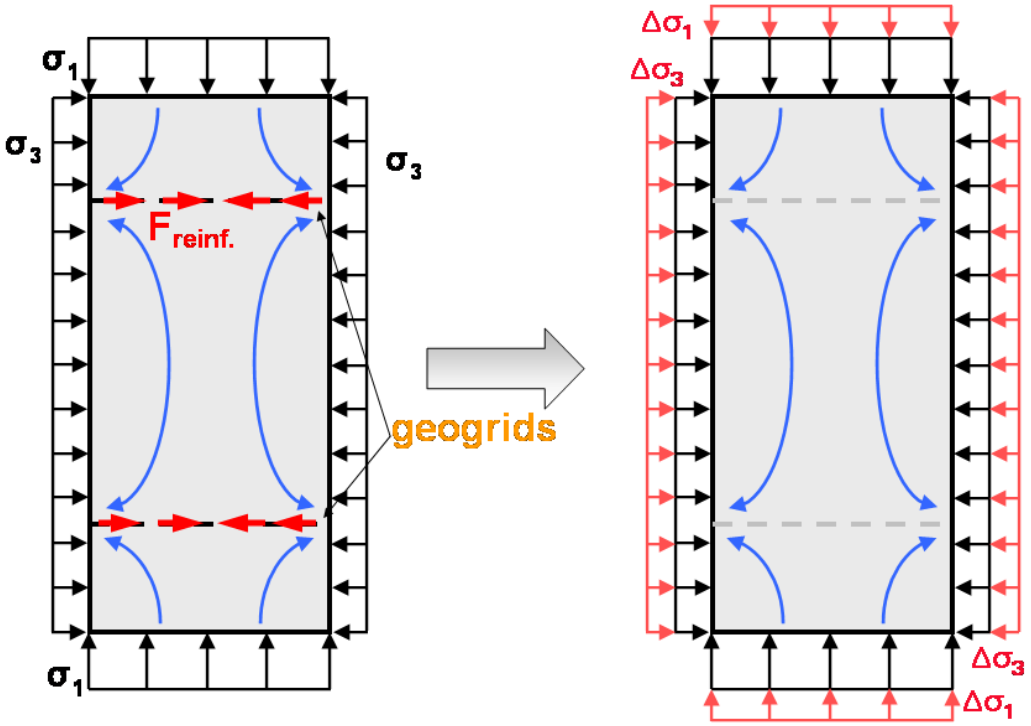

Figure 4-16: Increase of specimen strength due to reinforcement

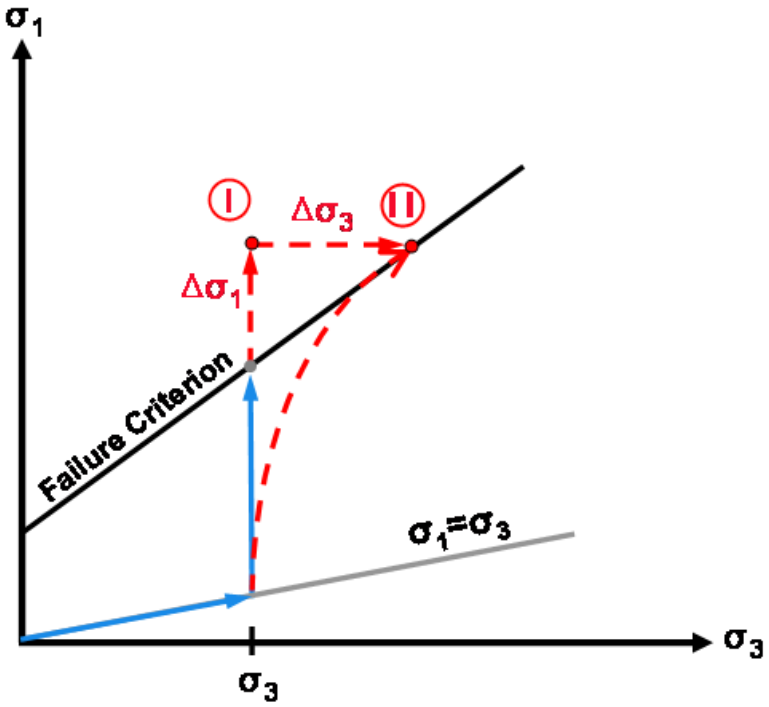

Figure 4-17: Stress path of the loading due to reinforcement

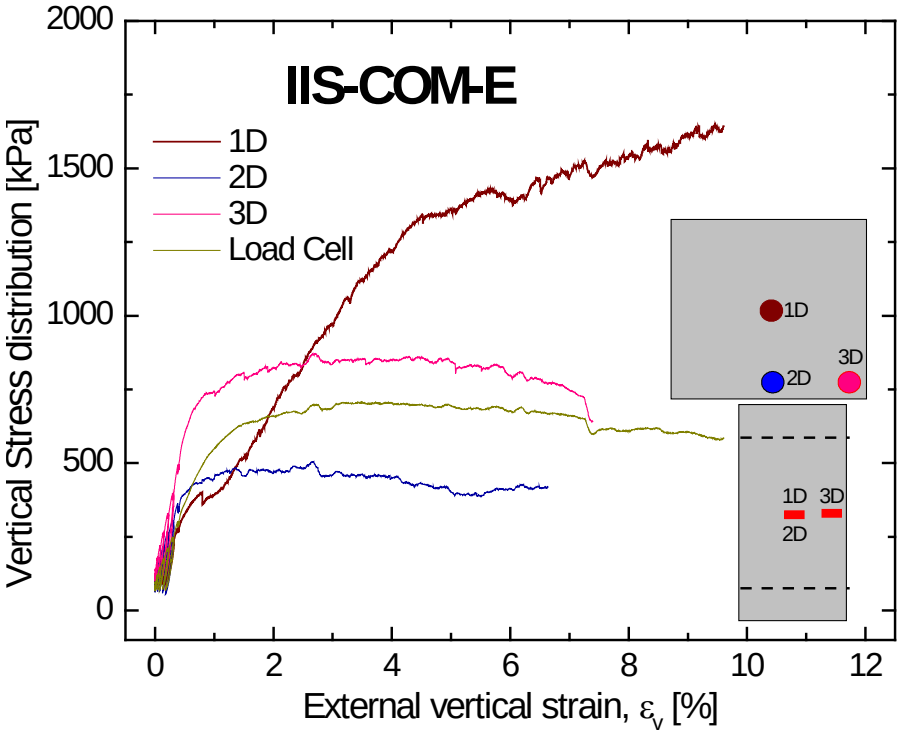

Figure 4-18: Vertical stress distribution in the reinforced test

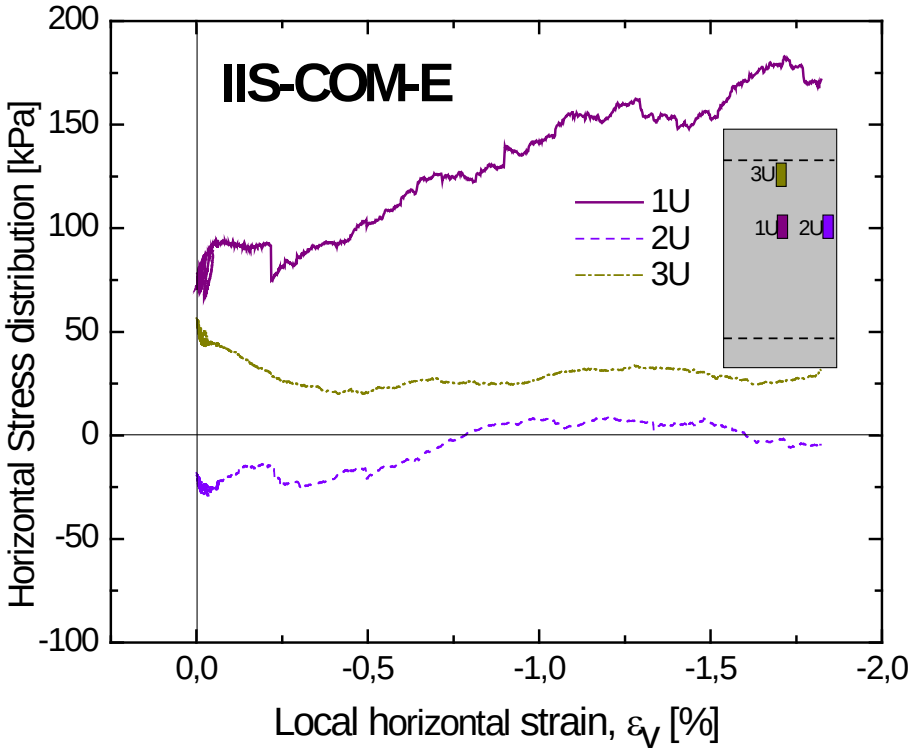

Figure 4-19: Horizontal stress distribution in the reinforced test

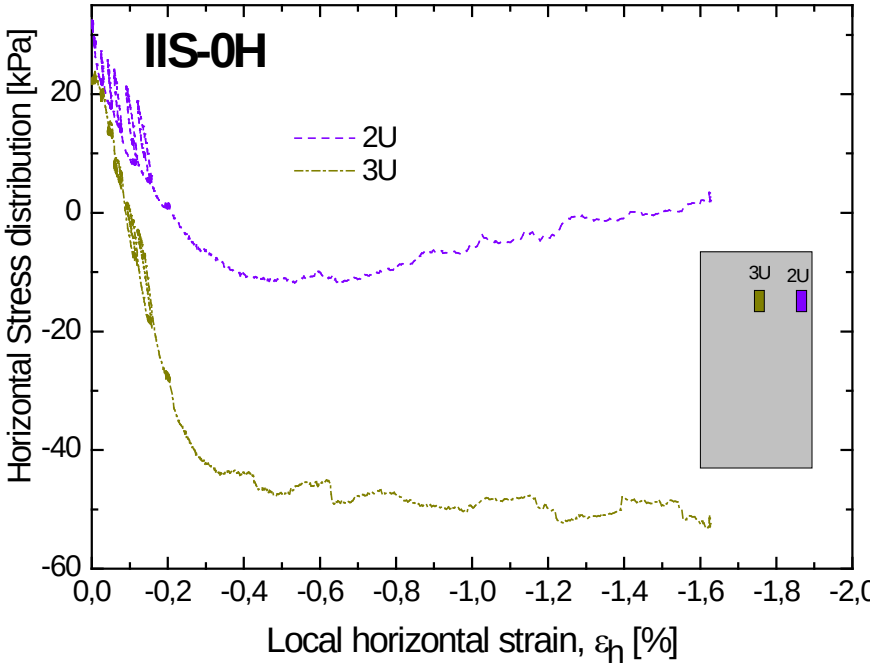

Figure 4-20: Horizontal stress distribution in the unreinforced test

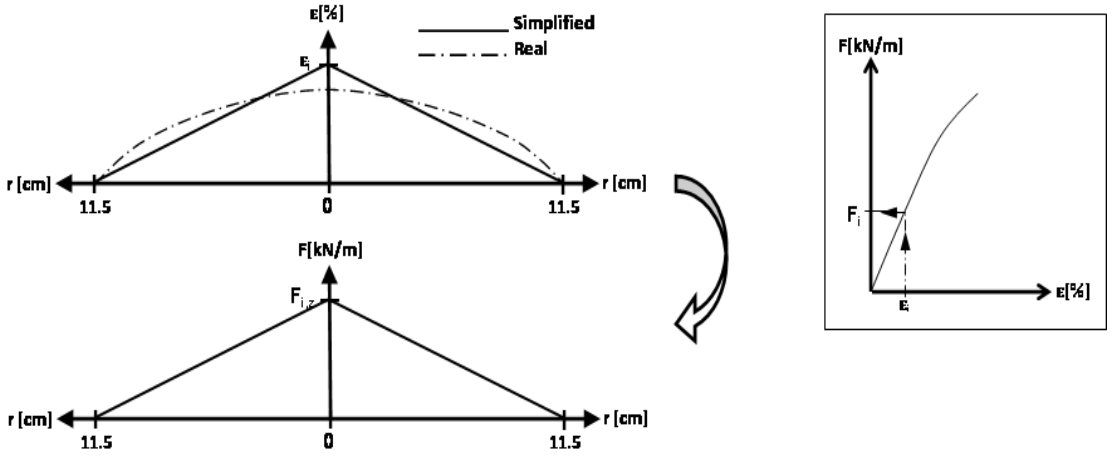

Figure 4-21: Simplified model of the real strain distribution in the grid

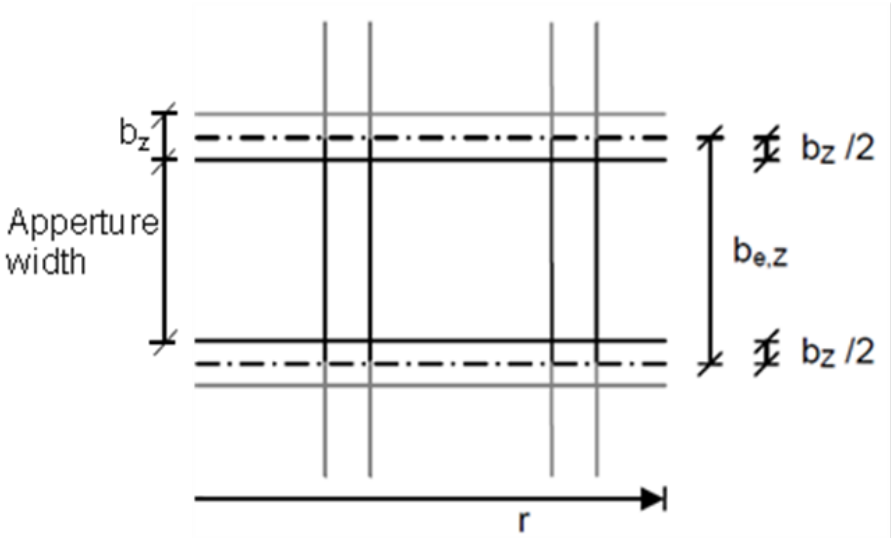

Figure 4-22a: Geometry transformation

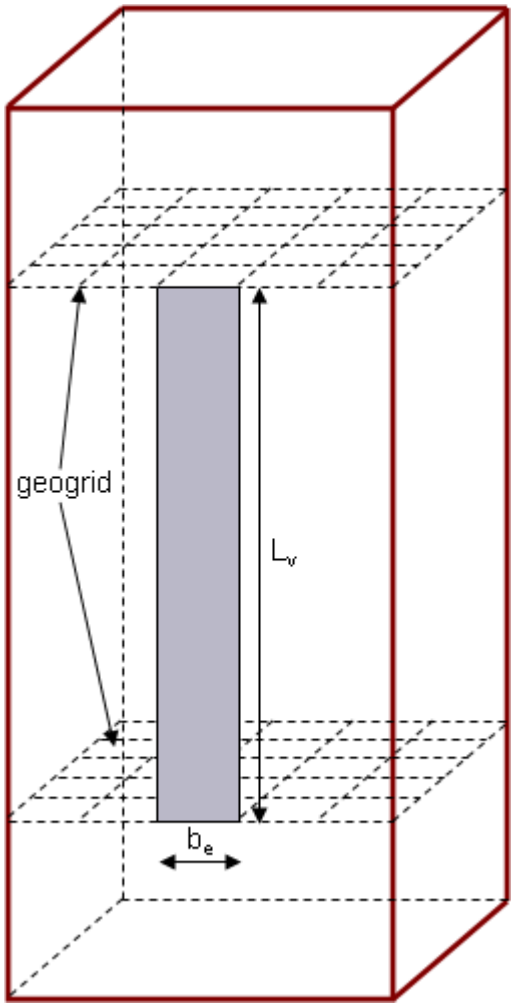

Figure 4-22b: Area of influence of a single longitudinal member

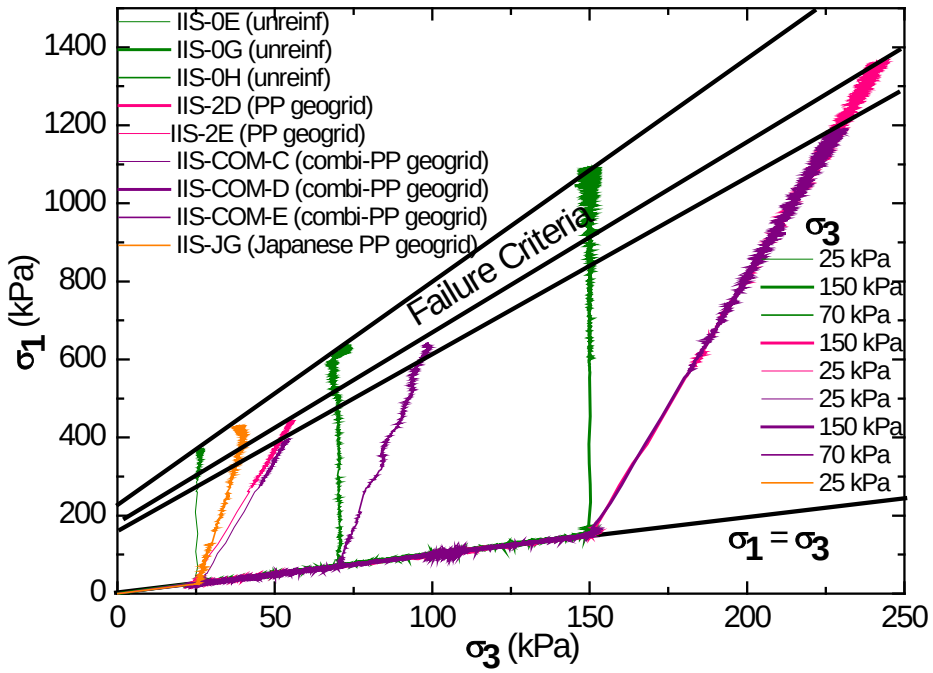

Figure 4-23: Stress path for unreinforced and reinforced tests

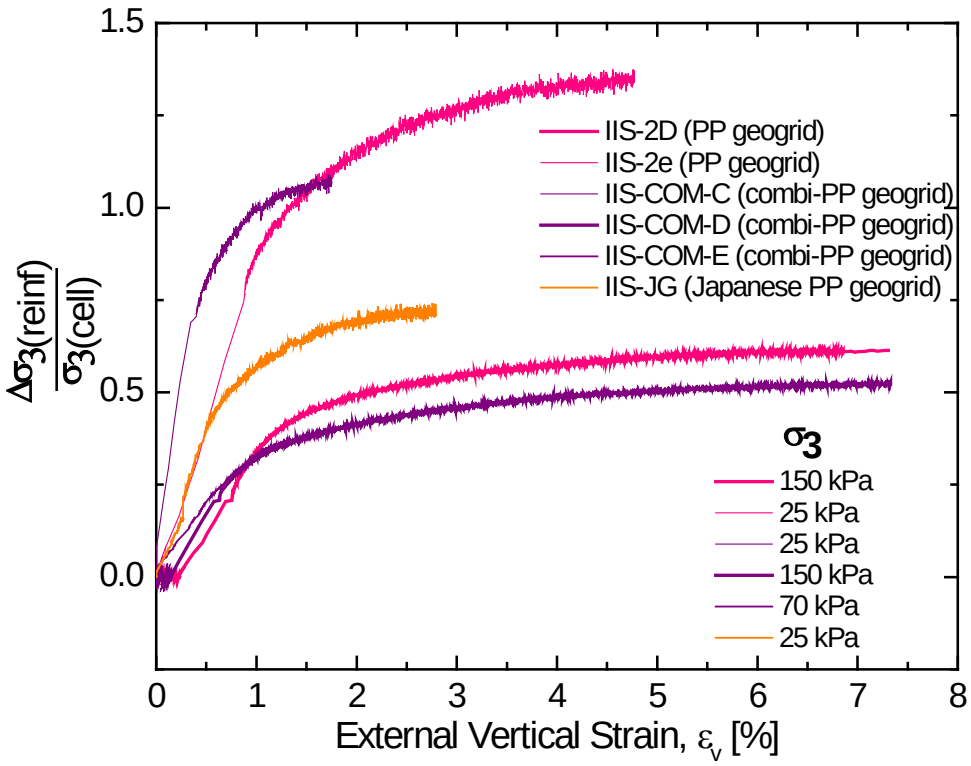

Figure 4-24: Confining effect due to reinforcement

References

Abu-Hejleh, N., Zornberg, J.G., Wang, T. & Watcharamonthein, J. 2002. “Monitored displacements of unique geosynthetic-reinforced bridge abutments”. Geosynthetics International, Vol. 9, No. 1.

Allen, T. M., and Bathurst, R. J. (2001). "Application of the K_0-stiffness Method to Reinforced Soil Wall Limit State Design." Final Research Report to Washington State Department of Transportation, Seatle, Washington State.

Allen, T. M., and Bathurst, R. J. (2001). "Prediction of Soil Reinforcement Loads in MSE Walls." Report WA-RD-522.1, Washington State Department of Transportation and Federal Highway Administration (FHWA).

Athanasopoulos, G.A. (1994). “On the Enhanced Confining Pressure Approach to the Mechanics of Reinforced Soil.” Geotechnical and Geological Engineering, 12, 122-132.

ASTM D4595 (1986). “Standard Test Method for Tensile Properties of Geotextile by the Wide-Width Strip Method.” American Society for Testing and Materials. USA.

Bassett, A.K. and Last, N.C. (1978). “Reinforcing Earth below Footings and Embankments.” Proc. Of the ASCE Spring Convention and Exhibit, Pittsburgh, PA.

Bathurst, R. J. and Cai, Z. (1994). "In-isolation Cyclic Load-extension Behavior of Two Geogrids." Geosynthetics International, 1(1), 1-19.

Ketchart, K. & Wu, J.T.H. 2001. “Performance test for geosynthetic reinforced soil including effects of preloading”, Federal Highway Administration, McLean, VA, USA, Report No. FHWA-R-01-018.

Kawamura, T., Umezaki, T., Ochiai, H., Yasufuku, N. and Hirai, T. (2000/10). “Confining Effect of Geogrid-reinforced Soil: Introduction into Design Method”, 2nd European Geosynthetics Conference (Bologna, Italy).

Moghaddas-Nejad, F. & Small, J.C. 2003. “Resilient and permanent characteristics of reinforced granular materials by repeated load triaxial tests”. Geotechnical Testing Journal, ASTM, Vol. 26, Issue 2.

Ochiai, H., Yasufuku, N., Yamaji, T., Guang-Li, X. and Hirai, T. (2001). “Experimental evaluation of reinforcement in geogrid-soil structure.”, Balkema, Int. Symp. on Earth Reinforcement, Fukuoka, Japan, (Ochiai et al., eds), Vol. 1, pp.249-254.

Ruiken, A. and Ziegler, M. (2008). “Effect of Reinforcement on the Load Bearing Capacity of Geosynthetic Reinforced Soil”. EuroGeo4, IGS, Edinburgh, UK, (Proceedings in CD).

Ruiken, A. and Ziegler, M. (2008). “Large Scale Laboratory Element Testing of Geogrid Reinforced Soil”. GIGSA GeoAfrica 2009.

Tatsuoka, F., Molenkamp, F., Torii, T., and Hino, T. (1997). "Preloaded and Prestressed Reinforced Soil." Soil and Foundations, Japan, 37(3), 79-94.

Tatsuoka, F. (1993). “Roles of Facing Rigidity in Soil Reinforcing.” Earth Reinforcement Practice, Ochiai, Hayashi, and Otani, eds., Balkema, Rotterdam, The Netherlands, 831-867.

Uchimura, T., Shinoda, M., Siddiquee, M.S.A. and Tatsuoka, F. (2001). “Deformation analysis of PLPS GRS bridge pier during construction and in service.” Swets & Zeitlinger, Landmarks in Earth Reinforcement, (Ochiai et al. eds), Vol 1, pp.293-298.

Uchimura, T., Tatsuoka, F., Sato, T., Tateyama, M. and Tamura,Y. (1996). “Performance of preloaded and prestressed geosynthetic-reinforced soil.” Balkema, Int. Symp. on Earth Reinforcement, Fukuoka, Japan, (Ochiai et al., eds), Vol. 1, pp.537-542.

Yasufuku, N., Ochiai, H., Kaneshige, M. and Kawamura, T. (2006). “Confining Effect of Geogrid-Reinforced Soil Linked with Soil Dilatancy and Its Application to Pratical Design Method.”, Millpress, Rotterdam, Geosynthetic, (Kuwano, J., and Koseki, J., eds), pp.1303-1306.

Ziegler, M. and Timmers, V. 2004. “A new approach to design geogrid reinforcement”. Proceedings of EuroGeo3, DGGT, Munich, Germany, Vol. 2, 661-666.

Ziegler, M. and Ruiken, A. (2008). “Progressive in Understanding of Geosynthetic/Soil Composite Material Behavior in Geosynthetic Reinforced Earth Structures”. Cancun Mexico 2008, pp. 1227-1236.

CHAPTER 5
CONCLUSIONS & RECOMMENDATIONS

5.1 Conclusions

The following conclusions can be drawn from the results obtained from unreinforced and reinforced large scale triaxial testing:

- The peak strength of the soil is increased significantly by all the geogrid reinforcements tested.
- Vertical and horizontal deformations are reduced considerably due to the reinforcement.
- Geogrid reinforced soils develop an additional confining effect due to activation of tensile force in the geogrids.
- The relative reinforcing effect is higher for small lateral confining pressures, as in case at small depths.
- The stiffness of reinforced specimens is higher than unreinforced specimens.
- Geogrid reinforcement does not show any significant improvement in the small strain stiffness of granular specimen, except for the case with Japanese geogrid.
- The tests using PP geogrid have a higher performance than the tests using combi-grid in case of using gravelly soil. Therefore there should be a consideration in using the correct type of geogrids corresponding to the construction materials.
- A method to determine the development of the confining effect due to the reinforcement is presented.

The results of the triaxial testing can be applied to various geogrid reinforced structures. The correlative strains depend on the lateral pressure of the surrounding soil. The confining pressure in the triaxial test has to be set similar to the field conditions, i.e. very low lateral pressure as it is the case in the near surface area. Actually, at triaxial testing the surrounding soil can only be simulated with a well defined, constant confining

pressure. Another shortcoming of the test method might be the missing anchorage of the reinforcement in the surrounding soil.

Test results obtained from triaxial testing show that deformations are reduced significantly for the tests using reinforcement compared to unreinforced soil. However, due to the missing possibility of anchoring the geogrids in the surrounding soil, it would underestimate the real peak strength of the composite material by far. Therefore, a concern with the reduction of deformations due to the reinforcement cannot simply be transferred from triaxial testing to field conditions.

5.2 Recommendations

Based on the present study, it is evident that further research in this field can yield practical and valuable result. Hence, future studies should focus on:

- Using the finite element model for the reinforced soil to simulate a full-scale geogrid reinforced approach construction using gravelly soil and compare the finite element results with field measurements from monitoring instrumental construction work.

- Developing advanced material models in order to better simulate the behavior of soil and unbound granular material.

- To provide actual soil strength properties, additional tests of soil strength properties under plane strain conditions should be carried out to obtain properties that duplicate field conditions.

- Quantitative verification of the proposed model on the confining effect, including evaluation local stress distribution in the reinforced specimens.